



Rutgers, The State University of New Jersey
Department of Industrial and Systems Engineering

Final Report
Defense Logistics Agency (DLA)
Industrial Base Innovation Fund
Contract No. SP4701-08-C-0025

**Title: Design and Implementation of an Innovative Manufacturing Process for
Aerial and Land Supply Needs**

Submitted to

Mr. John Dormer, Contracting Officer
Defense Supply Center Philadelphia
DLA Contracting Support Office DSCO-P
700 Robbins Avenue, Building 26-1
Philadelphia, PA 19111
215-737-2284
john.dormer@dla.mil

Principal Investigator

Dr. E. A. Elsayed
Department of Industrial and Systems Engineering
Rutgers University
96 Frelinghuysen Road
Piscataway, NJ 08854-8018
Phone: (732) 445-3859
Fax: (732) 445-5467
elsayed@rci.rutgers.edu

June 30, 2011

REPORT DOCUMENTATION PAGE					Form Approved OMB No. 0704-0188	
<p>The public reporting burden for this collection of information is estimated to average 1 hour per response, including the time for reviewing instructions, searching existing data sources, gathering and maintaining the data needed, and completing and reviewing the collection of information. Send comments regarding this burden estimate or any other aspect of this collection of information, including suggestions for reducing the burden, to Department of Defense, Washington Headquarters Services, Directorate for Information Operations and Reports (0704-0188), 1215 Jefferson Davis Highway, Suite 1204, Arlington, VA 22202-4302. Respondents should be aware that notwithstanding any other provision of law, no person shall be subject to any penalty for failing to comply with a collection of information if it does not display a currently valid OMB control number.</p> <p>PLEASE DO NOT RETURN YOUR FORM TO THE ABOVE ADDRESS.</p>						
1. REPORT DATE (DD-MM-YYYY) June 30, 2011		2. REPORT TYPE Final		3. DATES COVERED (From - To) November 10, 2008 - June 30, 2011		
4. TITLE AND SUBTITLE Design and Implementation of an Innovative Manufacturing Process for Aerial and Land Supply Needs				5a. CONTRACT NUMBER SP4701-08-C-0025		
				5b. GRANT NUMBER		
				5c. PROGRAM ELEMENT NUMBER		
6. AUTHOR(S) Elsayed, E.A.				5d. PROJECT NUMBER		
				5e. TASK NUMBER		
				5f. WORK UNIT NUMBER		
7. PERFORMING ORGANIZATION NAME(S) AND ADDRESS(ES) Department of Industrial and Systems Engineering Rutgers University 96 Frelinghuysen Rd. Piscataway, NJ 08854-8018				8. PERFORMING ORGANIZATION REPORT NUMBER		
9. SPONSORING/MONITORING AGENCY NAME(S) AND ADDRESS(ES) Defense Supply Center Philadelphia 700 Robbins Avenue, Bldg. 26-1 Philadelphia, PA 19111-5096 John Dormer 215-737-2284 john.dormer@dla.mil				10. SPONSOR/MONITOR'S ACRONYM(S)		
				11. SPONSOR/MONITOR'S REPORT NUMBER(S)		
12. DISTRIBUTION/AVAILABILITY STATEMENT DISTRIBUTION STATEMENT A. Approved for public release; distribution is unlimited.						
13. SUPPLEMENTARY NOTES						
14. ABSTRACT The objective of this project is to design and implement a fully automated innovative manufacturing process, based on patents co-authored by the principal investigator, for the development and production of flexible cushioning systems which have been tested in order for loads of supplies to be free-dropped from an aircraft at low altitude with aircraft flying at speeds higher than 70 knots. This is the first application and testing of free-drop of subpacks. Development of such innovative manufacturing process provides immediate capability for the Department of Defense to produce new sub-packs and low-cost reduced-volume delivery protection systems. The immediate use is the freedrop of supplies which was successfully tested in the field. This enables the freedrop (without parachute in DZs (drop zone areas) which are unreachable by land supply lines. This technology may result in new structures that might redesign the entire concept of supply chain for DoD.						
15. SUBJECT TERMS Industrial Base Innovation Fund, Manufacturing, Packaging, Packing Materials, Free Dropping, Aerial Delivery						
16. SECURITY CLASSIFICATION OF:			17. LIMITATION OF ABSTRACT	18. NUMBER OF PAGES	19a. NAME OF RESPONSIBLE PERSON	
a. REPORT	b. ABSTRACT	c. THIS PAGE			Dr. E.A. Elsayed	
U	U	U	U	146	19b. TELEPHONE NUMBER (Include area code) 732-445-5467	

Executive Summary

The objective of this project is to design and implement a fully automated innovative manufacturing process, based on patents co-authored by the principal investigator, for the development and production of flexible cushioning systems which have been tested in order for loads of supplies to be free-dropped from an aircraft at low altitude with aircraft flying at speeds higher than 70 knots. This is the first application and testing of free-drop of subpacks. It is observed that the structural attributes or characteristics of the package design itself can cause the supplies to land at the desired point in the area of operation with no damage to the supplies and in a condition that facilitates quick recovery and distribution. More specifically, the cushioning systems (for the packages) can be airdropped from an aircraft moving at between 90 and 130 Knots Indicated Air Speed (KIAS) from an altitude of 50 to 100 feet Above Ground Level (AGL) with 100 to 200 pounds (lbs) of supplies or cargo; and is quickly found and easily recovered from the Drop Zone (DZ) by one or two soldiers without Material Handling Equipment (MHE) in less than two minutes per package; and achieves very high survivability rate to meet mission needs. The packages include ammunition, MRE, blood pouches and water bottles. The investigators of this proposal have developed a geometric theory for folding flat sheets of material into intricate three-dimensional patterns. The theory ensures that the generated patterns can indeed be folded. By doing so, we are able to generate patterns with extensive geometric variations within the same family of patterns. The generated patterns can then be used, depending on the sheet material and type of applied loads, in many applications. It was shown through impact testing and field testing at Tobyhanna Army Depot that the new cushioning system is capable of absorbing high energy without damaging its contents. The work involved in this project resulted in the development and construction of a manufacturing process which is now fully automated to produce cushions and other protective systems and pallets with different capabilities of absorbing energy depending on the fragility of the cargo being shipped or air dropped and the condition of drop. The project demonstrates a prototype machine with many features that begin by using input data from the user such as the weight of the package content, the fragility of the items being transported (via air or land) and the altitude of the drop and other relevant information. In turn it calculates the optimum design of the cushioning system. Once accepted by the user, the software downloads the necessary parameters to produce this design to the machine's controller to begin the actual production process of the cushions. Once the required number of layers of the folded sheets is stacked to meet the desired size of the pad, the finished pad is ejected and the process continues for making the remaining pads.

Development of such innovative manufacturing process provides immediate capability for the Department of Defense to produce new sub-packs and low-cost reduced-volume delivery protection systems. The immediate use is the freedrop of supplies which was successfully tested in the field. This enables the freedrop (without parachute in DZs (drop zone areas) which are unreachable by land supply lines. This technology may result in new structures that might redesign the entire concept of supply chain for DoD. Of course, the latter requires extensive research in the ability to produce such geometric patterns inexpensively as well as demonstrate the unique characteristics they exhibit.

Table of Content

Executive Summary	
1. Introduction	4
2. Background of Sheet folding Theory and Technology:	4
2.1 Innovation and Background: pattern generation	4
2.2 Innovation and Background: applications in the production of sub-packs for freedrop	6
2.3 Innovation and Background: continuous sheet folding machine.....	7
2.3.1 Machine Description.....	7
3. Components of the Manufacturing Process	9
3.1 The Process of Designing a Cushioning System	9
3.2 Cushion Design and Manufacturing	10
3.2.1 Introduction	10
3.2.2 The data model	10
3.2.3 Use of database	11
3.3 Manual access to the database.....	14
4. Mechanical Design and Construction of the Folding Machine.....	14
4.1 Introduction	14
4.2 Machine basic operations.....	15
4.3 Main design units	15
5. Computer Control of the Folding Machine.....	16
5.1 Bridge Setting.....	16
5.2 Sensor Positioning Mechanism	17
5.3 Supervisor Controller.....	18
6. Patents by the Investigators	19

1. Introduction

During the eighteen years, Rutgers researchers have been working on a mathematical theory and technology that transforms flat sheet of material (metal, composites, paper) into three dimensional intricate structural patterns for many applications including cushioning systems that outperform honeycomb cushions and unique pallet designs among others. The theory and technology have been patented by Rutgers University (patent 7,115,089). The researchers have successfully been able to design a unique prototype machine capable of producing folded structures with different geometry and from different materials.

The US Army is interested in adding a new logistics supply capability named Low-Cost Low-Altitude Freedrop (LCLA-Freedrop). This will provide US Army with the capability to freedrop sub-packs containing ammos, electronic gear, food and blood pouches from high speed but low altitude aircraft. This capability will ensure delivery of supplies in war zones where delivery by other means will subject the delivery system to hostile fire or it is impossible to achieve due to terrain and accessibility of the drop zone such as the case in Afghanistan. In such situations the delivery is accomplished by using a sub-pack (weighs between 100 to 250 lbs) to be precisely dropped from low altitude using high speed aircraft in order to avoid enemy fire.

Rutgers researchers, in collaboration with Logistics Innovation Agency (LIA) of the Defense Logistics Agency, have developed two unique cushioning systems for freedrop of subpacks which contain the objects mentioned above. The cushioning systems have been successfully tested at Tobyhanna Army Depot. Further extensive testing were conducted at Aberdeen Proving Grounds over a three years period. Hundreds of subpacks containing a wide variety of supplies were freedropped and its contents were examined in details after each drop. This has lead to the development of two universal subpacks that can be used for freedrop of hundreds of items. The first subpack is referred to as FDS1 (Freedrop Design System 1) which is suitable for the drop of less fragile items such as ammos, generators, starters, motors and similar objects. This design is made of folded core paper that weights 61 lbs and a laminate paper of 61 lbs weight. The resulting cushion system can absorb the entire impact energy and causes no damage to the contents of the subpacks. The second cushion system is referred to as FDS2 (Freedrop Design System 2). It is made of a folded core paper that weighs 61 lbs and a laminate of 30 lbs weight. This system is suitable for the freedrop of fragile material such as Poland Spring Water, MRE, IV, hard disk drives, electronic gear and others.

The objective of this project is to produce these designs of the cushioning systems using a fully automated process. Rutgers researchers developed and constructed a fully automated process based on several patents. This process uses rolled paper that goes through a sequence of folding process and adds the laminated paper to the folding material to produce the desired cushion systems. This manufacturing process will add unique and important manufacturing capability to the DoD that does not exist in anywhere globally. It can also produce honeycomb-like structures that can replace the extensive applications of honeycomb throughout the DoD supply chain.

Before we describe the details of these components, we provide a brief background about sheet folding theory and technology which are the basis of this project.

2. Background of Sheet folding Theory and Technology:

2.1 Innovation and Background: pattern generation

The investigators of this project have developed a geometric theory for folding flat sheets of material into intricate three-dimensional patterns. The theory ensures that the generated patterns can indeed be *folded*. By doing so, we are able to generate patterns with extensive geometric variations

within the same family of patterns. The generated patterns can then be used, depending on the sheet material and type of applied loads, in many applications such sub-packs for low-cost low-altitude freedrop, pallets and other high energy absorption packaging systems for the US Army supply chain system. Figure 1 shows two patterns generated from flat sheets and both can be used as cores for different applications.

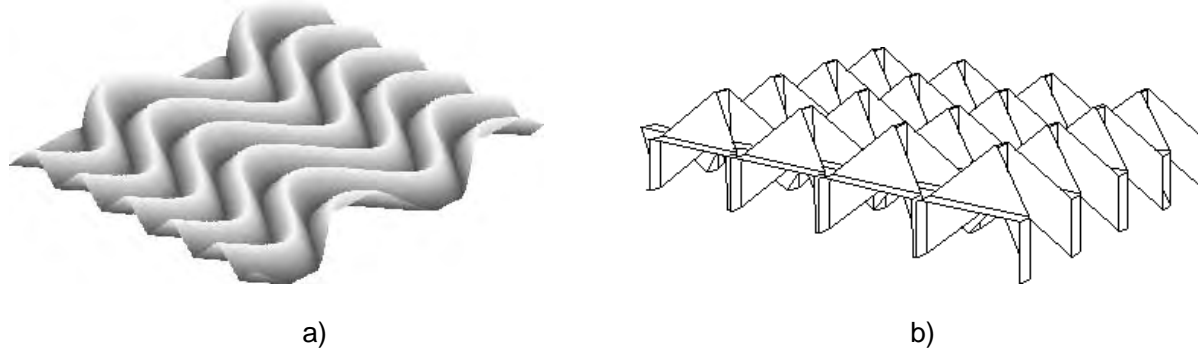


Figure 1: Planar Cores Produced from Folding Flat Sheets of Material

It should be emphasized that this is a *folding* technology for sheet material. Rolled sheet material is produced in advance in possibly one of the most efficient forming processes. This applies to a variety of materials including paper, aluminum, copper, steel, composites and plastics. The newly discovered mathematics extends the domain of folding to include sophisticated structural arrangements. Other production methods such as forging, casting, and assembly can produce three-dimensional arrays that appear approximately similar, but for time, energy or complexity reasons these processes are more costly. Moreover, some of the complex patterns generated by the geometric theory are indeed difficult, if not impossible, to produce by using other manufacturing processes than folding. **Thus the significance of the new theory of folding is that it will enable very intricate structures, previously available only to more costly production methods, to be available at the high-speed economy of a rolled sheet process using a single manufacturing process; namely *folding*.**

Moreover, this new sheet folding technology is capable of producing geometrically repetitive different patterns (shown in Figure 2) at high production rate and low cost, through use of the patented continuous manufacturing techniques developed by the authors at Rutgers University (see list of patents). The two folded sheets shown in Figure 2 are produced by using the same innovative folding machine. Figure 2(a) shows a folded roll which (named Chevron) which was used in making sub-packs for freedrop. Figure 2(b) shows honeycomb-like folded sheet which was produced in an one manufacturing step (unlike the traditional honeycomb that requires an entire factory for its production).

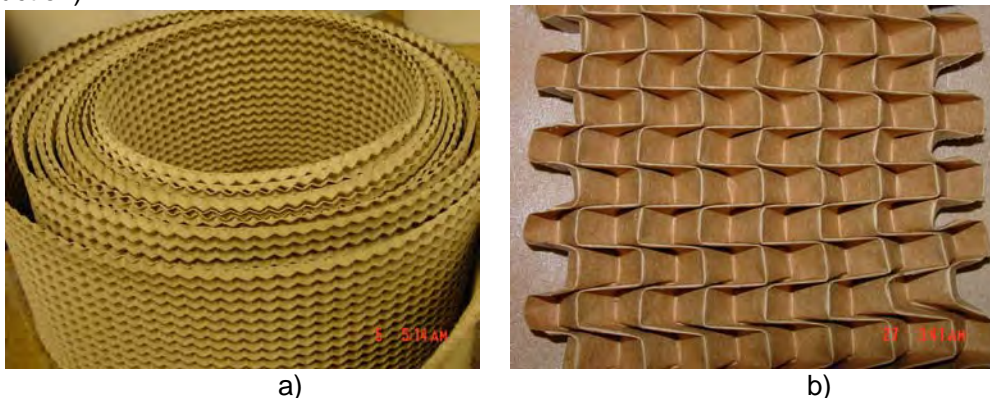


Figure 2. Folded 3-dimensions patterns generated by folding of flat sheet material

Folded patterns have one or more elementary flat surfaces, each of which has a specific geometrical shape which forms the basic building elements of the folded pattern., a combination or multiplication of these elementary flat surfaces of a specific geometrical shape constitutes the basic building cell of a folded pattern, as it is repeated in two dimensions, it creates a three-dimensional folded structure

2.2 Innovation and Background: applications in the production of sub-packs for freedrop

Rutgers researchers collaborated with US Army to design new cushioning system for freedrop as described earlier in this proposal. Folded KRAFT paper was produced using Rutgers sheet folding technology as shown in Figure 3(a). The folded sheets are then made (manually) into pads that were inserted in the sub-packs. A partially assembled sub-pack which contains two ammunition boxes with inert bullets is shown in Figure 3(b). It was shown through impact testing and field testing at Tobyhanna Army Depot that the new cushioning system is capable of absorbing high energy without damaging its contents. Figure 4 shows the freedrop test of the sub-packs.



Figure 3. (a) Sheet folding material produced using the continuous sheet folding technology
(b) Partially assembled sub-pack showing the cushions and ammo boxes

The cushioning system has been tested from different altitudes ranging from 75 ft to 150 ft without using parachutes. Figure 4 shows a freedrop at Tobyhanna.



a)

As shown in Figure 4, the sub-pack was subjected to significant energy due to the potential energy of the drop. In some instances the sub-pack fell on a steel plate with speeds ranging from 75 ft/sec to 130 ft/sec. The sub-pack was instrumented to measure the acceleration and impact force as shown.



b)

Figure 4. Freedrop of sub-packs and the contents of the sub-pack after drop.
Note how the cushion protected the ammo boxes.

2.3 Innovation and Background: continuous sheet folding machine

2.3.1 Machine Description

A prototype continuous folding machine is designed and is being used for experimental basis. The machine has the adaptability and precision for laboratory experimentation and is capable of producing consistent folded materials needed for testing the physical properties of these structures, and it convincingly demonstrates the capacity for low-cost industrial production.

The main breakthrough was achieved by progressive longitudinal folding technique, in which, the material is pre-gathered in rolling direction, by a series of mating roller pairs corrugations flutes running tangentially around the rollers. The first pair initiates one central flute into the sheet material, and successive pairs add an additional flute on both sides of the previous material producing a succession of 3,5,7,... flutes. This totally eliminates the keyed in effect and the associated sheet material slitting phenomenon. A top view of progressive longitudinal folding technique is illustrated in Figure 5.

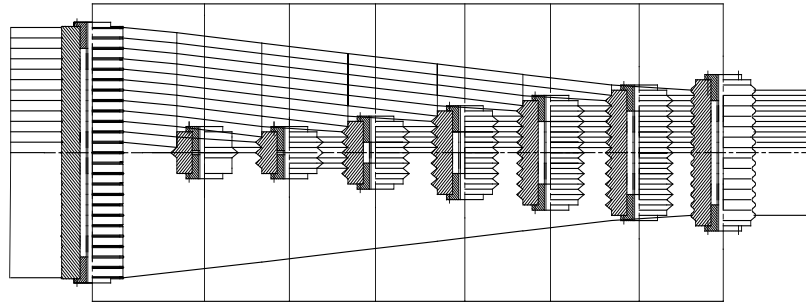


Figure 5. Progressive longitudinal folding

To enable the engagement depth of the roller pairs to be varied during machine operation, while preserving parallelism and synchronization of each pair and the entire successive pairs of rollers, three cross-helical gearboxes, linked by a vertical shaft, were used to drive each pair of rollers from the main horizontal drive shaft.

To produce the final pattern we engrave the pattern geometry on two sets of rollers which are driven by an identical mechanism, with the ability for the upper roller to be adjusted vertically while maintaining synchronicity and parallelism during machine operation. Figure 6 shows two views of the machine. Both of longitudinal folding rollers and the patterned rollers are driven separately by a permanent magnet DC geared motors fitted with 50:1 variable speed controller. Thus the rotation speed of the patterned roller pair is continuously variable and independent of the rotation speed of the pre-gathering rollers. These flexibilities of varying the engagement depths and the relative rates of the pre-gathered material to the patterned rollers are essential experimentation parameters on studying and optimizing the fold formation process in the transition area into the patterned rollers.

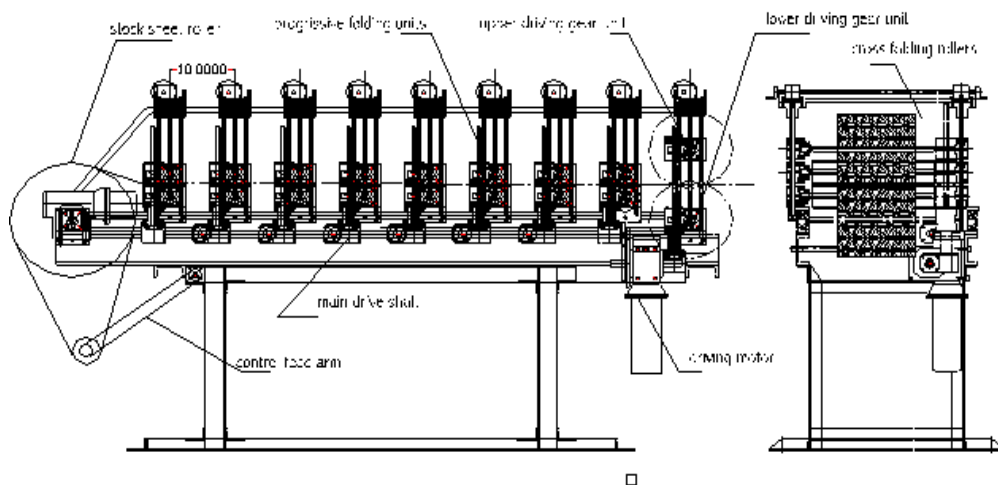


Figure 6. Side view of the continuous folding machine

Photographs of the machine sheet folding rolling sequence are shown in Figure 7. The machine successfully folds thin sheets of paper, copper, aluminum and stainless steel sheet material using this novel pre-folding technique. The rollers with engraved chevron pattern were machined using 4-axes CNC milling machine

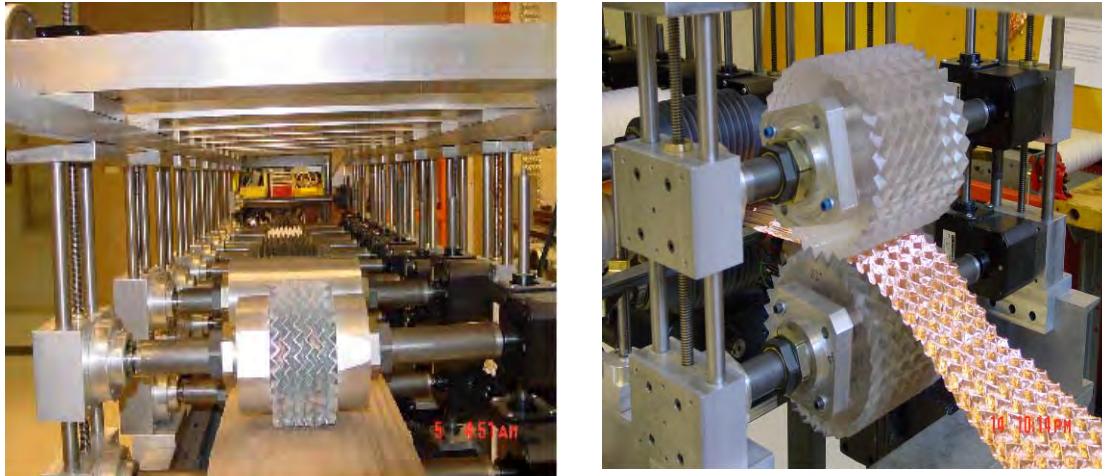


Figure 7. Photographs of the continuous sheet folding machine

3. Components of the Manufacturing Process

We now describe the details of the prototype machine and the three main components that have been developed and implemented in this project, they are: (1) The process of designing a cushioning system (2) Mechanical design of the machine and (3) Computer control and automation of the process.

3.1 The Process of Designing a Cushioning System

In order to determine the type of cushion (paper weight) and cushion dimensions we begin by using the input provided by the user which includes the weight of the item to be dropped, altitude of aircraft or Above Ground Level (AGL) drop height, speed of aircraft and fragility of the item (measured as the maximum acceleration that the object can withstand after impact without causing damage to the object). These inputs are then substituted in the necessary energy equations and the minimum cushion thickness (based on choice of paper combinations and fold height) is then estimated. These energy equations are based on the aerodynamics of the subpack (container) when it is released from the aircraft. The speed of the impact is calculated for different drop item weights, aircraft altitude and speed as shown in Appendix 1. Based on this Appendix we calculate the dimensions of the cushioning system for the items to be dropped as shown in Appendix 2. Further analysis that investigates the behavior of the subpack after drop in terms of interactions between the “cargo” of the subpack and the cushioning system and the effect of multiple impacts due to the rolling of the subpack after drop is shown in Appendix 3.

The energy equations and the results of the extensive experiments for different paper combinations and fold size are then used in a software developed for the calculations of the cushioning system dimensions and recommendation of paper combination as described below.

3.2 Cushion Design and Manufacturing

3.2.1 Introduction

This section describes and documents the design and manufacturing database. The database holds all the information about materials, designs, and the production parameters. When you design a cushion, the design program uses the database to retrieve information about material properties and previous items that have already been designed. When the user saves a design, it is also stored in the database. The information in the database is also used in the production process. At the beginning of the production of a cushion, users are asked to retrieve the correct production parameters from the database.

This section explains the structure of the database and how the information is stored and retrieved in each stage of the Airdrop delivery system. The first part of this report presents the data model. Then the use of the database is explained in relation to each process of the airdrop delivery system: designing, roller setting for folding machine, and production.

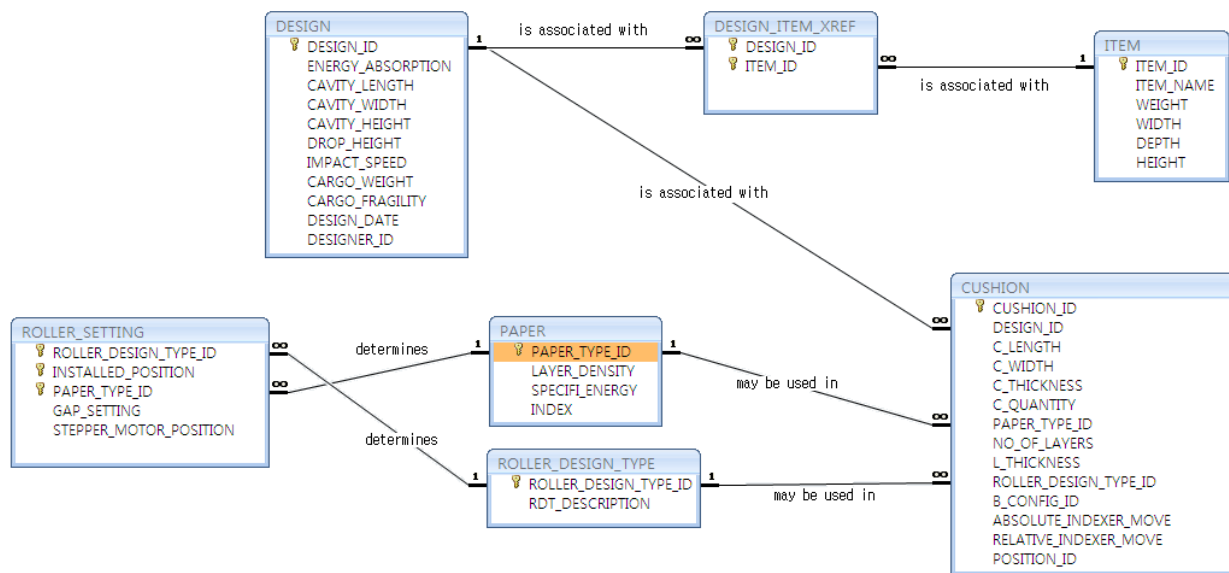


Figure 8. Data model

3.2.2 The data model

Figure 8 shows the data model, in which all the tables and their relationships are shown. The PAPER table and ITEM table hold some pre-stored information about the paper properties and dropping item. Users can add or delete an item in the ITEM table using the cushion design software. Users can add a paper type manually into the database, if desired. The ROLLER_SETTING table stores information about the setting of the rollers in the folding machine. The setting is determined by the paper type and the roller design type and may differ from position to position. The setting information is highly dependent upon the machine itself and also on the paper, and it requires on site manual calibration. The rest of the tables are filled with information that is generated from the cushion design software.

3.2.3 Use of database

1) Cushion design software and the database

The database is updated and retrieved automatically and users do not need to access the database manually in a normal operating condition. In this section, we will explain how the database is accessed and what information is transferred between each process of the airdrop delivery system and the database.

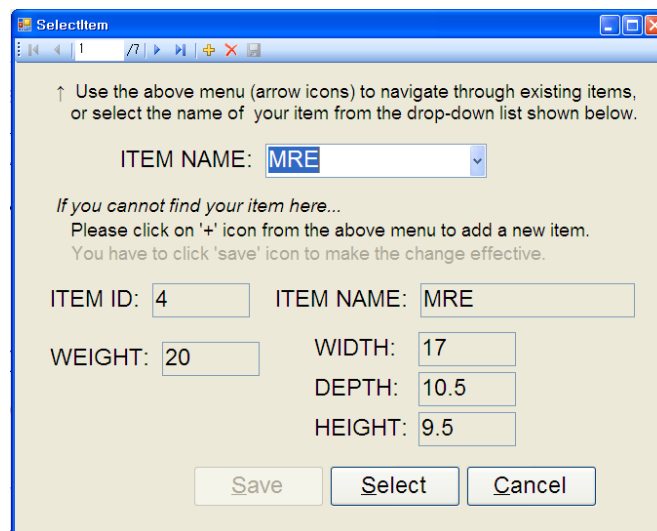


Figure 9. Item selection dialog

Figure 9 shows the item selection Dialog. On this dialog, readily available items are retrieved from the ITEM table and users can choose one from the list or add/delete an item in the database. Figure 10 shows a sample ITEM table in the database.

ITEM						
	ITEM_ID	ITEM_NAM	WEIGHT	WIDTH	DEPTH	HEIGHT
+	1	MRE	20	17	10.5	9.5
+	2	AMMO	33	12	7	6
+	3	Water bottles	40	15.5	10	8.5
+	4	Poland Sprin	40	15.5	10	8.5
+	5	Smart Water	40	16.5	11	9.25
+	6	Emergency D	33	19	11.5	6.125
+	7	DEX	19	17.5	12	7.5

Figure 10. Item table

When users design a cushion, the cushion uses a particular paper type whose material properties are given in the database. The design software calculates the amount of energy that can be absorbed using the material properties retrieved from the database (PAPER table).

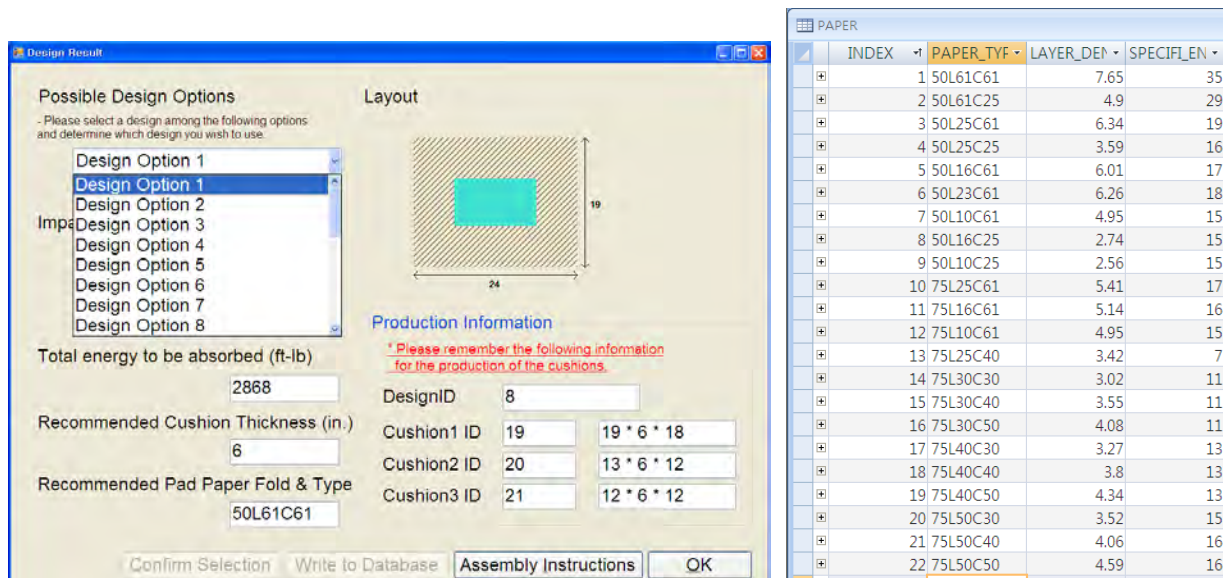


Figure 11. Design result dialog and PAPER table

Figure 11 shows a design result dialog. Users can see the possible design options in the dropdown list, which use different paper fold and type. The paper fold & type, the total energy to be absorbed by the design, and the resulting cushion thickness are shown. The results are based on the information from the paper properties given in the PAPER table.

When users select a design and save it to the database, a design ID and three cushion IDs that are associated with it are assigned. Those new design results can be found in the DESIGN and CUSHION tables (Figure 12).

DESIGN_ID	ENERGY_A	CAVITY_LEI	CAVITY_WI	CAVITY_HE	DROP_HEI	IMPACT_SF	CARGO_W	CARGO_FR	DESIGN_D	DESIGNER
1	15190.3854	20	12	8	85		90	200	2009-07-02	1
2	6150.5556	20	12	8	50		80	200	2009-07-02	14
3	5844.9012	15	10	8	50		126	80	2009-11-16	26
4	4373.2708	16	11	9	56		84	300	2009-11-16	14
5	5458.8517	19	11	6	56		105	110	2009-11-16	1

CUSHION	DESIGN_ID	C_LENGTH	C_WIDTH	C_THICKNE	C_QUAN	PAPER_TYF	NO_OF_LA	L_THICKI	ROLLER_DI	B_CC	ABSOLU	RELATIVE_J	POSITION
1	1	32	6	20	2	50L61C61	20	1.1			5000	2500	1
2	1	26	6	12	2	50L61C61	12	1.1			5000	2500	2
3	1	14	6	12	2	50L61C61	12	1.1			5000	2500	3
4	2	28	4	16	2	50L25C61	16	1.2			5000	2500	1
5	2	24	4	12	2	50L25C61	12	1.2			5000	2500	2
6	2	12	4	12	2	50L25C61	12	1.2			5000	2500	3

Figure 12. DESIGN and CUSHION tables

DESIGN_ITEM_XREF table is also filled in by the design software, ROLLER_DESIGN_TYPE_ID and ROLLER_SETTING tables can be filled in when the design is fixed because the paper fold & type determines the information for those tables.

2) Roller setting and the database

Once a cushion is designed, it is time to produce the cushion. According to the paper fold & type, the rollers in the folding machine must be set properly. Now, we need to position the rollers to have appropriate gaps between the upper and lower rollers. This can be done from the Graphical User

Interface (GUI) of the bridge setting software, which is shown below in Figure 13. The program for bridge setting is shown in Appendix 4.

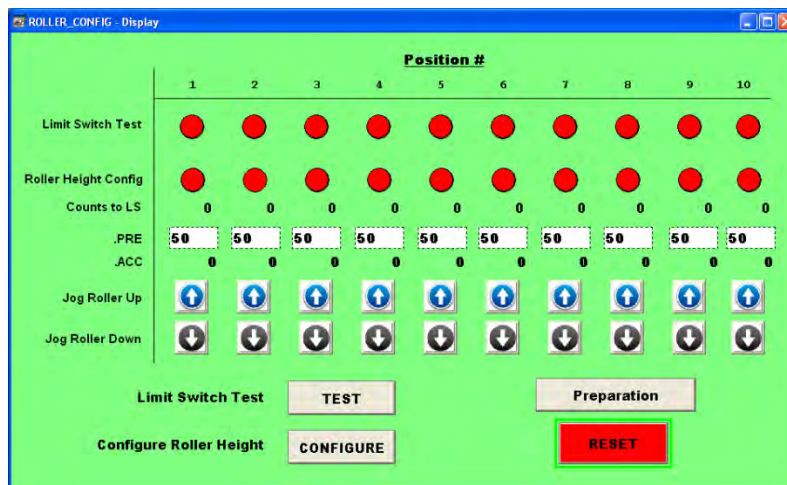


Figure 13. GUI for roller setting

When users click Preparation button, the Visual Basic for Applications (VBA) code running background downloads the roller setting data to the PLC. The values to be written are the number of clicks of stepper motors from the limit switch position to the appropriate position of the rollers. Once downloaded, they appear in the textboxes labeled as .PRE. The RSVIEW32®¹ software provides VBA data model, which enables us to write a VBA program to change the values of Tag database that is used in RSVIEW32 software. For the VBA code listing, see appendix I of this technical report.

3) Production and the database

Now that we have set our rollers, we are ready to produce the cushion. We need to download some more parameters for the production such as dimension of the cushion, number of layers, number of cushions, etc. This can be done from the subpack GUI shown in Figure 14a) and b).



Figure 14. a) Cushion ID lookup b) Operator screen

Figure 14a) shows the cushion ID lookup screen. When users enter a design ID and click the Look up Cushion IDs button, VBA code retrieves the cushion IDs from the database. Users can choose a cushion from the list, and then on the next screen, they can download the data by clicking the

¹ RSVIEW32 is automation software of Rockwell Software.

Download Data button. All the information about the cushion is downloaded to the PLC, including the location of sensors that are used to detect correct length and position of a layer in the machine. The VBA code for these actions is listed in Appendix 5 of this report.

A software program was developed for the design of the cushion system for an item after its dimensions, weight, item fragility in acceleration and speed and altitude of the aircraft. The software is included in the attached CD and its name is Airdrop. It is an executable file that can be easily installed and run.

3.3 Manual access to the database

For manual access to the database, user needs Microsoft Access 2003² or higher. The database is copied to the user's computer when the design software is installed. The user needs to enable hidden files from the explorer to see the database file.

4. Mechanical Design and Construction of the Folding Machine

4.1 Introduction

A preliminary schematic design of the folding machine is shown in Figure 15.

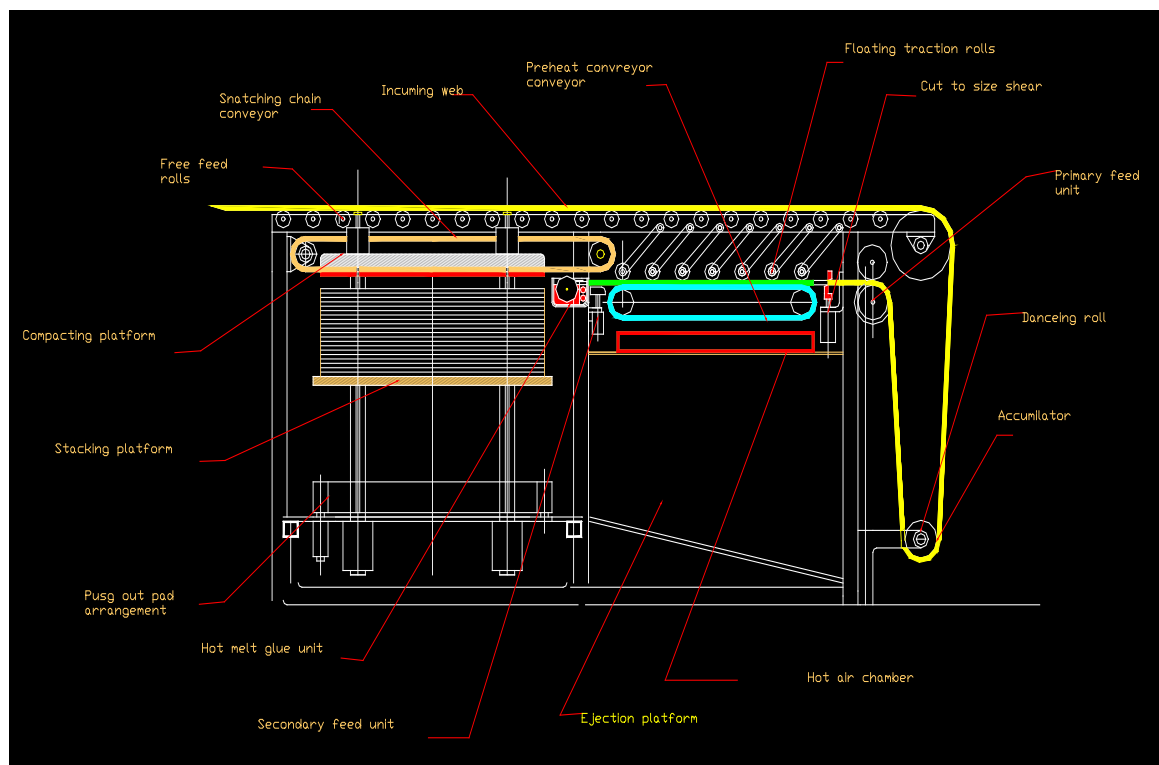


Figure 15. Schematic diagram of the folding machine

² Access is a database of Microsoft.

4.2 Machine basic operations

The design of the machine requires the following six main operations that need to be flexible to allow construction of pads with different dimensions and material:

1. Feeding of the paper (roll of paper)
2. Cutting (cutting the pad according to the desired length of the cushioning system)
3. Transporting (transporting the pad after cutting)
4. Gluing (applying glue to the bottom of pad)
5. Positioning/ Pressing (stacking the pads in order to produce the cushion with the desired thickness or number of layers of pads)
6. Ejection (Eject the completed cushion out of the system upon completion).

These tasks are synchronized using a fully automated computer control system as described later in this report.

4.3 Main design units

The machine design includes the design of individual units which are then assembled to make the final assembly of the machine. These units are listed below and their design details are given in Appendix 6.

- 1) The Machine Frame
- 2) The laminate hot melt glue unit
- 3) The laminating conveyor
- 4) The Web takeoff conveyor
- 5) The Web deflector
- 6) The web feed in rollers
- 7) The slab cutting unit
- 8) The slab holding unit
- 9) The slab measure to length/ positioning unit
- 10) The shuttle unit
- 11) The slab pick and place unit
- 12) The slab hot melt glue unit
- 13) The slab stacking unit
- 14) The pad labeling unit

- 15) The Pad Ejection Unit
- 16) The build in fork lift for loading the laminate feed roll stock
- 17) Construction an installation of built-in forklift for loading the core rolls
- 18) Design and construction of the Sensor Deploying Unit for Slab Cut/pickup
- 19) The pneumatic operating circuit
- 20) The signal/power interface circuit
- 21) The PLC control box
- 22) The Parker 6K8 control box

5. Computer Control of the Folding Machine

Full automatic control of the machine is achieved in every stage of the production process. It begins with the cushion design software which determines the type of paper to be used and the dimensions of the cushion and fold type in order to protect the subpack content. The information is then down loaded to the machine controllers. There are three major control actions: 1) The first control action involves the adjustments of the folding rollers and the distances between them to ensure proper fold. This is referred to as **bridge setting** since every set of folding rollers shown in Figure 16 constitute a bridge. 2) The second control action is the **positioning of the sensors** to meet the dimensions of the pad in order to prepare it for cutting. 3) The third control action involves the control of the entire **cushioning system** (synchronization of all necessary actions to produce the pad) and 4) The **supervisor controller (performed by 6K Controller)** which initiate all control actions mentioned above. We now present these three major control actions.

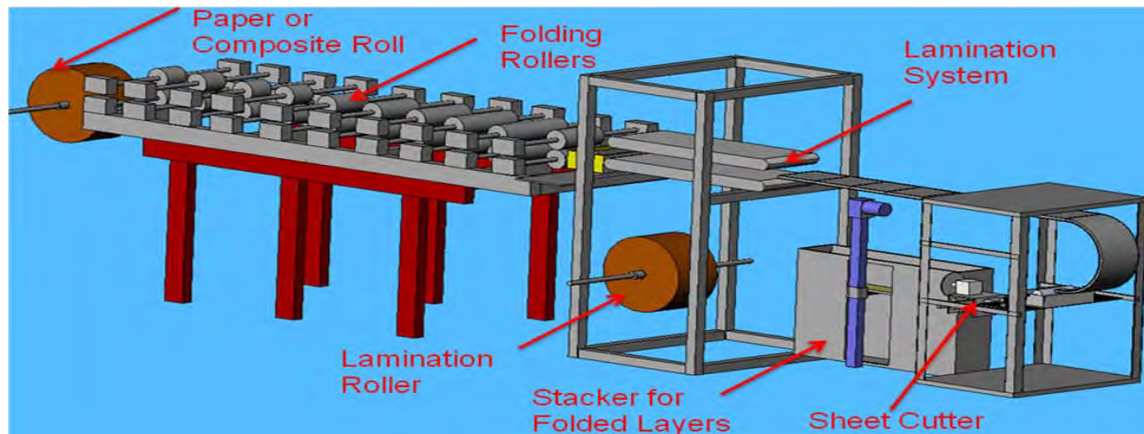


Figure 16. Schematic of the fully automated prototype folding machine

5.1 Bridge Setting

This working paper documents the control program logic and code for setting bridge heights on the folding machine. There are nine bridges the height of which is set in accordance with the paper type

that is being used to form the cushion layers. Each bridge height is independently set using stepper motors. The control sequence sets each motor position sequentially such that each roller has a proper gap with its opposing roller. This roller positioning is a one time setup that takes place at the beginning of a production run. Once set, the roller positions do not change during the production run. The roller position will change only when the paper type is changed or a new set of rollers are introduced.

A roller setting consists of moving the roller upward to find a home position limit switch and then moving the roller down a predefined distance to close the gap to the desired size. The actuator is a stepper motor. Closing the gap amounts to moving the stepper motor a predefined number of steps.

The control program has three parts. In the first part a test is run on the home position limit switches. Limit switches are wired as normally closed contacts because the predominant mode for a limit switch failure is as an open circuit. The program first tests that each limit switch reading is true, or closed. If a switch is false, or open, it has either failed or the bridge is at the limiting position. In that case, the stepper for that position is backed away from the limit switch by one turn of the motor. If the switch continues to indicate it is open, the operator is notified and must investigate the wiring. No further action is allowed. When the wiring problem is corrected, the operator can rerun the first part of the program. A successful run of the first part of the program will set a bit in controller memory that allows the bridge gaps to be set.

The second part of the control program is allowed to run when all limit switches have past initial testing. Here the bridges are first homed and, following that, they are moved to the nominal gap position. Indicator lamps on the operator panel will be lighted to show the operator that all positions are set.

The third part of the program is for jogging the rollers. Although the nominal roller setting is considered correct for a specific paper type, differences in manufacture as between lots of the same paper type may require slight adjustments of the roller. The jog buttons are available to the operator to make minor adjustments to the settings.

These three parts and detailed description of the bridge settings are given in Appendix 7.

5.2 Sensor Positioning Mechanism

An important component of the cushion fabrication subsystem is the sensor positioning mechanism that measures the length of pads that are to be cut, consistent with the design of the cushion that is assembled by gluing pads together. A two-sensor mechanism is implemented as shown in the drawing of Figure 17. Before material is fed into the gluing subsystem (from the right of Figure 1), sensor 1 has to be positioned to detect the material when it has reached the cushion design length. At that point the material is cut at the infeed rollers by a knife under program control. The material is then transported along a conveyor until it reaches sensor 2, which is used to signal the control program that the material has reached the pickup point. From there it is picked up by a linear transport pick up arm and taken to the gluing and stacking operation to become part of the cushion.

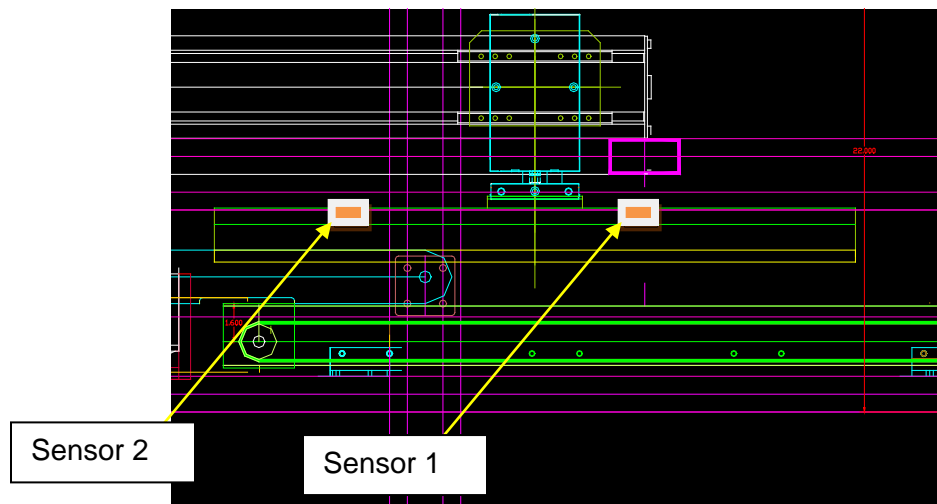


Figure 17. Sensors for length of cut and stopping point for pick up

This technical report documents the control program for the proper positioning of the sensors. The control program receives information on the length of the pad from the design program since the appropriate length of the cushion is defined at design time. The sensors are positioned by a set of lead screws that move them laterally along the conveyor. The lead screw for sensor 1 is driven by a stepper motor and the lead screw for sensor 2 is driven off the sensor 1 lead screw through a gear box having a 1:2 gear ratio. When sensor 1 is correctly positioned for the length of cut, sensor 2 will be automatically correctly positioned for the pick up of a pad of the designed length.

The lead screw pitch for sensor 1 is six revolutions per inch and the stepper motor resolution is 200 steps per revolution. Hence, 1200 steps are commanded from the control program for every inch of travel.

The stepper motor is driven from a PLC by the Allen Bradley 1746-HSTP1 stepper control module. In Section 2.0 we will describe the files that are used to command this module to control the stepper motor. Section 3 explains the program logic used to run the stepper control module. Section 4 contains the PLC ladder logic code for the sensor positioning program.

Detailed description of the sensor positioning mechanism is explained in Appendix 8.

5.3 Supervisor Controller

This technical report documents the 6K control program. A 6K controller is used to control the speeds of the first ten rollers on the folding machine and of the upper conveyor belts on the sub-pack system, so that they can be appropriately adjusted according to the speed of master folding roller, which is also controlled by the 6K controller. The control program described in this report is

written for the 6K controller, so that we can achieve desired responses from the motors which run the rollers.

The master folding roller DC motor is connected to axis 8 on the controller. The rest of the rollers on the folding machine are run by the other DC motor (axis 7 on the controller), and the sub-pack system upper conveyor belts are run by two servo motors (axes 5 and 6.) The program regulates the speed of the master motor and also adjusts the speed of other motors according to a programmed ratio of the speed of the master motor. The program also displays relevant information on a user interface, the RP-240 panel, and a user can manually override the control using this panel.

Details of this controller are shown in Appendix 9.

6.1 Patents by the Investigators

1. Basily, B. B., Elsayed, E. A. and Kling, D., 2004, Technology for Continuous Folding of Sheet Materials, Patent 7,115,089, October 3, 2006.
2. Basily, B. B., Elsayed, E. A. and Kling, D., 2004, Technology for Continuous Folding of Sheet Materials : Additional Claims, Patent Application, April 2006
3. Basily, B. B. and Elsayed, E. A., 2006, Technology for Continuous Folding of Sheet Materials into a Honeycomb-Like Configuration, Patent Application, Case 03-101US3

Appendix 1 - Aerodynamics of the Container

May 17, 2011

1 Introduction

This appendix describes the aerodynamics of a container that is dropped from a moving or stationary air vehicle and is allowed to drop freely, without a parachute or other device attached to it. We use standard methods of approximating the aerodynamic forces by means of a drag coefficient. We look at how much the aerodynamics forces affect the velocities during free fall, the time the container stays in the air, the distance traveled by the container before impact and drift of the container due to crosswinds.

During free fall, three forces act on the container, gravity, wind forces, and aerodynamic drag due to the relative wind speed. We analyze the effects of these forces and develop means of determining the speed of the container before impact, the amount of time the container travels in the air, and the amount of sideways drift in the presence of cross winds.

We begin with simple models and gradually make the models more sophisticated. Appendixes 2 and 3 will deal with the cushion model that is used when designing the container, and with the dynamics of the impact and subsequent tumbling, respectively.

2 Aerodynamics of Free Fall and Drag Force

We first consider the case of no wind forces acting on the container and consider vertical motion only, as in when the container is dropped from a crane or from a hovering aircraft. The forces affecting the box during its free fall are gravity and aerodynamic drag due to the motion of the container in an airstream, as shown in Fig. 1.

Considering the drop heights that are anticipated (50-100 ft), the time the container spends in the air will be around 2.5 seconds. It is difficult to develop a complete aerodynamic model of the box during free fall, as the airflow around the box does not reach steady-state during the very short time the box is in the air and a transient analysis has to be used. However, observations from drop tests indicate little transient behavior. The airflow causes very little rotational motion. Also,

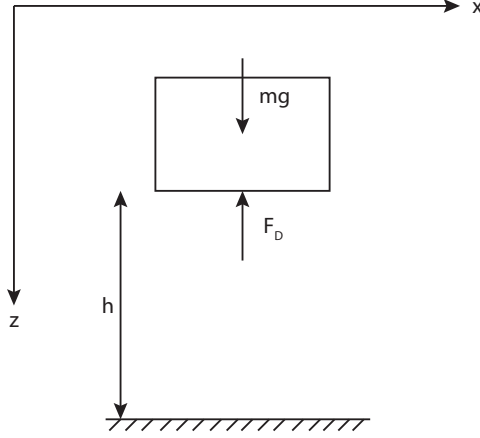


Figure 1: Free Body Diagram of One-Dimensional Motion

the actual drop height in a hostile environment will not be exactly the drop height that the boxes are designed for. Hence, one can reasonably justify the use of a simple aerodynamic model of the box during free fall.

We will neglect the angular velocity of the box during free fall. We have observed from actual drop tests (both from a crane and from a moving helicopter) that the angular velocity of the box remains almost constant during free fall. While one would expect for a longer flight that the box would align itself in a position that minimizes the drag force, there is little observed evidence from experimental data that this is happening during the short period of time that free fall takes place.

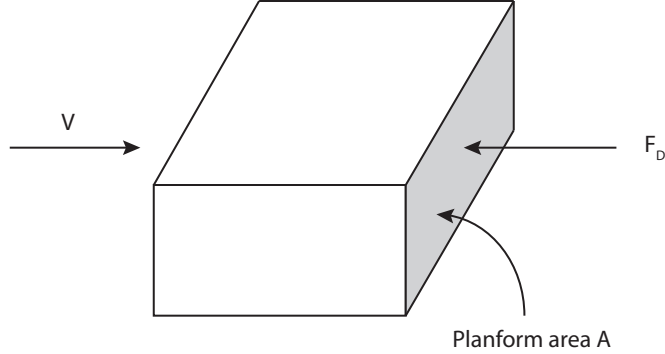


Figure 2: Body in an Airflow

We next discuss the force due to aerodynamic drag. Consider a body moving along a straight line in an airflow, such as the box of interest, as shown in Fig. 2. We can view this problem as the body is moving with speed v and the air is still, or the body is stationary and air is moving over the body with speed v . Assuming that the airflow far away from the body is uniform (known as *free stream velocity*), the streamlines, or the loci of points in the airflow, change direction as the airflow approaches the body, as shown in Fig. 3. This change is due to the resistance of the body to the airflow and creates the *aerodynamic drag force*. The aerodynamic drag force can be expressed

as

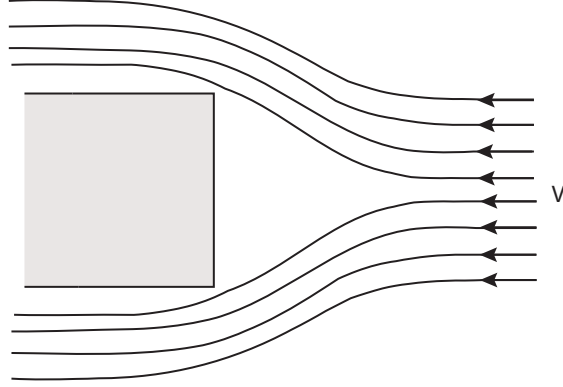


Figure 3: Streamlines over Body

$$F_D = \frac{1}{2} \rho C_D A v^2 \quad (1)$$

where ρ is the density of air, which we assume remains constant during free fall, v is the speed of

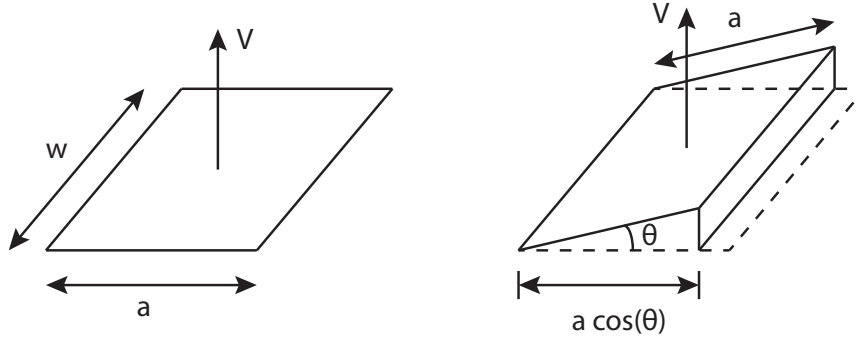


Figure 4: Planform Area

the box (or the free stream velocity), and A is the planform area, that is, the area of the surface of the box in contact with the air. For example, if a rectangular plate of dimensions a and w is moving such that its velocity is perpendicular to the plate, the planform area is $A = wa$, as shown in Fig. 4a. On the other hand, if the plate makes an angle θ with the horizontal, as defined by the orientation of the plate in Fig. 4a and as shown in Fig. 4b, the planform area is $A = wa \cos \theta$.

The dimensionless parameter C_D is the *drag coefficient*, and it indicates the amount of air resistance that opposes the flow. Its value depends on the shape of the object. In general, aerodynamic drag is not desired. In vehicles like airplanes and cars the drag force opposes the thrust and results in wasted energy. Airplanes and cars are designed so that their drag coefficient is as small as possible. In our case, however, the drag force is welcome, as drag reduces the impact velocity of the container. The drag coefficient of a blunt shaped object, such as the container considered here, is large, usually around $C_D \approx 1$.

For a flat surface, such as the one shown in Fig. 5a (side view shown), the drag coefficient is estimated as $C_D \approx 1$, and for a wedge shape, as shown in Fig. 5b $C_D \approx 0.8$.

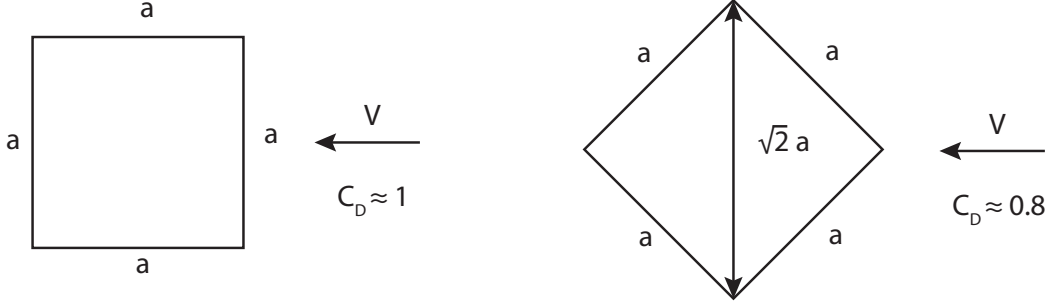


Figure 5: Drag Coefficients for Blunt Shapes (side view shown). a) Flat Plate, b) Wedge.

Consider the object in Fig. 5 (side view). The box is square with sides a and its width is w . In Fig. 5a, the airflow is perpendicular to one of the sides, so the planform area is aw and drag coefficient is approximated as 1, so the quantity $C_D A = C_D aw \approx aw$. In Fig. 5b, the airflow is perpendicular to the hypotenuse, which is of length $\sqrt{2}a$ and the drag coefficient is 0.8, making the quantity $C_D A = 0.8\sqrt{2}aw \approx 1.13aw$. It follows that for any other orientation where one of the equal sides makes faces the airflow $C_D A$ will be between $1aw$ and $1.13aw$, so we can conservatively estimate it as $1aw$ for all of our simulations. This is what we will do in our approximate analysis.

The freedrop project has considered boxes of different but relatively similar dimensions and weight. One is a container designed to drop ammunition, with dimensions of $24 \times 21 \times 33$ in., and a weight of 120 lb, including the cargo. The other is a container designed to drop softer cargo, such as water bottles and MREs, with dimensions around $32 \times 25 \times 23$ in. and weighing around 100 lb. Because we have little control on the the way the box is dropped and which surface (or corner) of the box makes impact, we need to take an estimate of aw , which can vary from 3 and 6 square feet.

In all cases, we began with using a cushion thickness of 6 in. Considering the free body diagram of the box, shown in Fig. 1 and summing forces in the vertical direction, the equation of motion becomes

$$+ \downarrow m\dot{v} = mg - F_D = mg - \frac{1}{2}\rho C_D A v^2 \quad (2)$$

with the velocity v is taken as positive downwards.

3 Terminal Velocity and Velocity Right Before Impact

A very interesting property of objects falling down in an airfield is terminal velocity. In the absence of drag forces the equation of motion above becomes simpler, the acceleration is constant, $a = g$, and the speed of a falling object is obtained from the constant acceleration formula as

$$v^2 = 2ah = 2gh \quad \rightarrow \quad v = \sqrt{2gh} \quad (3)$$

in which h is the height from which the object is dropped. In the presence of air resistance the speed of the object slows down due to drag. If the object is dropped from a sufficient height a time comes where the drag force becomes equal to the force of gravity. The velocity of the object at that condition is called *terminal velocity* (v_T), which can be calculated by setting $\dot{v} = 0$ in the equation of motion. We obtain

$$F_D = F_g = \frac{1}{2}\rho C_D A v_T^2 = mg \quad \rightarrow \quad v_T = \sqrt{\frac{2mg}{\rho C_D A}} \quad (4)$$

For the box considered here, if we set $mg = 100$ lb, $C_D A = 5$ sq. ft. and the density of air as $\rho = 2.36 \times 10^{-3}$ slug/ft³, we arrive at the terminal velocity as

$$v_T = \sqrt{\frac{2mg}{\rho C_D A}} = \sqrt{\frac{200}{2.36 \times 10^{-3} \times 5}} = 130.2 \text{ ft/sec} \quad (5)$$

Figure 6 plots the terminal velocity as a function of the drag times area ($C_D A$).

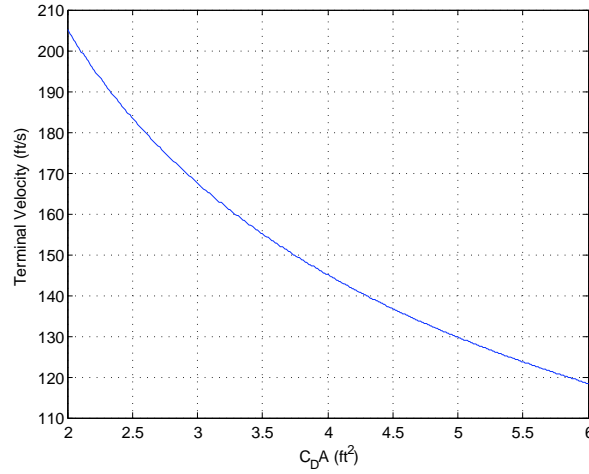


Figure 6: Terminal Velocity as a Function of Drag ($C_D A$)

To find the minimum height from which the box needs to be dropped so that it reaches terminal velocity just before impact we need to integrate the equation of motion. We also need to add the kinematic expression relating position to speed, $\dot{z} = v$, so that the two describing equations can be written as

$$\dot{z} = v \quad m\dot{v} + \frac{1}{2}\rho C_D A v^2 = mg \quad (6)$$

Using a numerical integration package and integrating the describing equations we can obtain the velocity before impact, which we denote by v_0 . Figure 7 plots the velocity before impact as a function of drop height for different values of $C_D A$. We see that the speed before impact comes to within 20% of terminal velocity after a height of 300 ft when $C_D A = 5$ ft². The general conclusion is that for the values of the drag, box dimensions and box weight of interest to us, once the box is dropped from an altitude of about 300 ft or higher the vertical velocity at impact is similar. Figure 8 plots the velocity before impact as a function of drop height and drag $C_D A$. The results of this figure can be generalized to any value of the drag.

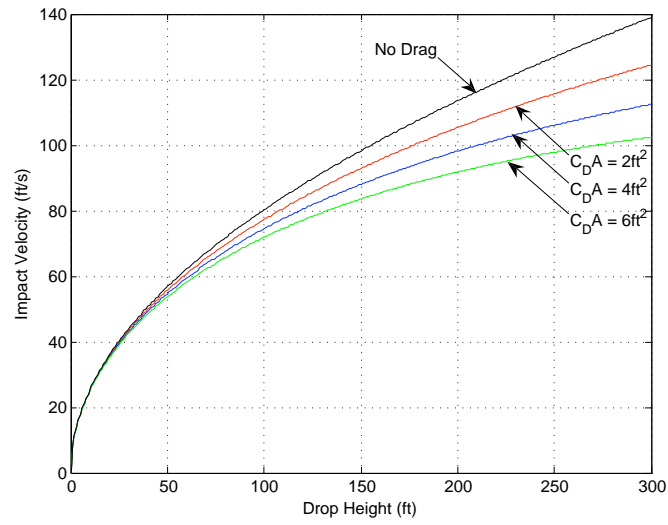


Figure 7: Impact Velocity v_0 as a Function of Drop Height

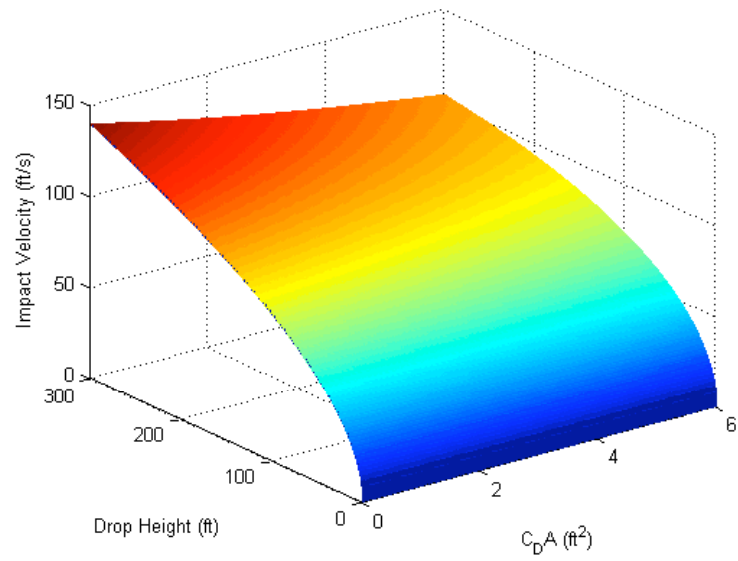


Figure 8: Impact Velocity v_0 as a Function of Drag ($C_D A$) and Drop Height

The drop height and impact velocity are denoted by h and v_0 , respectively. Because of aerodynamic effects, energy is lost during the fall and $mgh \neq \frac{1}{2}mv_0^2$. It is interesting to find the height the container would have to be dropped, so that it in the absence of aerodynamic drag the container would have the same kinetic energy $\frac{1}{2}mv_0^2$. Referring to this height as *effective height* and denoting it by h^* , we have

$$mgh^* = \frac{1}{2}mv_0^2 \quad (7)$$

so that the equivalent height has the form

$$h^* = \frac{1}{2} \frac{v_0^2}{g} \quad (8)$$

Table 1 shows the time to impact, vertical velocity before impact and effective height, for the case when the planform area is $A = 5$ sq. ft. and for different values of the drag coefficient. As before, the box is dropped from an altitude of 100 ft. We see that changes in the drag coefficient do not produce large changes in the time to impact but they affect the final velocity.

C_D	Time to Impact (sec)	Velocity before Impact (ft/sec)	Effective Height (ft)
0	2.49	80.2	100
0.8	2.56	74.5	86.1
1.0	2.57	73.1	83.1
1.2	2.59	71.9	80.2

Table 1: Time to Impact and Velocity Before Impact. $A = 5 \text{ ft}^2$, $h = 100 \text{ ft}$

It should be reiterated that the analysis here is based on a very simple model of having a constant drag coefficient and that the drag coefficient is sufficient to capture all the effects of aerodynamic drag and that the product of the drag coefficient and planform area do not change as the box falls down.

4 Effect of Drag When Horizontal Speed is Involved

When both horizontal and vertical speeds are involved, as is the case when the box is dropped from a moving airplane or helicopter, the aerodynamics becomes more complicated. This is because the vertical speed changes as the box drops, which results in a change in the direction of the resultant velocity and hence of the planform area. In addition, we need to be more concerned about the rotational moment caused by the drag force.

We will use the same assumption as in the previous subsection about modeling drag and the planform area. We will continue to assume that the product of the drag coefficient and planform area remains the same, $C_D A = \text{const}$, as the resultant velocity changes. Figure 9 shows the free

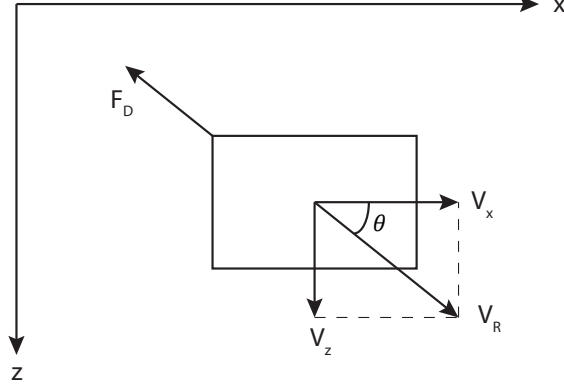


Figure 9: Free Body Diagram of Box.

body diagram of the box. We again use a particle model for the box, neglecting any rotational motion.

We write the velocity of the container as $\mathbf{v} = v_x \mathbf{i} + v_z \mathbf{k}$, so that in our simulations v_x and v_z are always positive. The force balances in the horizontal and vertical directions are

$$ma_x = m\dot{v}_x = m\ddot{x} = -F_D \cos \theta \quad ma_z = m\dot{v}_z = m\ddot{y} = -mg - F_D \sin \theta \quad (9)$$

where $F_D = \frac{1}{2}\rho C_D A v_R^2$ is the drag force and $v_R = \sqrt{v_x^2 + v_z^2}$ is the resultant velocity of the box. The angle θ shows the orientation of the resultant velocity, with

$$\tan \theta = \left| \frac{v_z}{v_x} \right| \quad (10)$$

so that

$$\cos \theta = \frac{v_x}{v_R} = \frac{v_x}{\sqrt{v_x^2 + v_z^2}} \quad \sin \theta = \frac{v_z}{v_R} = \frac{v_z}{\sqrt{v_x^2 + v_z^2}} \quad (11)$$

Substituting the above into the equations of motion we obtain

$$m\dot{v}_x + \frac{1}{2}\rho A C_D v_x \sqrt{v_x^2 + v_z^2} = 0 \quad m\dot{v}_z + \frac{1}{2}\rho A C_D v_z \sqrt{v_x^2 + v_z^2} = mg \quad (12)$$

The above equations can be integrated numerically to obtain plots of the velocity of the box before impact. Figure 10 plots the horizontal and vertical velocities vs. time, for different values of $C_D A$. The initial horizontal velocity is taken as 100 ft/sec. We see that, as expected, the vertical velocity reaches terminal velocity and the horizontal velocity eventually becomes zero. Of course, for this to happen the box needs to be dropped from a very large height (over 1500 ft) so it will remain in the air for over 10 seconds.

For the time of flight of interest to us, which is at around 2.5 seconds, we see that the horizontal velocity roughly becomes half its initial value. This may seem counterintuitive, but note that the drag force is dependent on the resultant velocity. From the equation of motion above, the drag force in the horizontal direction is greater than the drag force that would be present in the absence of horizontal velocity ($v_x^2 < v_x \sqrt{v_x^2 + v_z^2}$) and the same is true for the drag force in the vertical direction ($v_z^2 < v_z \sqrt{v_x^2 + v_z^2}$). As a result, the box slows down more rapidly.

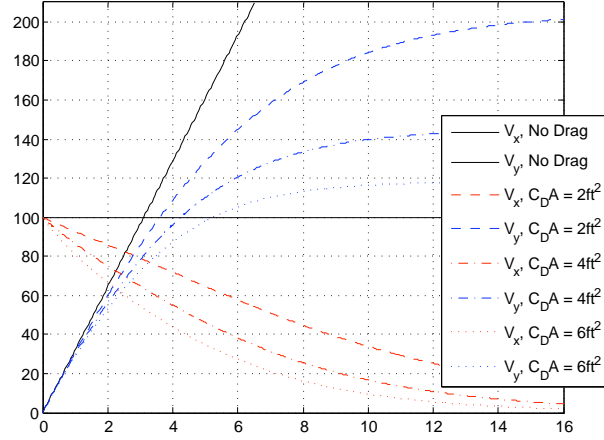


Figure 10: Vertical and Horizontal Velocity as a Function of Time.

5 Distance Traveled in Air

When a container is dropped from a moving vehicle, the container moves horizontally as it falls. It is of interest to calculate how much the container travels in the horizontal direction before it makes impact with the ground. In military drop zones that are small, the distance the cargo travels in the horizontal direction, as well as how much the cargo tumbles after it makes impact, can help the pilot to pinpoint where to drop the cargo. Appendix 3 will discuss tumble length. Figure 11 illustrates the process.

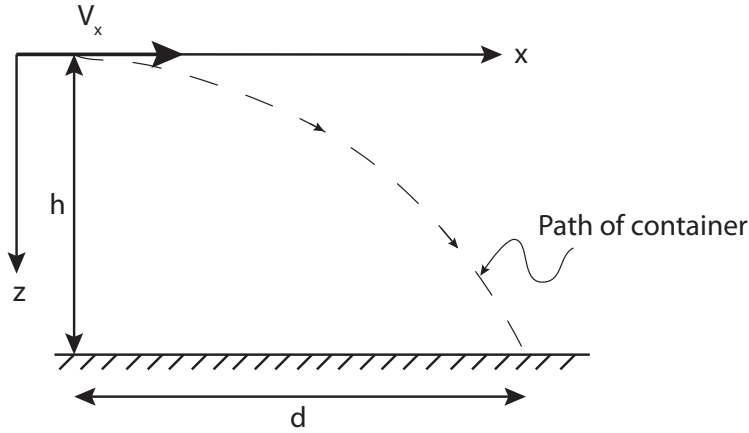


Figure 11: Drop Distance

To calculate the distance the cargo travels in the air, we take Eq.(12) and add to it the two kinematic equations that relate the distance to velocity in each direction

$$\dot{x} = v_x \quad \dot{z} = v_z \quad (13)$$

These four equations can then be integrated numerically to find the distance traveled. We performed

these integrations and found that the horizontal distance traveled was almost linearly proportional to the horizontal velocity. This is expected, as the horizontal distance, in the absence of aerodynamics, should be $x = v_x t$ and the time t depends on the drop height. Because of the large number of variables (horizontal speed, drop height, box dimensions) we are not providing plots. Rather, based on interpolation of the numerical solutions, we developed empirical relationships for the container of dimensions $32 \times 25 \times 23$ in. and weight 100 lb.

Drop Height	Horizontal Distance Traveled (ft)
50 ft	$130 + 1.4(v_x - 80)$
65 ft	$148 + 1.6(v_x - 80)$

Table 2: Empirical Relations for Horizontal Travel Distance (v_x in ft/sec)

For example, a container dropped from a height of 65 ft and with a speed of 100 ft/sec will travel 180 ft in the air before it makes contact with the ground.

6 Three-Dimensional Motion and Drift due to Cross-wind

The models we have used so far have been two-dimensional, dealing with motion in the direction of the horizontal velocity and vertical height. This model is adequate in the absence of cross-winds, as nothing happens in the sideways direction. However, in the presence of cross-winds we need to consider three-dimensional motion. In addition, if we are going to consider cross-winds, we should also consider head and tailwinds.

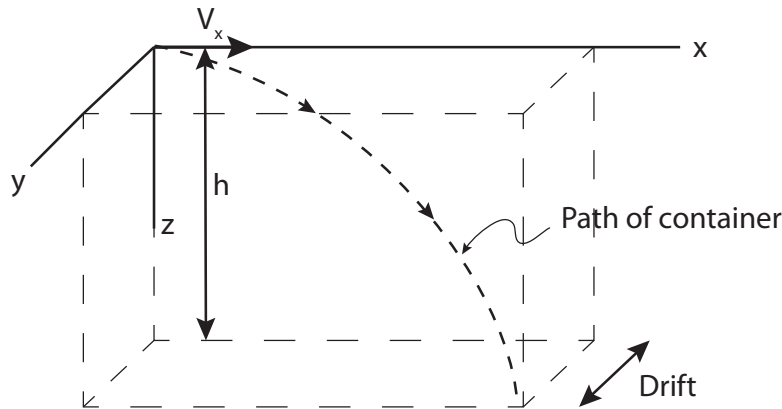


Figure 12: Drop Distance with Drift

Figure 12 describes the geometry. We select the x direction as the direction of the vehicle releasing the container, the z direction is the vertical, and y is the side or drift direction. v_x , the horizontal speed of the container, and v_z , the vertical speed are as always positive. We define by $\mathbf{V} = V_x \mathbf{i} + V_y \mathbf{j} + V_z \mathbf{k}$ the wind velocity at the location where the container is dropped. According

to our notation, because the horizontal velocity of the container is always positive, a positive V_x is a tailwind, which reduces drag, and a negative V_x is a headwind, which increases drag. V_y is the crosswind, which causes the sideways drift, so that the container has a displacement in the y direction, and V_z is a vertical gust. It follows that the relative velocity that the cargo has with respect to the air is

$$\mathbf{v}_{rel} = \mathbf{v} - \mathbf{V} = (v_x - V_x)\mathbf{i} + (v_y - V_y)\mathbf{j} + (v_z - V_z)\mathbf{k} \quad (14)$$

and the aerodynamic forces are dependent on the relative velocity. We can write the drag force as

$$F_D = \frac{1}{2}\rho C_D A v_{rel}^2 \quad (15)$$

where

$$v_{rel} = \sqrt{(v_x - V_x)^2 + (v_y - V_y)^2 + (v_z - V_z)^2} \quad (16)$$

is the the magnitude of the relative velocity, or the *relative speed*. Note that the above equation continues using the assumption that the quantity $C_D A$, which is the product of planform area of the container and drag coefficient, remains the same, regardless of the orientation of the container.

Based on previous developments, we can now write the aerodynamic equations in three dimensions and in the presence of wind speed as

$$m\dot{v}_x + \frac{1}{2}\rho A C_D (v_x - V_x) v_{rel} = 0 \quad (17)$$

$$m\dot{v}_y + \frac{1}{2}\rho A C_D (v_y - V_y) v_{rel} = 0 \quad (18)$$

$$m\dot{v}_z + \frac{1}{2}\rho A C_D (v_z - V_z) v_{rel} = mg \quad (19)$$

As can be seen, the three equations are nonlinear and coupled. We add to these equations the three first-order kinematic equations relating the distance traveled to the speed

$$\dot{x} = v_x \quad \dot{y} = v_y \quad \dot{z} = v_z \quad (20)$$

These six equations above are the describing equations of the container and they can be integrated to find the displacement and velocity of the cargo as it is dropped. The results for the sideways drift in the y direction are given in Tables 3-5 below, for a container of 100 lbs, dimensions $32 \times 25 \times 23$ in for different values of the wind gust V_y , with no headwind or vertical gusts ($V_x = V_z = 0$).

As expected, the drift amounts vary nonlinearly. For example, if we look at the amount of drift when there is no horizontal speed and a 65 ft drop (dropped from a hovering aircraft) the drift is 2.52 ft when the side wind is 13 knots. When wind speed is 26 knots (almost doubled) the same drop conditions result in a drift of 7.18 ft, almost three times the drift when $V_y = 13$ knots. We expect this result, because the aerodynamic force varies by square of the relative speed. By contrast, and also as expected, the magnitude of a horizontal speed affects the drift linearly.

The above results represent the worst possible case, that of a constant wind gust while the container is in the air. In general, wind gusts are not constant and they change direction. As a result, under more realistic circumstances, we can expect to have the drift to have smaller values.

Drop Height (ft)	Horizontal Speed (ft/sec)	Sideways Drift (ft)
50	0	1.85
65	0	2.52
50	84.4	5.01
65	84.4	6.47
50	118.1	6.53
65	118.1	8.40

Table 3: Drift Amounts due to a Wind Gust of $V_y = 13$ knots = 21.94 ft/sec

Drop Height (ft)	Horizontal Speed (ft/sec)	Sideways Drift (ft)
50	0	3.11
65	0	4.17
50	84.4	7.09
65	84.4	9.26
50	118.1	9.15
65	118.1	11.92

Table 4: Drift Amounts due to a Wind Gust of $V_y = 18$ knots = 30.38 ft/sec

Drop Height (ft)	Horizontal Speed (ft/sec)	Sideways Drift (ft)
50	0	5.41
65	0	7.18
50	84.4	10.22
65	84.4	13.29
50	118.1	13.00
65	118.1	19.91

Table 5: Drift Amounts due to a Wind Gust of $V_y = 25$ knots = 42.20 ft/sec

The sideways drift while the container is dropped should be compared with the drift of the container when it is dropped by parachute. Because cargo dropped by parachute stays longer in the air, drift is much larger.

Appendix 2 - Modeling of Containers, Cushions, and Cushion Stiffness

May 17, 2011

1 Introduction

This appendix describes the mathematical models and design criteria developed for the cushion pads that surround the cargo of the container used in free drop experiments. It is assumed that the container has both a horizontal and vertical velocity upon impact. The model takes into consideration the fact that impact can take place at any point on the container.

The freedrop method of aerial resupply or delivery encompasses the releasing of cargo payloads from an aircraft at a given altitude and allowing the payload to free-fall to the ground or drop zone (DZ) without any aerodynamic decelerator, such as a parachute. Since there is no parachute that stabilizes the orientation of the load so that it lands at a predictable angle and reduces its impact velocity with the DZ, the structural attributes or characteristics of the Freedrop Delivery System (FDS), or package, itself must insure that the supplies incur no damage and are in a condition that facilitates quick recovery and distribution to the receiving units and Soldiers. To be successful, this concept requires highly effective impact attenuation (cushioning) materials, which encapsulate the cargo to overcome the effects of tumbling that forward movement of the aircraft induces, and which absorb very high levels of impact energy.

The cushion that is modeled here takes into consideration one-dimensional impact. This modeling decision was taken in order to simplify the mathematical model and the design of the cushion, the type of the cushion and the thickness of the cushion.

2 Requirements on the Cushion

The container consists of the following parts:

- An outer box made of corrugated cardboard. The box holds the cargo to be dropped and the cushion pads. The box design consists of two components, a container and a lid that has

the same shape as the container, but fits right over it. This design ensures no glue is used to seal the box. In addition, after freedrop has occurred and the container has landed, persons receiving the container can open it and retrieve the cargo inside quickly. After the cushion pads and cargo are placed inside the box and the lid is placed over the container, the assembly is taped shut in order to prevent the lid and container from moving against each other and to provide more stiffness. Details about the container design are given in other parts of our report.

- **Cushion pads.** Six cushion pads are used to completely surround the cargo. There are three pairs of cushions of different sides. The manufacture and placement of the cushions in the container is demonstrated in the business case analysis. The cushion pads are not glued or attached to each other or to the container walls. Instead, they are cut to precise dimensions so that they are held tightly together. This tightness provide additional stiffness, as will be discussed later.
- **The cargo.** The type and thickness of the cushion pads, as well as the dimensions of the container, depends on the characteristics of the cargo. These features include the weight of the cargo, the stiffness and hardness.

When designing the cushion to absorb the energy of the payload and survive the drop undamaged, we need to consider the following issues:

- The cushion must be able to absorb the energy of impact. If the energy of impact is less than what the cushion can absorb, the cushion will not deform completely. On the other hand, if the energy of impact is higher than what the cushion can absorb, then the cushion will completely deform and will reach its *solid height*, after which it will behave like a very strong spring. This will cause the container to bounce back.
- The cushion must be thick enough to reduce the speed of the cargo in a way so that maximum acceleration levels, also known as fragility, are not exceeded. On the other hand, the cushion cannot be prohibitively thick, as this would make a very large container that would take up too much space. Such a container will not be easily navigated in and out of the aircraft, as well as by the troops on the ground receiving them.
- The cushion needs to be soft enough so that the cargo can crush it through it once the cargo makes contact with the cushion. If the cushion is too rigid with respect to the cargo, then it may not deform during impact, in which case the cargo absorbs the energy of impact and gets damaged. This issue is especially important when dealing with cargo that is not rigid, such as water bottles and ammunition cans.

The above requirements are competing requirements and have different levels of importance for different types of cargo. For example, hard cargo, such as ammunition cans, are heavy and they need a strong cushion to absorb all the energy. Cushion pads designed for ammunition cannot be used for softer, more flexible cargo, such as water bottles and MREs, as the cushion would be very stiff with respect to the cargo and it would not deform or absorb any impact energy.

3 Assumptions for Cushion Analysis

In this section, we discuss the energy absorbed by a cushion as a cargo that is dropped from a height and protected by a cushion.

We will begin with a simple model and gradually increase the model complexity and consider other cases. We make the following initial assumptions about the cargo and the cushion:

- The cargo is rigid. An example to this is an ammunition can, which does not deform too much when dropped from a height.
- We know the maximum acceleration level that the cargo can withstand, before damage occurs to the cargo. This maximum acceleration is referred to as *fragility* and is measured in *gs*, where g is the acceleration due to gravity, $g = 32.2 \text{ ft/sec}^2$.
- We know the properties of the cushion, which are measured by its energy absorbing capability.
- The cushion is *isotropic*, that is, its properties in each direction is the same. We have observed from our impact as well as compression tests that the folded paper technology developed at Rutgers is much closer to an isotropic material than other previously developed cushion material, such as honeycomb.
- When the cushion deforms, there is a very small elastic deformation region, which is followed by a near horizontal plastic deformation region, as in the load-deformation curves shown below. The load deformation curves show different levels of resistance, depending on the impact velocity. Based on test results, we approximate the load deformation curve as a horizontal line. This approximation has turned out to be reasonably accurate for the folded material, as we have observed little in the form of elastic effects after impact.

Suppose a container containing cargo and the cushioning material that has a total mass of m is dropped from a height h . In the absence of aerodynamic effects (aerodynamic effects are discussed in Appendix 1) the energy of the container is $mgh = Wh$, where $W = mg$ is the weight. The kinetic energy of the container is

$$T = \frac{1}{2} \frac{W}{g} v^2 = Wh \quad (1)$$

from which we calculate the impact velocity as

$$v_{\text{impact}} = \sqrt{2gh} \quad (2)$$

Note that the impact speed, in the absence of aerodynamic effects, is independent of the weight of the cargo. In the presence of aerodynamic effects, as discussed in Appendix 1, the speed of the cargo is reduced by aerodynamic drag. If we know the impact speed from aerodynamic analysis, we can calculate an *effective height* h^* , which, in the absence of aerodynamic effects, would result in the same impact speed as a drop from height h in the presence of aerodynamic effects.

4 One-Dimensional Impact Model

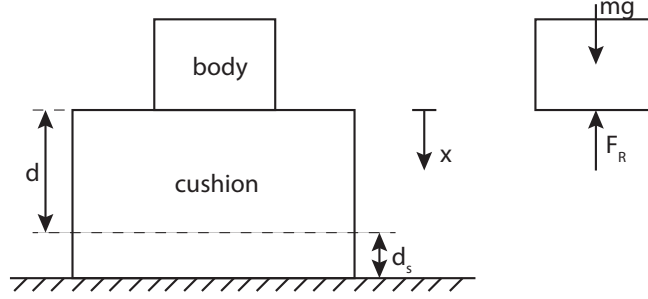


Figure 1: Body Falling on a Cushion and Free Body Diagram

Let us consider the simplest form of impact, that of a body falling on a cushion as described in Fig. 1. The cushion is of initial thickness $d + d_s$ and when fully compressed has a *solid height* of d_s . While it is being compressed, the cushion provides a resistive force F_R on the body. This force usually has the form

$$F_R = f(x, \dot{x}) \quad (3)$$

For the most general case the resistive force is nonlinear and it varies with the speed of contact. In general, the resistive force is larger when resisting a body that falls faster. The modeling of this resistive force is a research topic and it varies for different materials. Researchers have developed approximate models, but the validity of each model has to be verified experimentally for a given type of cushion. Our testing has shown that the chevron-patterned folded paper material that we have developed at Rutgers generates a resistive force that is two or three times larger for fast moving loads, than it is for slow moving or quasi-static loads.

The resistive force versus deformation (or stress-strain) curve of the cushioning material we have developed is almost a horizontal line, as shown in Fig. 2. The force F_0 denotes the minimum amount of force that needs to be applied to the cushion before the cushion begins to deform nonlinearly. The figure above can be divided into three ranges:

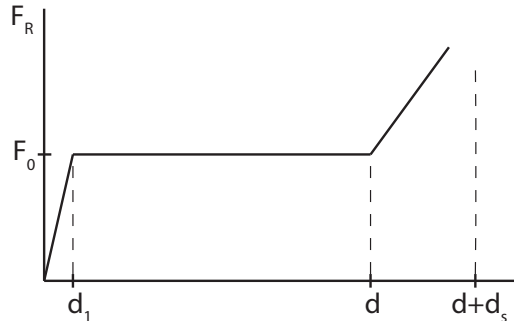


Figure 2: Load-Deformation Curve for Ideal Cushion

- A small linear range, ($0 \leq x \leq d_1$), where the force deformation curve increases as a straight line.
- A much larger range, ($d_1 \leq x \leq d$), where the resistive force is almost constant, at F_0 . This range indicates plastic deformation and the crushing of the cushion material.
- The range where the cushion reaches solid height ($x > d$). Here, the cushion acts as a very strong spring and provides very high resistive forces. This is a region we would like to avoid, as the cushion very stiff, possibly stiffer than the cargo. In such a scenario, the cargo begins to absorb energy instead of the cushion and damage to the cargo may occur.

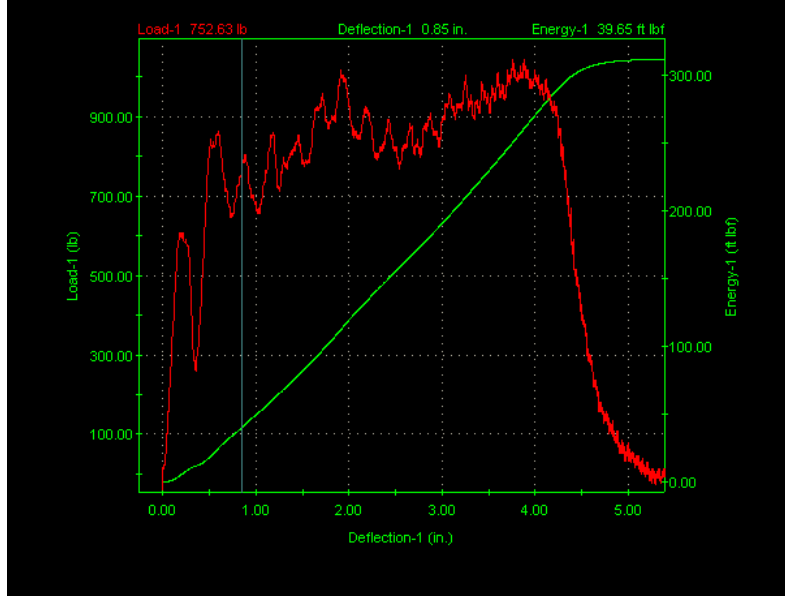


Figure 3: Load-Deformation Curve Test Results for Chevron Patterned Cushion

Figure 3 shows actual test results generated on an impact testing machine at Rutgers, using an MTS Universal Testing instrument (INSTRON Dynatup 9200 Series Drop Tower Impact Tester) having a maximum compressive load capability of 10,000 lbs. During a test, an impacting head of weight W_i is raised to a height h_i and then released so that it has an impact energy of $W_i h_i$ (ignoring aerodynamics effects, as the distance traveled is short. For developing higher energy levels, the impact head is also pushed against a spring, which increases the potential energy. The testing equipment is shown in Fig. 4.¹

The cushion used in the impact test was of thickness 6 inches, with the solid height at 1 inch. Because we knew from prior test results that a cushion made of the chevron-patterned folding paper five inches thick could absorb a maximum energy of 300 lb-ft (for a cushion surface area of 6 by 6 inches), we set the energy level of the impact to 300 lb-ft, so that the deformation of the cushion would not exceed solid height. Exceeding solid height on an impact testing machine would lead to very high resistive forces and possibly damage the machine. The continuously increasing line in the above figure denotes the absorbed energy. As can be seen, if we filter the resistive force plot, we come very close to the ideal curve in Fig. 2.

¹See Figs. 8 and 9 for pictures of sample cushions made of chevron patterned folding material and honeycomb.

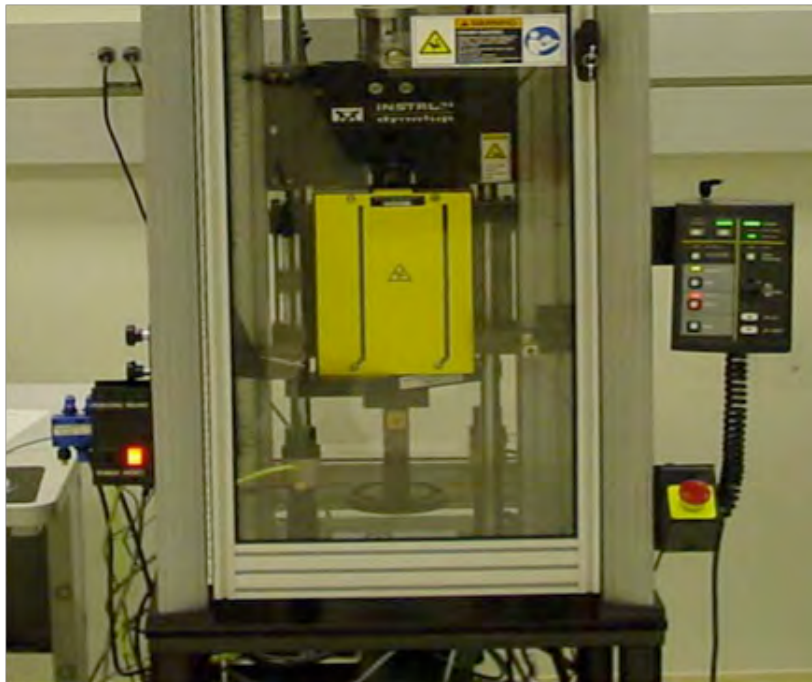


Figure 4: Impact Machine

A horizontal load deformation curve is preferred, as it can absorb the largest amount of energy, $F_0 d$, as opposed to any other curve with a maximum amplitude of F_0 . One of our goals in the freedrop project was to develop cushioning materials that have load-deformation curves that are near horizontal.

Let us now take a look at the deformation test conducted for honeycomb. Figure 5 shows the same test with the same energy level on honeycomb. It is interesting to note that, while honeycomb provides a higher level of resistance for a brief time (1700 lb vs 1000 lb for chevron), the resistance fades away and we get a much less uniform deformation curve.

From here on, we will assume that the resistive force vs. deformation curve is horizontal for the chevron folded cushion material developed at Rutgers. This basically means that the resistive force that the cushion applies on the falling object is constant. Denoting the thickness of the cushion by d , we conclude that the maximum energy that can be absorbed by the cushion material, which is the area under the curve in the above figure, is

$$E_{max} = F_0 d \quad (4)$$

Note that the maximum force F_0 is dependent on the area of the cushion material, which we denote by A . It is of interest to denote the resistive force per unit area, which we define as the *strength of the cushion* (or energy density) σ_0 as

$$\sigma_0 = \frac{F_0}{A} \quad (5)$$

where σ_0 has the units of stress (force over area, or energy over volume). In essence, σ_0 is a material property of the cushion. Now, let us conduct a drop test. We select a cushion of cross-sectional

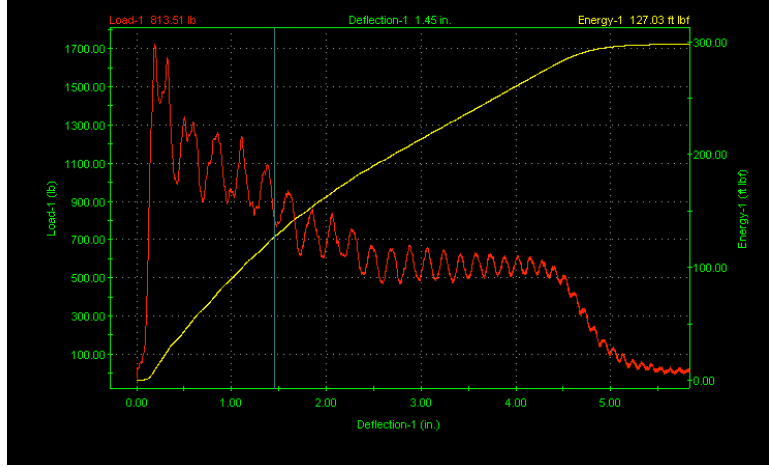


Figure 5: Load-Deformation Curve Test Results for Honeycomb

area A and thickness d and drop onto it a rigid object of the same cross-sectional area A . Let us select the potential energy of the object before the drop test as E . It follows that the maximum amount of energy that the cushion is able to absorb, E_{max} , is

$$E_{max} = \sigma_0 A d \quad (6)$$

or, $\sigma_0 = E_{max}/Ad$ is the maximum energy per unit volume that the cushion material can absorb. When designing the cushion material one can calculate the value of σ_0 from drop tests using the relation

$$\sigma_0 = \frac{E}{A\delta} \quad (7)$$

where E is the energy of the dropped object and δ is the measured deformation. A properly designed cushion should give the same value for different energy levels.

In summary, if an object is dropped on a cushion of strength σ_0 , area A and thickness d , the cushion will deform by an amount $\delta = E/\sigma_0 A$ and as long as the energy of the drop is less than E_{max} the cushion will not reach *solid height* and there will be room for more energy absorption. Once the energy of the impact reaches E_{max} the cushion reaches solid height. The term solid height is borrowed from coil spring design problems, where in a compression spring the maximum deflection of the spring the unstretched length of the spring minus the solid height.

We are interested in what happens to the cushion and to the dropped object when the energy of the dropped object is higher than the maximum energy the cushion can absorb. Obviously, the cushion reaches solid height, and it begins to behave similar to a solid made of the cushion material, with a very high resistive force. It is difficult to observe this effect in the laboratory, when using an impact testing machine, as an impact testing machine can sustain damage if we enter the solid height zone. Our observations from actual drop tests, from a crane or helicopter, has led us to develop the following theory.

The impact takes place in three stages, as shown in Fig. 6:

1. The object is released with a certain energy level. Some energy is lost during free fall due to aerodynamic drag, and immediately before impact the object has a energy level of E_0 . The energy is entirely kinetic: $E_0 = \frac{1}{2}mv_0^2$, where v_0 is the vertical velocity of v_0 immediately before contact with the cushion material.
2. The object makes contact with the cushion and begins to compress the cushion. The cushion has an energy absorbing capability of E_{max} . If the cushion is able to absorb all of the impact energy, then the object comes to a rest and the impact ends. If not, the cushion is compressed to its solid height. The energy level at this stage is $E_1 = E_0 - E_{max}$ and the velocity of the object now is

$$v_1 = \sqrt{\frac{2(E_0 - E_{max})}{m}} \quad (8)$$

We reiterate that if all the energy of the cargo is absorbed by the cushion $v_1 = 0$ and the impact ends.

3. If the cushion reaches solid height and the object still has a velocity, a continuing collision takes place between the object and the cushion, which is now in solid form. The solid form cushion has some elasticity but it is also very strong, so that the collision is not purely plastic. Once can look at this as the solid cushion acting like a very strong spring. Because we do not know the properties of this collision well, we will estimate the effects of the collision with a coefficient of restitution e . Hence, the velocity of the object immediately after impact becomes

$$v_2 = -ev_1 \quad (9)$$

It should be noted that while we modeled the cushion as a perfectly plastic material, there is some small level of elasticity in it and this elasticity will force to body to bounce back. This elasticity is yet another factor that contributes to the coefficient of restitution. For freedrop experiments, we have estimated the coefficient of restitution experimentally, by determining how much the body rises. Indeed, if the body has velocity v_2 when it bounces back, it has energy of $E_2 = \frac{1}{2}mv_2^2 = \frac{1}{2}e^2mv_1^2$. Equating it with the energy level reached at maximum height after the bounce, $E_2 = mgh_2$, we can estimate the coefficient of restitution as

$$e = \sqrt{\frac{2gh_2}{v_1^2}} \quad (10)$$

A better measure of the impact and how we relate it to the entire drop is to compare the velocity before impact v_0 and relate it to the final velocity, v_2 . We can do this by noting that

$$\frac{1}{2}mv_2^2 = e^2\frac{1}{2}mv_1^2 = e^2(E_0 - E_{max}) = e^2(\frac{1}{2}mv_0^2 - \sigma_0Ad) = e^2(mgh^* - \sigma_0Ad) = mgh_2 \quad (11)$$

which, when solved for the coefficient of restitution, gives

$$e = \sqrt{\frac{h_2}{h^* - \frac{\sigma_0Ad}{mg}}} \quad (12)$$

It is this latter value of e that we use in Appendix 3, when we discuss the impact model.

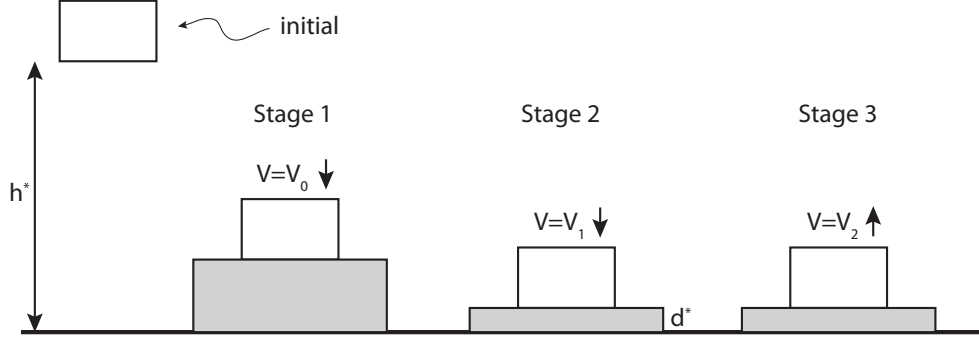


Figure 6: The Three Stages of Impact with a Cushion

At this time, it is useful to have a discussion on what type of coefficient of restitution is preferable for our purposes. Consider the collision two bodies. When the coefficient of restitution $e = 1$ the collision is called elastic, and no energy is lost. When $e = 0$ the collision is called plastic and all energy along the line of impact is lost. The energy is lost usually due to damage to the colliding bodies or to internal damping in the bodies. Most collisions involve a coefficient of restitution between 0 and 1, where there is some energy loss as well as some bouncing back. It is clear that in our design, the coefficient of restitution depends on the properties and thickness of the cushion that we are using.

One may initially think that having a low coefficient of restitution is better, as in our case the container will not bounce back. However, a low coefficient of restitution means that the impact energy is absorbed by the colliding bodies. When the impact energy is higher than the energy the cushion can absorb, $E_0 > E_{max}$, solid height is reached and, since the solid height cushion does not absorb as much energy, then the falling object absorbs all the remaining energy $E_0 - E_{max}$, which may result in damage.

On the other hand, when we have a higher coefficient of restitution, the impact energy is not dissipated as much and some of the impact energy is transferred back to the falling object in the form of kinetic energy. Thus, there is less energy absorbed by the cargo and hence the object suffers less damage.

There are two possibilities when an object is dropped on a cushion and it basically does not bounce back at all, or bounces a very small distance.

- The first possibility is that the cushioning material absorbs all of the energy of the object and that the object comes to rest before solid height is reached. This, obviously, is the desired situation. In realistic cases of airdrop, though, a very thick cushion would be required to accomplish this.
- The second possibility is that the cushioning material reaches solid height and then the crushed cushion has a zero or very low coefficient of restitution. In this case, the dropped object absorbs the remaining energy and possibly sustains damage.

The above two possibilities should be considered when designing a cushion. In general, unless sophisticated finite element models are developed, one has to conduct experimental analysis to design the cushion.

5 Simple Cushion Design Based on Fragility Level

We are dropping an object from a height of h and the object has a fragility level of a_0 , that is, the maximum acceleration it can withstand before damage is a_0 . One usually denotes fragility levels as a function of the gravitational constant g . We want to design a cushion that the dropped object comes to a rest before solid height is reached.

Let us ignore, for the sake of argument, the aerodynamic drag forces (or, treat h as the equivalent height). Let us also assume that the entire energy of the object is absorbed by the cushion just as the cushion reaches solid height. From the previous discussions, we also assume that the cushion provides a constant resistive force while it is being compressed by the object. Hence, we identify the first two stages of the motion as constant acceleration motions. In stage 1, that is, free fall, the acceleration of the object is g , acceleration of gravity. In the second stage, the acceleration of the object is a . The energy before the impact (mgh) is absorbed completely by the cushion. Noting that the force applied by the cushion is constant at $F = ma = \sigma_0 A$ and the distance traveled is d , the energy absorbed by the cushion becomes mad . Equating these two energies, we come up with a very interesting relation

$$mgh = mad \quad \rightarrow \quad \frac{d}{h} = \frac{g}{a} \quad (13)$$

so that the ratio of the cushion thickness to the drop height is the inverse of the acceleration ratios. For example, if we are dropping from a height of 100 ft and the fragility level (or maximum acceleration a body can sustain) of the object is $a_0 = 200g$, which is a reasonable estimate for a bullet, we replace a in the above equation with the fragility a_0 and the expression for the cushion thickness becomes

$$d = \frac{gh}{a_0} = \frac{100g}{200g} = 0.5 \text{ ft} \quad (14)$$

We can adjust the result above to reflect the amount of energy absorbed by the drag forces. Assuming, for the parameters that we are considering, that 20% of the energy of the object is lost to drag, we replace gh in the above equation by $0.8gh$, which gives a desired cushion thickness of $0.4 \text{ ft} = 4.8 \text{ in}$.

Next, let us use these results and calculate the energy density σ_0 , that is, the strength of the cushion. The contact area between the object and cushion is A , and the force required to resist the speed of the falling object is $F_R = \sigma_0 A$. Equating this force to the acceleration of the object while it makes contact with the cushion we obtain

$$F = \sigma_0 A = ma_0 \quad \rightarrow \quad \sigma_0 = ma_0/A \quad (15)$$

Therefore, in order to completely crush the cushion and to not cause damage to the cargo, we need a cushion that has a strength of $\sigma_0 = ma_0/A$ and has thickness of $d = 0.8gh/a_0$. Of course,

one should keep in mind that the thickness that we are talking about here is the amount that the cushion can deform before solid height is reached, and not the actual thickness of the cushion.

In essence, if we look at the two design criteria developed above, one involves energy and the other involves acceleration.

6 Theory vs. Reality

The derivations above are based on the assumptions that the impacting body is the same size as the cushion and that the impacting body does not make impact at an angle with the cushion. Neither one of these assumptions hold true in an actual drop.

The fact that the surface area of the cushion is larger than the contact area of the object works to our advantage, as long as the object does not shear the cushion as it compresses the cushion. Looking at Fig. 7, we want the cushion to not rip. If the cushion rips, then the only part of the cushion that provides stiffness is the surface area of the object. It is preferable to have a cushion where the parts of the cushion not in contact with the dropped object still provide some stiffness. We see from Fig. 7a that when the cushion does not shear, a larger area of the cushion deforms, thus absorbing more energy. Test results conducted in a Rutgers laboratory, using an MTS Universal Testing instrument having a maximum compressive load capability of 10,000 lbs, for chevron patterned folded paper and honeycomb are shown in Figs. 8 and 9. In both tests, cushion samples 6 by 6 by 6 inches in size were impacted upon a 4 by 4 in metal head.

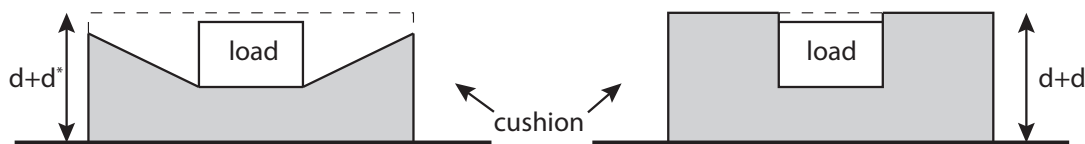


Figure 7: Cushion Compression Scenarios: a) No Shearing, b) Shearing

The second assumption deals with the object falling on the cushion completely flat. This, of course, does not happen and the object most likely makes contact with the cushion in the fashion shown in Fig. 10.

This type of contact is typical of side impact or when there is corner impact. Such impact reduces the strength of the cushion, as the amount of resistance the cushion puts up is less. On the other hand, a larger part of the cushion comes into contact with the cargo. We are currently working on finite element models to quantify the effects of such impact. Figures 11 and 12 show an outer container, and damage to cushion for an angled drop. Figures 13 and 14 show the inside of another container manufactured out of chevron patterned folding material after an angled drop. The cargo inside the container were two ammunition cans.



Figure 8: Chevron Shear Test



Figure 9: Honeycomb Shear Test

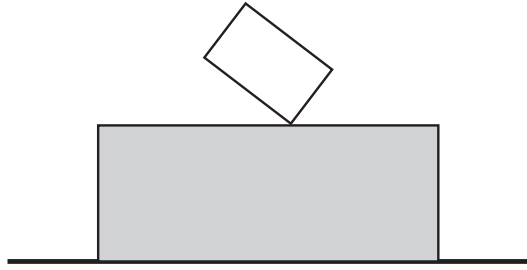


Figure 10: Angled Contact Between Object and Cushion



Figure 11: Outer Box after Angled Impact



Figure 12: Inner Box after Angled Impact



Figure 13: Inside of Box after Angled Impact - With Cargo



Figure 14: Inside of Box after Angled Impact After Cargo is Removed

6.1 Accuracy of the Impact Model

The impact model described above has several shortcomings as discussed below:

- First, the dropped container changes shape as it makes contact. The coefficient of restitution is traditionally used to model impact between two relatively hard objects (e.g., steel vs. steel, rubber on glass) so its accuracy for our container is questionable.
- Even if using the coefficient of restitution is a reasonable assumption measurements for the coefficient of restitution are usually taken by bouncing spherical objects onto flat surfaces. When corners impact, the coefficient of restitution changes. Thus, we have little means of calculating the coefficient of restitution other than experimental observations. The coefficient of restitution is a quantity that depends on a variety of factors, including the relative speed of the impacting bodies along the tangential direction. We earlier discussed a simple way of estimating it. We will have more discussion of the coefficient of restitution in Appendix 3, when we discuss the impact model.
- As will be discussed in Appendix 3, the idea of an impulsive friction force has been questioned by many. The coefficient of friction associated with impulsive forces is also a quantity that needs to be determined from experimental measurements.
- As discussed earlier, the impact location changes during impact. We have very little means of determining the exact location of impact.
- Construction of box. As per Army specifications, the cushion pads are not glued to the container walls or to each other, but they are cut precisely so that they snugly fit inside the box. This snug fit simulates a cushion that is made of one piece. However, if somehow the cushion pads do not have snug fit, there will be vastly diminished cushion stiffness and the cargo will experience very high contact forces.

7 Cushion Design Process

The cushion design process involves the selection of the stiffness of the cushion, as well as the thickness of the cushion, given the characteristics of the cargo and drop conditions. Building a cushion of any desired strength σ_0 out of folded paper is unrealistic and will require the storing of a very large number of types of paper. Instead, based on test results and prior experimentation, we decided to concentrate on a small number (usually around three or four) cushion types and we select the cushion to use from this group. Hence, our cushion design process selects the type of cushion to use among the cushions we have and determines the thickness of the cushion.

The cargo that is to be dropped is characterized by its size (outer dimensions), weight, hardness, and fragility level. In many cases, it is not possible to know the hardness level and fragility level of the cargo accurately, especially for soft cargo, such as water, IVs or MREs.

As discussed in Section 2, we use three criteria in selecting the cushion. We begin with the cushion stiffness σ_0 , which is observed experimentally. We then determine a modified stiffness σ_1 ,

based Fig. 8a. When the cushion does not shear under impact, a greater amount of the cushion is compressed. Consequently, more energy is absorbed.

Denote the area of the cargo that makes contact with the cushion by A and the maximum compression of the cushion by d . Given cushion stiffness of σ_0 , the maximum energy absorbed by the cushion is $E_{max} = \sigma_0 Ad$, as discussed earlier.

The displaced volume for the case of no shear is calculated by simple geometry. We take the contact area, add to it an estimated 6 in. of cushion thickness and calculate the compressed volume of the cushion, assuming that the compression not under the immediate area can be approximated by a straight line. We make this assumption because this is what we observed during testing, both with the impact machine and with the drop tests. Let us denote this volume by V . It follows that this volume V is larger than Ad and more energy can be absorbed by the cushion. Denote this absorbed energy by $E_1 = \sigma_0 V$. We define the enhancement ratio $e_R = \frac{V}{Ad}$. We arrive at a modified stiffness by dividing E_1 by Ad , so that

$$\sigma_1 = \frac{E_1}{Ad} = \frac{\sigma_0 V}{Ad} = e_R \sigma_0 \quad (16)$$

so that, by using the cushion material developed in our project, we can absorb more energy than a material that shears.

Given the energy of the cargo, defined as weight multiplied by drop height, and contact area of the cargo, then the cushion thickness d should be such that the energy absorbing capability of the cushion, $\sigma_1 Ad$ is greater than the energy of the cargo, mgh^* , where h^* is the equivalent height based on the aerodynamics, or

$$d \geq \frac{mgh^*}{\sigma_1 A} \quad (17)$$

We next add the two additional requirements. First, the cargo should be able to deform the cushion. For this to happen, at the initial point of contact, there must be deformation of the cushion. We refer to this criterion as *impact stress* and we define the criterion as d should be such that the energy absorbing capability of the cushion immediately under the payload, $\sigma_0 Ad$ is less than the energy of the cargo, mgh , or

$$d \leq \frac{mgh^*}{\sigma_0 A} \quad (18)$$

The second added requirement pertains to fragility. As the cargo compresses the cushion, the force acting on the cargo is $\sigma_0 A$. Equating this to the inertia ma , where a is the deceleration, we get a deceleration level of

$$a = \frac{\sigma_0 A}{m} \quad (19)$$

This deceleration must be less than the fragility of the cargo. To better visualize this relationship, we continue with our assumption that the acceleration remains near constant during compression

of the cargo, and calculate the work done by the inertia force as $W = F_{inertia}d = mad$. Setting this as greater or equal to the energy of the cargo mgh^* , we obtain

$$d \geq \frac{mgh^*}{ma} = \frac{gh^*}{a} \quad (20)$$

Defining the fragility as f as the maximum acceleration the cargo can endure, so that $a_{max} = fg$, the requirement for d becomes

$$d \geq \frac{h^*}{f} \quad \text{or} \quad \frac{h^*}{d} \leq f \quad (21)$$

To summarize, the three conditions that the cushion thickness d needs to satisfy are

$$d \geq \frac{mgh^*}{\sigma_1 A} \quad d \leq \frac{mgh^*}{\sigma_0 A} \quad d \geq \frac{h^*}{f} \quad (22)$$

We at Rutgers team have developed a software product that conducts a decision making scheme that takes into consideration these three requirements and determines the type of cushion to use and the lowest cushion thickness that will not lead to damage.

8 Dealing with Soft Cargo

The developments and results above were for a rigid object dropped onto a cushion. Our results show that we can model ammunition boxes and generators and design cushions for them by assuming that they are rigid and they absorb very little energy during impact. For softer cargo, such as water bottles, MREs and medical supplies like IVs, the design above has to be modified. This is because the cargo itself absorbs some of the energy. Moreover, the impact stress criterion has to be satisfied.

As an example, consider dropping MREs using cushion material developed for ammunition cans. The MREs are much softer than the cushion, so that in a contact between the two would be similar to a car hitting a solid wall. The cushion would not absorb any energy and all the energy would be absorbed by the cargo, most likely damaging the cargo.

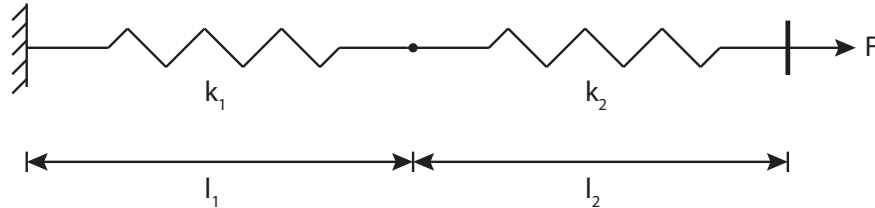


Figure 15: Springs in Parallel

To understand how to deal with softer cargo, let us consider a simple model, involving two springs. Consider two springs in parallel, with constants k_1 and k_2 , as shown in Fig. 15. The

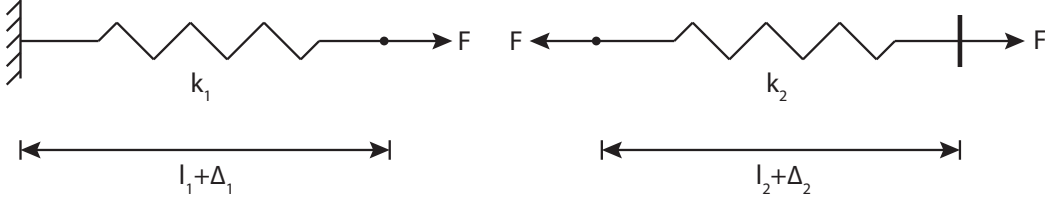


Figure 16: Free Body Diagrams

undeformed lengths of the cushions are l_1 and l_2 , respectively. We draw the free body diagrams in Fig. 16. The force transmitted by each spring is going to be the same. The deflection of the springs is denoted by Δ_1 and Δ_2 , and equating the two spring forces we obtain

$$k_1 \Delta_1 = k_2 \Delta_2 \quad (23)$$

which lets us relate the spring deflections as

$$\Delta_2 = \frac{k_1}{k_2} \Delta_1 \quad (24)$$

so that the deflections are inversely proportional to the spring rates. This is to be expected, because the weaker spring will end up deflecting more.

Next, let's write the energy and see how much energy each of the springs absorbs. Writing the energy absorbed by each spring as

$$E_1 = \frac{1}{2} k_1 \Delta_1^2 \quad E_2 = \frac{1}{2} k_2 \Delta_2^2 \quad (25)$$

and substituting the value of Δ_2 from the previous equation we have

$$E_2 = \frac{1}{2} k_2 \Delta_2^2 = \frac{1}{2} k_2 \left(\frac{k_1}{k_2} \Delta_1 \right)^2 = \frac{1}{2} \frac{k_1}{k_2} k_1 \Delta_1^2 = \frac{k_1}{k_2} E_1 \quad (26)$$

We see that the energy absorbed is proportional to the spring ratio. If we say that $k_2 > k_1$ (spring 2 is stronger than spring 1), so that $\frac{k_1}{k_2} < 1$, then the energy absorbed by the second (that is, stronger) spring is less than the energy absorbed by the weaker spring. The weaker spring absorbs much more of the energy.

We can extend this analogy to our cushion, even though we are not dealing with linear deformations. Consider two cushions, each with the same cross-sectional area A , but with different energy densities σ_1 and σ_2 , that are glued together. The combined cushions are impacted by a load with total energy E . Denote the energy absorbed by each cushion as E_1 and E_2 , so that $E_1 + E_2 = E$ and each cushion deflects by

$$\delta_1 = \frac{E_1}{\sigma_1 A} \quad \delta_2 = \frac{E_2}{\sigma_2 A} \quad (27)$$

To ascertain how the two energies E_1 and E_2 and hence the two deflections related, we will use the argument that the force transmitted by the two cushions is the same. Without loss of

generality, let's say $\sigma_2 > \sigma_1$. When the energy density of the load, $\frac{E_0}{Ad}$, is smaller than $\sigma_1 A$ then there will be no deformation, as the cushions will withstand the force without crushing. When the energy density is between $\sigma_1 A$ and $\sigma_2 A$ then the weaker cushion will start buckling first and the stronger cushion will remain intact.

When the load is stronger than both cushions, both cushions will collapse. We will assume that the energies absorbed by the cushions are inversely proportional to the strengths of the cushions. We have

$$\frac{E_1}{E_2} = \frac{\sigma_2}{\sigma_1} \quad (28)$$

and, introducing the expressions

$$\delta_1 = \frac{E_1}{\sigma_1 A} \quad \delta_2 = \frac{E_2}{\sigma_2 A} \quad (29)$$

to the above relation we obtain a relation between the two deflections as

$$\frac{\delta_2}{\delta_1} = \left(\frac{\sigma_1}{\sigma_2} \right)^2 \quad (30)$$

so that the deflections of the cushions are related to the square of the strengths of the cushions. So, if one cushion has strength of 30 psi and the other 10 psi, the weaker cushion will deform 9 times more than the stronger cushion. Also, it should be noted that all of the cushion materials we develop have a linear range of deformation. Even though this range is very small, there is some small deformation in the stronger cushion.

In order to design a cushion for soft cargo, we need to determine the energy absorbing capability of the cargo. To this end, we conduct impact tests for the cargo the same way we conducted tests on cushions. The results of these tests give us an idea on how much energy the cargo absorbs and what the fragility is. We also get ideas on how to select the cushion for softer cargo. For example, we tested several types of water bottles and identified containers that do not do well in drop tests as well as in impact tests on the impact machine.

Once we calculate the energy per volume of the cargo, we compare it with the cushion types that we have and calculate which part of the energy is absorbed by the soft cargo and which part by the cushion. This percentage is used as a factor to obtain a modified energy absorption capability, which is then used in the cushion design calculations in Eqs.(22).

9 Isotropy of the Cushion Material

All of the developments above are based on the assumption that the properties of the cushion that we are designing are the same, regardless of the orientation of the cushion. This assumption is not very accurate. Our tests have shown that the assumption is more accurate for the chevron patterned folded paper than it is for honeycomb.

Consider Figs. 8 and 9, which depict the cushion samples used in impact testing. The *flat direction* is perpendicular to the table on which the cushions rest in the above-mentioned figures.

The shear tests on these specimens were conducted by impacting the specimen in the flat direction. For the chevron patterned folded paper developed in this project, the other two directions are referred to as the *machine direction* (the direction in which the folding machine produces the folded material) and *cross direction*. Tests have shown that the impact strength, as measured by the cushion stress σ_0 , is strongest for the cross direction and weakest in the machine direction, with a ratio of about

$$\frac{\sigma_{0_{cross}}}{\sigma_{0_{machine}}} \approx 1.7 \quad (31)$$

We expected this result and have been comfortable with it. We have observed that a difference in energy density of the magnitude we have does not make a significant difference for drops from varying angles.

For honeycomb, properties of the directions perpendicular to the flat direction are nearly identical. We will refer to these directions as the *cross directions*. It turns out that honeycomb is strongest in the flat direction, actually stronger than chevron, but is very weak in the cross directions. The strength ratio that was measured from our tests is

$$\frac{\sigma_{0_{flat}}}{\sigma_{0_{machine}}} \approx 8 \quad (32)$$

This difference is cause for concern for honeycomb, especially when there is an angled drop, where the container makes impact with the ground at a corner. We have observed the effects of difference in impact strengths in different directions, in both the resistance forces generated, as well as the energy absorption capability. The concept is illustrated in Fig. 17 for an angled drop. The lines in the cushion are in the flat direction, which for honeycomb provide eight times more resistance than the cross direction.

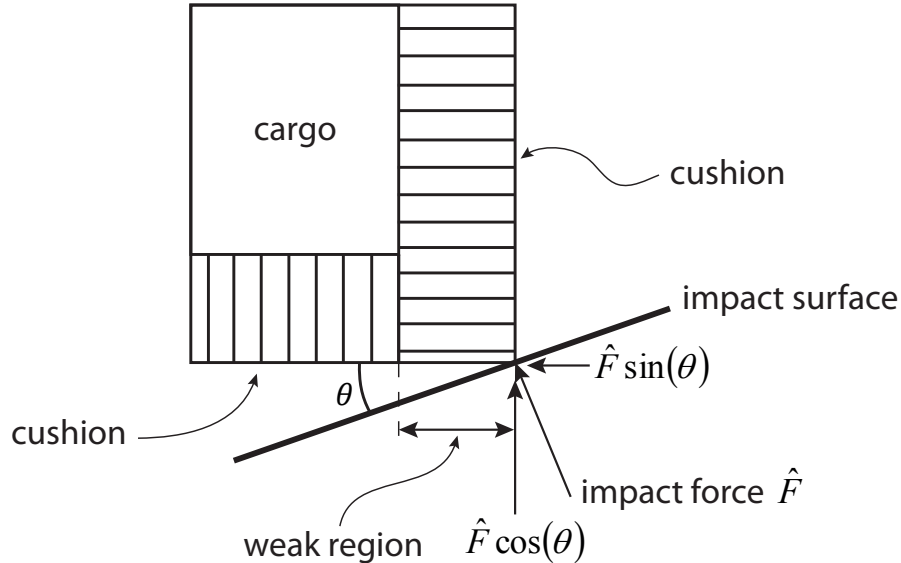


Figure 17: Angled Drop, with Impact Force on the Cushions

The vertical cushion shields the right side of the cargo. This cushion provides stronger resistance to an impact force along the horizontal direction. The horizontal cushion shields the

bottom of the cargo and it provides stronger resistance to an impact force that is vertical. No matter how we select the cushions, there will be a weak region due to the difference in the cushion resistance. For example, in the figure above we could have selected the lower cushion as wider and the side cushion shorter. The corner weakness would still be there.

Now, consider an impact with a surface that is more horizontal than vertical. It follows that the impact force, which is perpendicular to the impact surface, will have a larger component in the vertical direction, where the cushion is weak. Consequently, there will be less energy absorption and more damage. Because in an actual airdrop from a moving aircraft one does not have control over which corner of the container will make impact with the ground, it is always a safer idea to select a cushion that has comparable strength in either direction.

We have observed this phenomenon during drop tests conducted at our labs, during drops from cranes at the Army Depot in Tobyhanna, Pa., as well as in drop tests from moving helicopters at the Aberdeen Proving Grounds. There was more damage to corner elements when honeycomb was used as the cushion element than when chevron was used. The difference was as not as large as what we expected, though, because impact with the ground also generates a horizontal impact force, due to friction. Also, the compression of the cushions against each other provides additional strength. We will discuss impact forces in more detail in Appendix 3.

Appendix 3 - Impact Modeling

May 17, 2011

1 Introduction

This appendix describes the mathematical model of the impact of the container used in free drop experiments. It is assumed that the container has both a horizontal and vertical velocity upon impact. The velocities and angular velocities immediately after impact are calculated based on the assumption that the impact takes place instantaneously. The model is developed such that impact can take place at any point on the container.

This report does not include details on the properties, manufacture and the design of the cushioning material, as that information has been discussed in other reports and in Appendix 2. It is assumed that the properties of the cushion and the nature of frictional forces during impact can be modeled by means of a coefficient of restitution and a coefficient of friction. The model developed here considers two- as well as three-dimensional motion and it also looks at subsequent impacts and the tumbling of the container.

2 Nomenclature and Geometry of Impact

Figure 1 describes the falling container. We are using an inertial coordinate system xyz , with x denoting the horizontal and y the vertical directions. The initial model considers that the motion of the container is in the xy plane, so that there is only one angular velocity component involved. According to our coordinate system a positive rotation is counterclockwise.

The impact location is denoted by P and the center of mass by G . Note that the impact location does not have to be a corner. The velocity of the center of mass is denoted by

$$\mathbf{v}_G = \bar{v}_x \mathbf{i} + \bar{v}_y \mathbf{j} \quad (1)$$

The container is dropped from a height with an initial horizontal velocity so that it is moving in the positive x direction and negative y direction before impact. The difference in location between the center of mass and the point of impact is described by the distance R between the two points and the angle γ that the line joining G and P makes with the vertical. When γ is positive (counterclockwise)

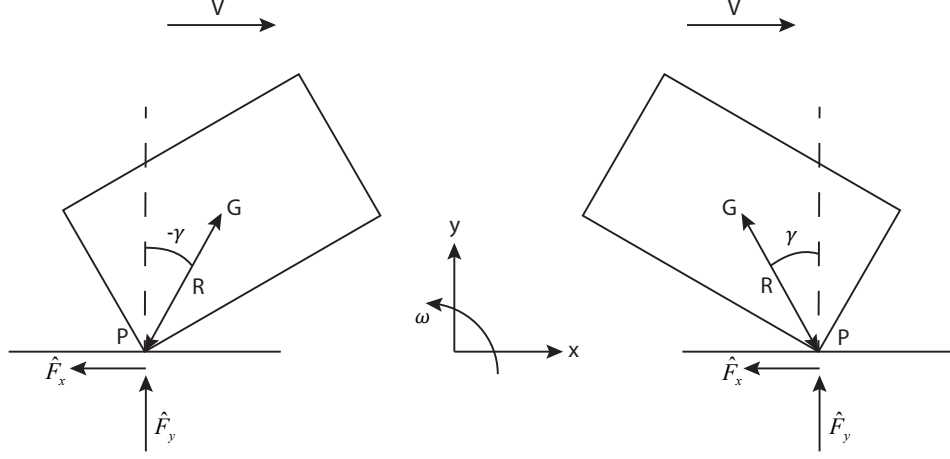


Figure 1: Impacting Box

the impact position is in front of the center of mass and when γ is negative (clockwise) the impact position is behind the center of mass.

The forces generated during impact are denoted by \bar{F}_x and \bar{F}_y . The magnitude of the vertical impact force is related to the *coefficient of restitution* e associated with the impact. The horizontal impact force depends on the friction coefficient μ and whether there is sliding or not at the instant of impact. The *impulses*, also called impulsive forces, that are generated during impact are denoted by \hat{F}_x and \hat{F}_y . They are calculated by integrating the impact forces over the duration of impact. Denoting the duration of impact by Δ , we calculate the impulses by

$$\hat{F}_x = \int_0^\Delta \bar{F}_x dt \quad \hat{F}_y = \int_0^\Delta \bar{F}_y dt \quad (2)$$

The relationship between the impact forces and time during impact is not very well known, even when a smooth object impacts with a surface. If we add to this that most of the container undergoes plastic deformation, the impulsive forces become very hard to model. The impulsive forces \hat{F}_x and \hat{F}_y are shown in Fig. 1.

We assume the container to be rigid, but the fact that a coefficient of restitution is used is an indication that the container has some internal flexibility. This being the case, an issue comes to mind as to where the real point of impact is. To illustrate this point, let us look at Fig. 2, which shows a cross-section of the container, with the cargo and cushioning material. The cargo is in the form of two ammunition cans, separated by a cushioning layer. Upon impact, the cushioning material gets crushed to a solid thickness and the cargo presses against the cushioning. So, is the impact location where the container hits the ground first or is it where the corner of the ammunition box presses into the solid thickness cushion? Our analysis of experimental data, obtained from high-speed video, together with theoretical developments, indicate that the impact point is closer to the point where the cargo penetrates the cushion material.

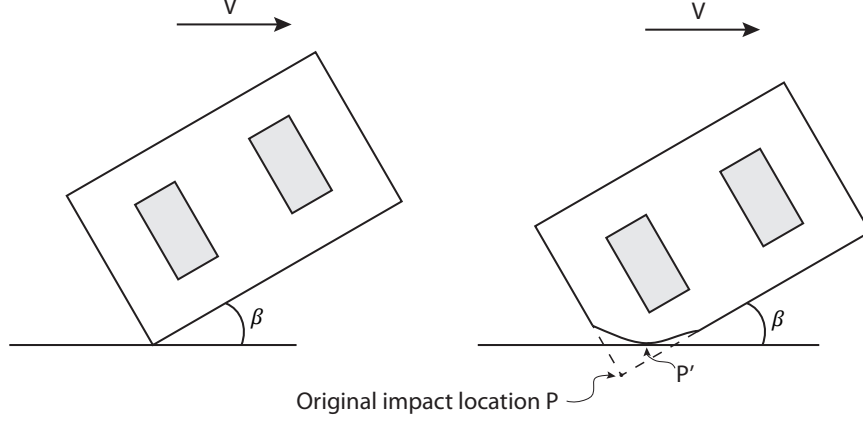


Figure 2: Cross-section of container. a) Before compression, b) After compression

3 Governing Equations of Impact

We will use impulse-momentum principles to write the equations of impact. The velocities and angular velocity immediately after impact will be denoted with primes, so we will have \bar{v}'_x , \bar{v}'_y , and $\bar{\omega}'$. The impulse-momentum relationship in the horizontal (x) direction for immediately before and immediately after impact is

$$m\bar{v}_x - \int_0^\Delta \bar{F}_x dt = m\bar{v}'_x \quad \text{or} \quad m\bar{v}_x - \hat{\bar{F}}_x = m\bar{v}'_x \quad (3)$$

Similarly, in the vertical direction we have

$$m\bar{v}_y + \hat{\bar{F}}_y = m\bar{v}'_y \quad (4)$$

and the angular impulse momentum relationship becomes

$$I_G\bar{\omega} + \hat{\bar{M}}_G = I_G\bar{\omega}' \quad (5)$$

where I_G is the mass moment of inertia of the box and $\hat{\bar{M}}_G$ is the angular impulse about the center of mass in the z direction. It is convenient to express this moment in vector form as

$$\hat{\bar{M}}_G \mathbf{k} = \mathbf{r}_{P/G} \times \hat{\mathbf{F}} \quad (6)$$

where

$$\mathbf{r}_{P/G} = R \sin \gamma \mathbf{i} - R \cos \gamma \mathbf{j} \quad \hat{\mathbf{F}} = -\hat{\bar{F}}_x \mathbf{i} + \hat{\bar{F}}_y \mathbf{j} \quad (7)$$

so the impulsive moment becomes

$$\hat{\bar{M}}_G = R \sin \gamma \hat{\bar{F}}_y - R \cos \gamma \hat{\bar{F}}_x \quad (8)$$

We have three equations and five unknowns, which are \bar{v}'_x , \bar{v}'_y , and $\bar{\omega}'$, the velocities immediately after impact, and the two impulsive forces, $\hat{\bar{F}}_x$ and $\hat{\bar{F}}_y$. We hence need two more equations to

solve for the unknowns. Both these equations come from the impact condition. The first equation comes from the description of impact and it involves the coefficient of restitution. It relates the component of the velocity of the impacting point in the vertical direction and has the form

$$\mathbf{v}'_P \cdot \mathbf{j} = -e \mathbf{v}_P \cdot \mathbf{j} \quad (9)$$

where e is the coefficient of restitution. The velocity of the point of impact is

$$\mathbf{v}_P = \mathbf{v}_G + \bar{\omega} \times \mathbf{r}_{P/G} = (\bar{v}_x + R \cos \gamma \bar{\omega}) \mathbf{i} + (\bar{v}_y + R \sin \gamma \bar{\omega}) \mathbf{j} \quad (10)$$

so the vertical impact relation becomes

$$\bar{v}'_y + R \sin \gamma \bar{\omega}' = -e(\bar{v}_y + R \sin \gamma \bar{\omega}) \quad (11)$$

The fifth relation is related to what happens in the horizontal direction during impact and it involves friction. As in all problems involving friction, one has to address the issue of whether there is sliding or not. Here, we are looking at the instant of impact and we are concerned with whether there is sliding during impact. Three scenarios are possible:

1. There is **sliding** of the impact point during impact. In this case, we do not know the sliding velocity, but we know that the horizontal impulsive force is related to its vertical counterpart by

$$\hat{F}_x = \mu \hat{F}_y \quad (12)$$

where μ is the coefficient of friction between point P on the container and the impact surface. The above equation becomes our fifth relation.

2. There is **no sliding** at the point of impact in the horizontal direction, so we have $\mathbf{v}'_P \cdot \mathbf{i} = 0$. It is as if the container is rolling about the impact point, at least when the horizontal motion of the container is visualized. Considering the expression for the velocity of point P in Eq. (10), the fifth equation for the case of no sliding becomes

$$\bar{v}'_x + R \cos \gamma \bar{\omega}' = 0 \quad (13)$$

3. The container pivots about the impact point. Hence $\mathbf{v}_P = \mathbf{0}$. Here, the coefficient of restitution in Eq. (33) is $e = 0$. We have

$$\bar{v}'_x + R \cos \gamma \bar{\omega}' = 0 \quad \bar{v}'_y + R \sin \gamma \bar{\omega}' = 0 \quad (14)$$

In essence, the third scenario is a special case of the second scenario, with $e = 0$. This scenario is encountered very rarely.

3.1 Accuracy of the Impact Model

The impact model described above has several shortcomings:

- First, the freedropped container changes shape as it makes contact. The coefficient of restitution is traditionally used to model impact between two relatively hard objects (e.g., steel vs. steel, rubber on glass), so its accuracy when applied to our impact problem is questionable.
- Even if using the coefficient of restitution is a reasonable assumption measurements for the coefficient of restitution are usually taken by bouncing spherical objects onto flat surfaces. When corners impact, the coefficient of restitution changes. Thus, we have little means of calculating the coefficient of restitution other than experimental observations. We expect that the coefficient of restitution will be a quantity that depends on a variety of factors and we discuss means of estimating the coefficient of restitution in subsequent chapters of this report.
- Most impact analysis considers a positive coefficient of restitution. However, when the container is dropped onto a surface like a marsh or a lake, the container will proceed to move down. In such a case, a negative coefficient of restitution needs to be used. It is extremely difficult to determine the value of the coefficient of restitution under such circumstances. Also, given a desired drop zone, one should know how much the container travels in the air in the horizontal direction (analyzed in Appendix 2) and how much the container tumbles after impact (analyzed in this Appendix) before dropping the container from a moving aircraft.
- The idea of an impulsive friction force has been questioned by many. The coefficient of friction associated with impulsive forces is also a quantity that needs to be determined from experimental measurements.
- As discussed earlier, the impact location changes during impact. We have little means of determining the exact location of impact.

4 Solution of the Impact Equations

We now have five equations and five unknowns for each of the possible scenarios. Before solving these equations, though, it is convenient to non-dimensionalize them. For example, dividing Eq. (4) by $m\bar{v}_y$ and introducing the non-dimensional parameters

$$v'_y = \frac{\bar{v}'_y}{\bar{v}_y} \quad \hat{F}_y = \frac{\hat{\bar{F}}_y}{m\bar{v}_y} \quad (15)$$

where v'_y is the nondimensional vertical velocity after impact, we obtain for the linear momentum relationship in the vertical direction

$$1 + \hat{F}_y = v'_y \quad (16)$$

Similarly, we define the non-dimensional parameters

$$v'_x = \frac{\bar{v}'_x}{\bar{v}_y} \quad \hat{F}_x = \frac{\hat{\bar{F}}_x}{m\bar{v}_y} \quad \omega = \frac{\bar{\omega}R}{\bar{v}_y} \quad I = \frac{I_G}{mR^2} \quad (17)$$

as well as the ratio of the initial velocities

$$\rho = \frac{\bar{v}_x}{\bar{v}_y} \quad (18)$$

we rewrite the second through fourth describing equations as

$$\rho - \hat{F}_x = v'_x \quad I\omega + \hat{F}_y \sin \gamma - \hat{F}_x \rho \cos \gamma = I\omega' \quad v'_y + \omega' \sin \gamma = -e(1 + \omega \sin \gamma) \quad (19)$$

The fifth equation for the cases of sliding, no sliding or pivoting during impact become

$$\text{for sliding } \hat{F}_x = \mu \hat{F}_y \quad \text{for no sliding and pivoting } \omega' = -v'_x \quad (20)$$

As expected, the resulting describing equations are much simpler in non-dimensional form. It should be noted that because \bar{v}_y is a negative quantity, all of non-dimensional velocities and angular velocities have a different sign than their dimensional counterparts.

We now proceed to solve the describing equations for the unknowns. One can easily accomplish to do this by means of solving five linear equations for five unknowns. However, we can also accomplish this in closed form, by means of manual substitution. This process involves several algebraic substitutions and we only list the results here. We simplify the problem by assuming that the initial angular velocity of the container is negligible, so $\bar{\omega} = 0$. This assumption is realistic because the angular velocity of the container immediately after impact is far higher than the initial angular velocity.

4.1 Solution for the Case of Sliding at Point of Impact

Neglecting the initial angular velocity of the container, the relation for the impact velocity equation becomes

$$\omega' \sin \gamma = -e \quad (21)$$

and the other equations of impact become

$$1 + \hat{F}_y = v'_y \quad \rho - \hat{F}_x = v'_x \quad I\omega + \hat{F}_y \sin \gamma - \hat{F}_x \rho \cos \gamma = I\omega' \quad \hat{F}_x = \mu \hat{F}_y \quad (22)$$

Defining the dimensionless parameter

$$a = \frac{\sin \gamma - \mu \cos \gamma}{I} \quad (23)$$

and solving for the unknowns we obtain the solution for the case of sliding of the point of impact as

$$\hat{F}_y = -\frac{a(1+e)}{1+a \sin \gamma} \quad \hat{F}_x = \mu \hat{F}_y \quad v'_x = \rho - \mu \hat{F}_y \quad v'_y = 1 + \hat{F}_y \quad \omega' = a \hat{F}_y \quad (24)$$

4.2 Solution for the Case of No Sliding at Point of Impact

For the case of no slip (but bouncing in the vertical direction) the solution is a bit more complex. We again assume that the initial angular velocity of the container is negligible. The governing equations are

$$1 + \hat{F}_y = v'_y \quad \rho - \hat{F}_x = v'_x \quad I\omega + \hat{F}_y \sin \gamma - \hat{F}_x \rho \cos \gamma = I\omega' \quad \omega' \sin \gamma = -e \quad \omega' = -v'_x \quad (25)$$

Carrying out the algebra we obtain the solution for the angular velocity immediately after impact as

$$\omega' = -\frac{(1+e)\sin\gamma + \rho\cos\gamma}{I+1} \quad (26)$$

and

$$v'_x = -\omega' \cos\gamma \quad v'_y = -e - \omega' \sin\gamma \quad \hat{F}_x = \rho - v'_x \quad \hat{F}_y = v'_y - 1 \quad (27)$$

4.3 Solution for the Case of Pivoting at Point of Impact

In this case, the container pivots about the point of impact and the impacting point has zero velocity in both the horizontal and vertical directions immediately after impact. The solution for this case can be obtained by setting $e = 0$ in the previous case. Or, we can compare angular momentum about the impact point. The result can be shown to be

$$\omega' = -\frac{\sin\gamma + \rho\cos\gamma}{I+1} \quad (28)$$

and

$$v'_x = -\omega' \cos\gamma \quad v'_y = -\omega' \sin\gamma \quad \hat{F}_x = \rho - v'_x \quad \hat{F}_y = v'_y - 1 \quad (29)$$

5 Relating the Different Cases

We consider two types of cases when dealing with the impact equations and their solution: First, we can solve the problem of given initial conditions on the speed, angular velocity, and drop orientation, as well as the coefficients of friction and of restitution, we solve for the velocities and angular velocity immediately after impact. Or, given the initial conditions and measured data from immediately after impact we estimate the impact parameters.

When solving for the conditions immediately after impact we do not know which set of equations to use, as at that point we do not know whether there is sliding or not. In such cases, one can first assume that there is no sliding. Once one obtains the expressions for the impulsive forces, one checks the ratio of $\frac{\hat{F}_x}{\hat{F}_y}$. If this quantity is less than the coefficient of friction, then assuming that there is no sliding is correct. If, on the other hand, the ratio of the impulsive forces is greater than the coefficient of friction, this means that the available friction is not sufficient sustain no sliding and we have to consider the case of sliding.

From the simple analysis above, we conclude that the case of no sliding at the instant of impact requires higher levels of friction. Similarly, one can determine whether there is pivoting at the instant of impact or not based on the coefficient of friction.

When simulating the impact equations, one has to determine whether there is sliding or no sliding at the instant of impact. To determine this, we use the following procedure:

1. Begin with the assumption that there is no sliding and use Eqs.(26)-(27) to calculate the parameters after impact.
2. The horizontal impulsive force (friction force) should be such that it is less than or equal its maximum value. Compare \hat{F}_x with $\mu\hat{F}_y$. If $\hat{F}_x \leq \mu\hat{F}_y$ then the no sliding assumption is correct, as the horizontal impulsive value is less than its maximum value. If not, then the horizontal impulsive force that is needed is larger than the maximum frictional force than can be sustained. Hence the container slides. Use Eqs.(24) to calculate the after impact parameters.
3. Alternatively, one can begin with the assumption that the container slides during impact and obtains the impact parameters using Eqs.(24). Then, the validity of this assumption is tested by calculating the horizontal velocity of the impact point using the after impact horizontal and vertical velocities of the center of mass, as well as the angular velocity, to see if the calculated velocity is indeed greater than zero.

6 Three-Dimensional Impact

While the two-dimensional impact formulation is sufficient for most types of calculations (we select the x direction as the velocity direction of the falling container) we consider here the three-dimensional equations of impact.

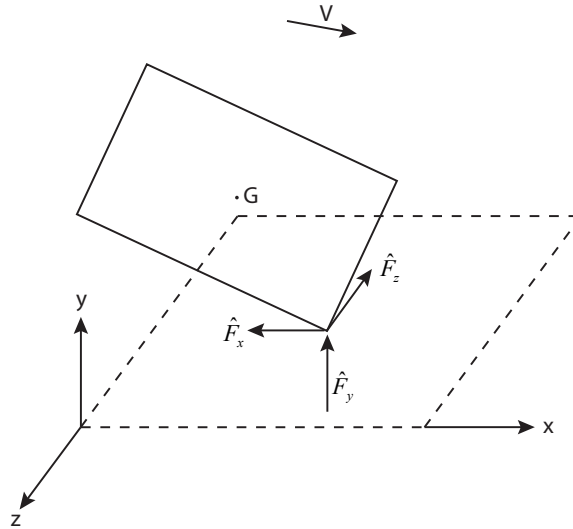


Figure 3: Three-Dimensional Impact

Suppose select our fixed coordinate system so that we have a container with horizontal and vertical velocities after impact. In this case, during impact the container is acted upon by three

forces, as shown in Fig. 3: The vertical impact force, \hat{F}_y , which is perpendicular to the plane of impact (xz plane) and two horizontal impulsive forces, \hat{F}_x and \hat{F}_z , which constitute the friction forces. In addition, we have three translational velocities (velocity components of the center of mass) and three angular velocities to find. We hence have a total of nine parameters to calculate, which necessitates that we develop nine equations that describe the impact. The first six equations come from the dynamics:

- Three equations for the translational velocities

$$m\mathbf{v}_G + \hat{\mathbf{F}} = m\mathbf{v}'_G \quad (30)$$

where $\mathbf{v}_G = v_x\mathbf{i} + v_y\mathbf{j} + v_z\mathbf{k}$ are the velocity components of the center of mass and $\hat{\mathbf{F}} = \hat{F}_x\mathbf{i} + \hat{F}_y\mathbf{j} + \hat{F}_z\mathbf{k}$ is the impulsive force vector. Note that \hat{F}_x and \hat{F}_y are impulsive friction forces.

- Three equations for the angular momentum balance

$$[I_G]\{\omega\} + \{\hat{M}_G\} = [I_G]\{\omega'\} \quad (31)$$

where $[I_G]$ is the inertia matrix of the container, $\{\omega\} = [\omega_x \ \omega_y \ \omega_z]^T$ is the angular velocity vector and $\{\hat{M}_G\}$ is a column vector describing the impulsive moment generated about the center of mass

$$\hat{\mathbf{M}}_G = \mathbf{r}_{G/C} \times \hat{\mathbf{F}} \quad (32)$$

Note that, because we are using a fixed coordinate system xyz , and the inertia matrix is constant only when we consider a coordinate system fixed to the body, the inertia matrix here changes with the orientation of the container.

We need three more equations to solve for the nine impact parameters

$$v'_x, v'_y, v'_z, \omega'_x, \omega'_y, \omega'_z, \hat{F}_x, \hat{F}_y, \hat{F}_z$$

These three conditions come from the impact condition. One equation is associated with the coefficient of restitution and the velocities of the impact point before and after impact

$$\mathbf{v}'_P \cdot \mathbf{j} = -e\mathbf{v}_P \cdot \mathbf{j} \quad (33)$$

The remaining two equations are related to whether there is sliding or no sliding at the point of impact. To deal with the sliding scenario, one can proceed by defining a tangential direction t , in the plane of motion. We denote the velocity of the impact point in the plane of motion by \mathbf{v}_H and express it as

$$\mathbf{v}_H = (\mathbf{v}_P \cdot \mathbf{e}_t)\mathbf{e}_t = \mathbf{v}_P - (\mathbf{v}_P \cdot \mathbf{j})\mathbf{j} = v_H\mathbf{e}_t \quad (34)$$

where $v_H = \mathbf{v}_P \cdot \mathbf{e}_t$ is the horizontal speed of the impact point. It follows that whether there is sliding or not, the component of the velocity in the horizontal plane perpendicular to the tangential direction is zero. Defining this direction as the normal direction n , with unit vector \mathbf{e}_n , we have $\mathbf{v}_P \cdot \mathbf{e}_n = 0$. This relation holds true before impact as well as after impact, so

$$\mathbf{v}'_P - (\mathbf{v}'_P \cdot \mathbf{j})\mathbf{j} - (\mathbf{v}'_P \cdot \mathbf{e}_t)\mathbf{e}_t = \mathbf{v}'_P \cdot \mathbf{e}_n = 0 \quad (35)$$

which constitutes our second impact equation. To get the third equation, we need to consider the scenario of whether there is sliding or no sliding along the tangential direction. As shown in Fig. 4, the impulsive friction force \hat{F} is in the tangential direction. If there is sliding, then the total friction force is equal to its maximum possible value, or

$$\hat{F} = \sqrt{\hat{F}_x^2 + \hat{F}_z^2} = \mu \hat{F}_y \quad (36)$$

If there is no sliding during impact, then the horizontal velocity immediately after impact is zero, or

$$\mathbf{v}'_P \cdot \mathbf{e}_t = 0 \quad (37)$$

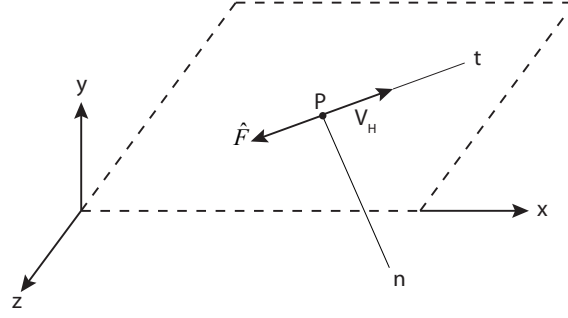


Figure 4: Impulsive Frictional Force

The resulting nine equations are all coupled to each other and are impossible to solve by hand. Using a symbolic manipulator to solve these equations yields very lengthy results that are impossible to interpret, so a simple numerical analysis of solving nine equations and nine unknowns is the preferred procedure.

As in the two-dimensional case, one has to determine whether there is sliding or no sliding at the instant of impact. We again begin with the assumption of no sliding, calculate the impulsive forces and check to see if the impulsive friction forces are less than the maximum value they can have, or

$$\sqrt{\hat{F}_x^2 + \hat{F}_z^2} \leq \mu \hat{F}_y = \mu \hat{N} \quad (38)$$

If not, we use the equation corresponding to sliding.

The above equations assume that the coefficient of friction on the plane motion is the same in each direction. If not, we need to consider more than one friction coefficient.

We have conducted simulations of the impact in three-dimensions and the results follow the results we have obtained in the two-dimensional case, with little additional information learned from the three-dimensional case, especially when there is horizontal speed involved. For this reason, we will proceed with the two-dimensional analysis when we consider in the next section the tumbling of the container after impact.

7 Tumbling after Impact

As we saw in the previous sections, the impacted container may have both translational and rotational velocities after impact. The magnitude of these quantities depend on the drop conditions (height, horizontal speed, coefficient of friction, coefficient of restitution), as well as the angle with which the container makes contact with the impact surface. The question is what happens to the container immediately after impact.

Because the container has some angular velocity, we expect it to tumble in the air and then make another impact. We have observed from our simulations that if there is no horizontal speed of the container before impact, even though the container may develop some horizontal speed, the speed is not very large and the subsequent impact absorbs most of the remaining energy in the container. To understand this scenario better, let us consider Fig. 5, where a container dropped without a horizontal velocity and no angular velocity makes contact at point A . The impact force \hat{F}_y is upward, which creates a clockwise angular velocity ω' . The clockwise angular velocity creates a velocity at point A in the negative x direction and hence the impulsive friction force \hat{F}_x is in the positive x direction. Hence, the resulting horizontal velocity of corner A is in the x direction.

The container tumbles in the air. If the tumbling amount is small, the container makes second contact at point B , even though if the impulsive force \hat{F}_y is large, it may make contact at point C or D . As discussed earlier, all these results depend on the initial conditions of the drop (impact velocity, orientation of the container). Our analytical simulations and experimental observations show that if the container is dropped without a horizontal velocity, then the container makes two or at most three additional impacts. All of these impacts are very small in magnitude, so that in essence all one needs to be concerned with is the initial impact, as far as damage analysis and failure of the container are concerned. The main goal of a tumbling analysis is to understand how much the container travels after initial impact, especially when it is dropped with an initial horizontal velocity.

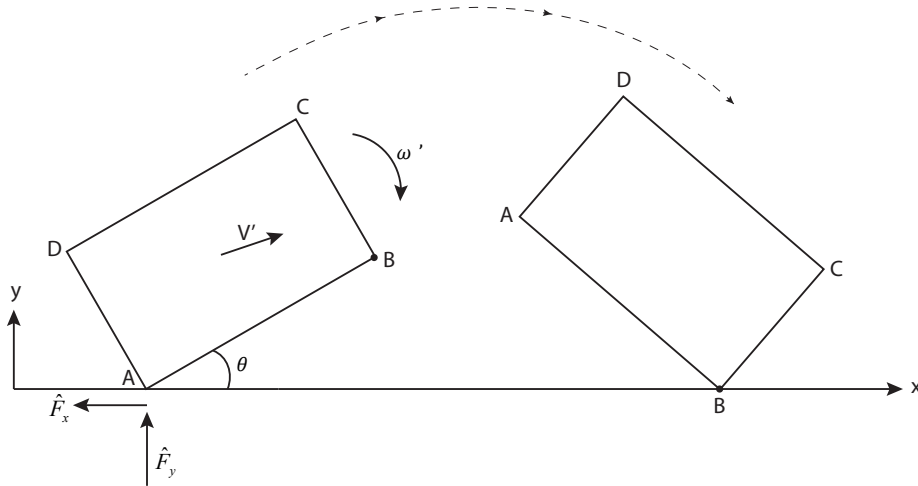


Figure 5: Tumbling after Impact

The situation is different when there is horizontal speed involved. In that case, the impact condition is always sliding at the instant of impact and the container tumbles and rolls for a much longer period of time.

We have added a module to our impact simulation model that calculates when the container makes the second and subsequent impacts. A typical simulation result of the tumbling is shown in Fig. 6.

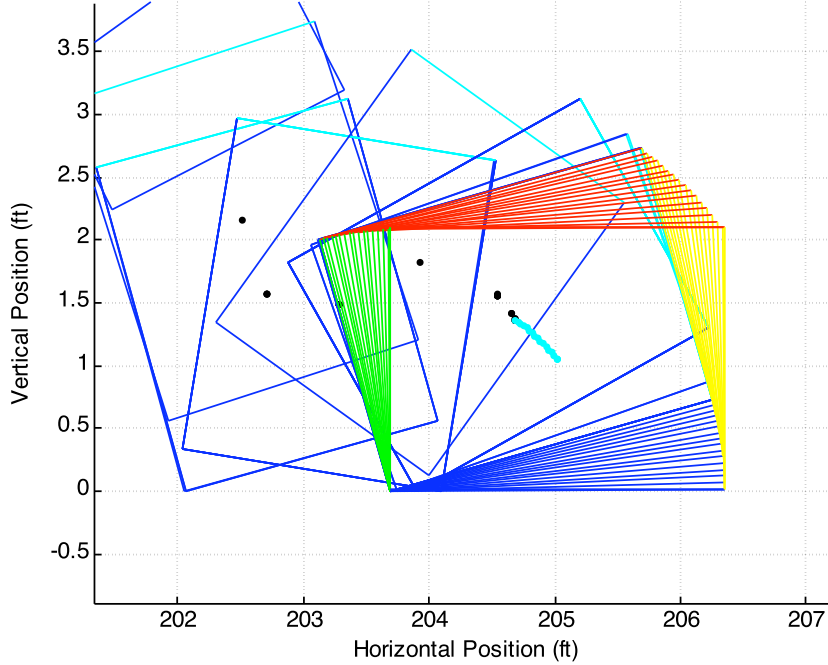


Figure 6: Simulation of Tumbling

Using estimated values for the impact parameters coefficient of restitution $e = 0.25$ and friction coefficient $\mu = 0.7$, we ran several simulations. Figures 7 and 8 give the impact data for two situations, one a 50 ft drop and the other a 65 ft drop of a 100 lb container, whose dimensions we discussed in previous appendices. The figures compare the distance traveled versus horizontal speed when the containers are released from a moving vehicle (labeled Release Velocity in the figures). The figures also compare the horizontal distance travelled by the containers while they are in the air.

As can be seen, for the drop angles shown, where θ is marked in Fig. 5, the distance traveled varies almost linearly with the horizontal speed. Interestingly, when the drop angle is positive we have larger distances of tumbling, as opposed to negative drop angles. This can be visually verified from Fig. 5, as when the drop angle is positive the impulse force provides an angular velocity in the direction of tumbling and the reverse happens for negative angles.

As the drop angle becomes smaller, indicating a near horizontal orientation of the container

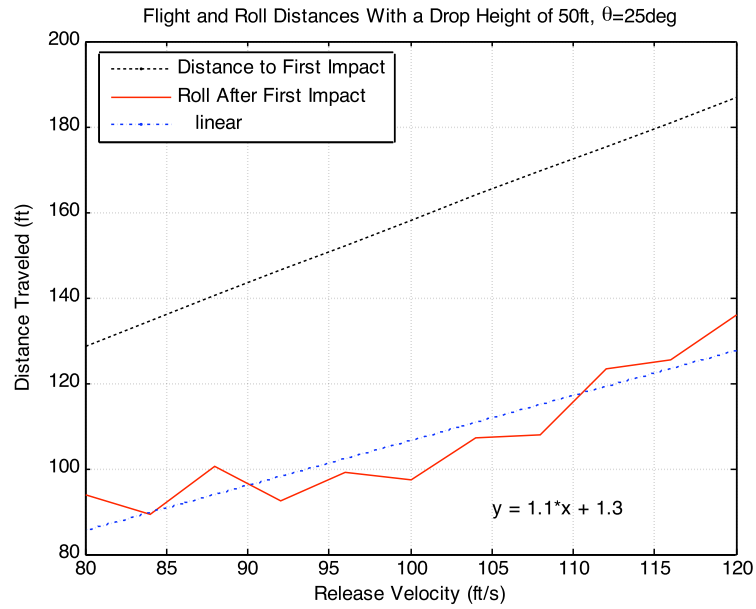


Figure 7: Tumbling Distances after Impact

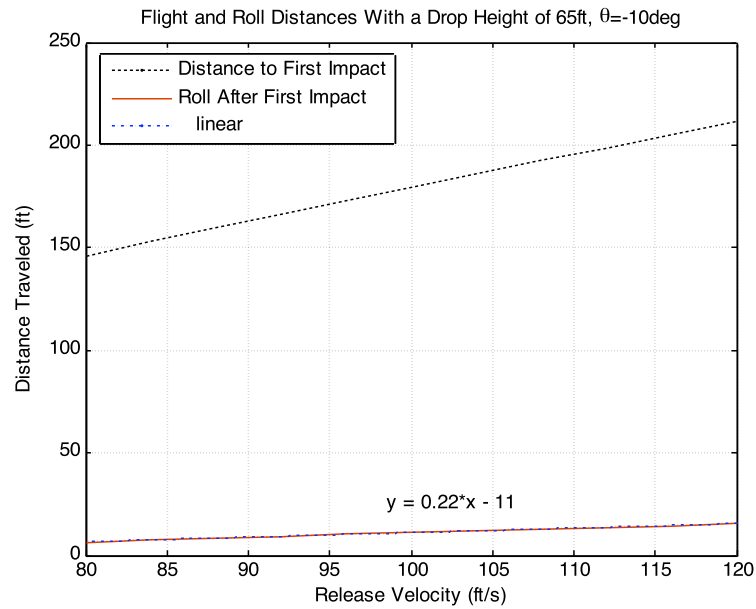


Figure 8: Tumbling Distances after Impact

at time of impact, the tumbling distances do not vary linearly with the horizontal speed but have a random nature, as seen in Fig. 9. Of course, a near zero tumbling distance indicates a mathematically possible but physically unrealizable case of the impact energy being dissipated at the instant of impact. We have not seen any example to this in our experimental analysis, indicating that under certain conditions, and especially when the drop angles are very small, our mathematical model is not accurate. It should be noted that we are using a very simple model here, in order to be able to gain some insight and draw some simple conclusions.

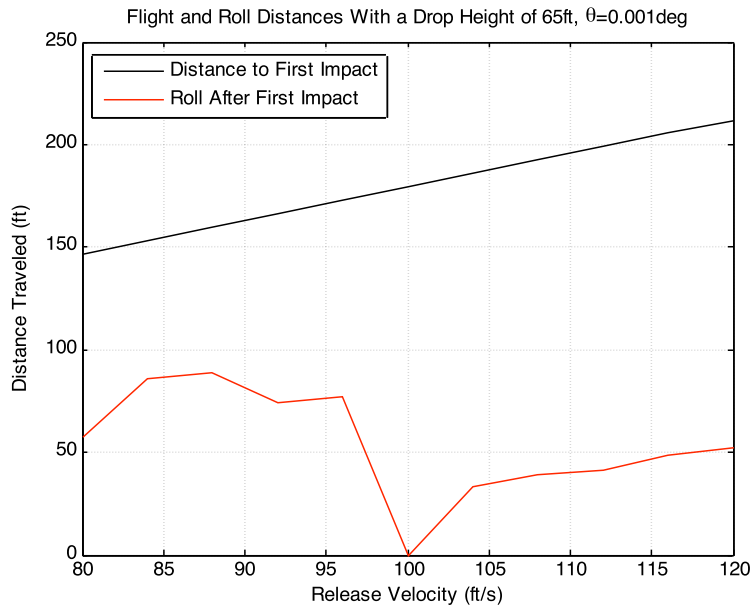


Figure 9: Tumbling after Impact, Near Horizontal Orientation

On the other hand, when we compare experimental data and analytical data for, say drop angles of $\pm 25^\circ$, we see close correlation between the two. A statistical analysis was conducted by the Logistics Innovation Agency on the tumbling distances based on drop height and speed, and a linear correlation was found with horizontal velocity. This result closely matches our results. This linear analysis did not consider correlation with drop angles, as it was difficult to determine drop angles from video of the drops and subsequent tumbling.

In order to estimate the roll distance, given the drop height, we have conducted simulations of tumbling distances as a function of drop angles and horizontal velocities. The simulated drops and subsequent tumbling were averaged to come up with an expected value of the roll distance. We used this analysis to estimate the coefficients of friction and restitution. The simulation results closely match experimental results. It is not easy to come up with an empirical formula that estimates the roll distance as a function of height and horizontal speed. Because the tumbling impact equations and plots are very lengthy, we are including those results as a separate paper at the end of this appendix.

8 More on Impact with Horizontal Speed

In our research on impact of containers that are dropped from a height, we have considered two types of initial conditions:

- The container is dropped from a height with no initial horizontal speed. This is the case when the container is dropped from a crane or from a hovering helicopter. As a result, when the container makes contact with the ground it only has a vertical velocity. We are ignoring any small amount of horizontal velocity generated by wind.
- The container is dropped from an airplane or from a moving helicopter. As a result, when the container makes impact it has both a horizontal and vertical velocity.

It follows that when dropped from the same height, the container that has an initial horizontal velocity will have a higher total velocity than the container dropped with no horizontal velocity. Assuming that the vertical velocities are the same at impact (these values may change somewhat due to the aerodynamics), the presence of horizontal velocity increases total velocity and adds to the energy.

It would appear from this observation above that one would expect damage to the container to be much higher when horizontal speeds are present. Yet, when we dropped containers from moving helicopters, we did not observe any such phenomenon. Comparing the helicopter drop experiments with experiments involving drops from cranes we observed the following:

- In most cases, damage was less when horizontal speeds were involved.
- Increasing the horizontal speed of the containers had the effect of slightly reducing the amount of damage.

These two observations are contrary to what one would expect. In order to understand these observations we need to look at what happens during impact. Fig. 10 below shows the impact forces that result of the impact of an object with horizontal speed. In essence, the impact point moves, as impact takes place.

To get a general idea, let us consider an impact with a horizontal speed of 60 ft/sec. From our accelerometer measurements (albeit taken with no horizontal speed), the duration of impact is about 1/100 seconds. Putting the two numbers together, we estimate the distance travelled by the impact force as $d = v\Delta = 60/100 = 0.6$ ft. Hence, vertical the impact force is applied over a distance of 0.6 ft, rather than being applied to the same point.

The horizontal impact force, on the other hand, depends on the amount of friction between the container and the ground. It is well-known that the coefficient of friction becomes smaller when sliding (as compared to the static coefficient of friction), and that the coefficient of friction goes down even further as the relative speed of the sliding surface becomes faster.

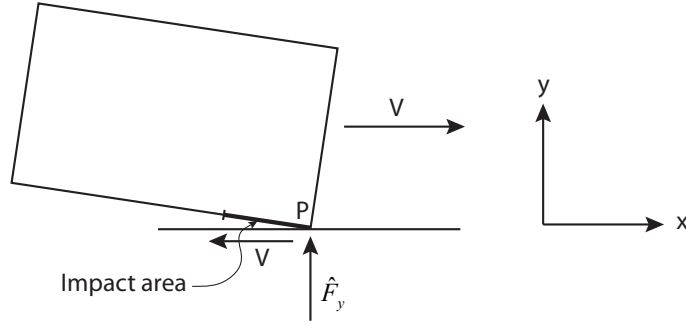


Figure 10: Impact with Horizontal Speed

Our analytical results, literature search, as well as our observations from actual drop tests indicate that as the horizontal speed is increased we have more sliding, hence the following results:

Table 1: A Comparison of Different Conditions and the Resulting Effect

Condition	Result
Higher levels of friction	Higher horizontal force
Higher horizontal speed	Lower amounts of friction, lower horizontal force
Lower horizontal speed	Higher amounts of friction, higher horizontal force

Based on these results, we have created the following table that summarizes expected damage levels for drop tests involving horizontal speeds as compared to no speeds.

There is also another argument that explains why there is less damage to the container when there is a horizontal speed. As Fig. 2 shows, because of the rotation of the container during impact the impact location on the container changes. This change in impact location during impact is larger when the impact point slides, as opposed to when it pivots. Hence, having a higher horizontal speed, which leads to more of a sliding effect than a pivoting effect, has the effect of changing the impact location and distributing the impact force over a greater area. The pivoting motion becomes more like rolling. This results in lower amounts of damage.

To observe this phenomenon more closely, consider a quarter circle that is making impact and rolling, as shown in Fig. 11. As a result of the rolling, the impact force is evenly distributed. Let us denote the magnitude of the impact force by \hat{F} . In Fig. 11b, the figure is rotated to show the geometry more. Let us also say that the amount of rotation during impact is θ_0 and it takes Δ amount of time, so the angular velocity during impact is $\omega = \theta_0/\Delta$ and we assume this quantity to be constant. Let us calculate the total impulsive force during impact. If the container does not change orientation during impact, the total force experienced by the impact location is $\hat{F}\Delta$. As the corner rotates, the magnitude impulsive force becomes $\hat{F} \cos \theta$. Integrating over the time of impact

Table 2: Observed Effects as Related to Initial Conditions

Initial Condition	Observed (and Expected) Damage
Dropped from same height onto hard flat surface	More damage when no horizontal speed is present Amount of damage decreases with increased horizontal speed
Dropped onto softer flat surface	Difference in damage for the cases of horizontal speed and no horizontal speed becomes less
Drop surface gets even softer	More damage when horizontal speed is involved, because of pivoting effect. Even though there is more energy absorption in the vertical direction, due to softness of surface, there is more pivoting and higher horizontal forces.
There is a vertical impediment (small or large wall or a mound) at impact point, or a rough surface	Much more damage when horizontal speed is present. The vertical impediment generates large horizontal impact forces which are larger than the pivot forces

we get

$$F = \int_0^{\Delta} \hat{F} \cos \theta dt = \frac{1}{\omega} \int_0^{\theta_0} \hat{F} \cos \theta d\theta = \frac{1}{\omega} \hat{F} \sin \theta_0 = \hat{F} \Delta \frac{\sin \theta_0}{\theta_0} \quad (39)$$

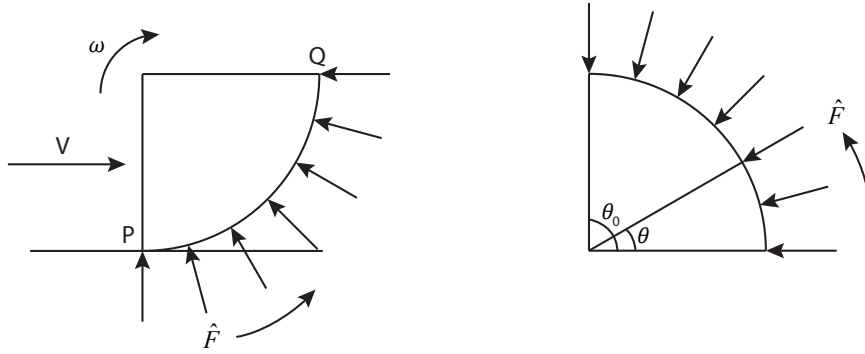


Figure 11: a) A Quarter Circle that is Rolling, b) Rotated View

For small values of θ_0 , $\frac{\sin \theta_0}{\theta_0}$ is almost 1, so total impact force does not change, but as θ_0 gets bigger, the magnitude decreases. This is another reason why the impact force is less when there is sliding and rolling of the container during impact.

In conclusion, having a horizontal speed during impact results in lower horizontal forces, which has the effect of reducing damage, because

- The impact point slides and rolls, instead of pivots, during impact, resulting in an impact force that lasts a bit longer and causes the impact force to be spread over a larger area

- The amount of friction becomes lower with increased horizontal speed, thus lowering the horizontal force
- The impact location on the container moves more, thus distributing the impact force over a larger area

It should be noted that the above results are valid only when the impact surface is flat so that the forces generated in the horizontal direction are sliding forces and not impact forces. If the impact surface is rough (in essence higher amounts of friction), has stones, dead trees, or other vertical impediments, the reaction in the horizontal direction becomes one of impact as well, and this can increase the resultant impact forces to high levels. However, we have not observed this phenomenon at all during actual drop tests from a moving helicopter, indicating that the horizontal friction forces are strong enough to counter any impediments on the drop surface.

Appendix 4

VBA code for Bridge Setting

```
Sub CFG_PRE()
    Dim myConn As New ADODB.Connection
    Dim connectionString As String

    'For machines that have only Access2003, we have to use MS Jet provider.
    'If you have Access2007 on your machine, you can use Microsoft.ACE.OLEDB.12.0 as the
    provider.
    connectionString = "Provider = Microsoft.Jet.OLEDB.4.0;Data Source = C:\Documents and
    Settings\USERNAME\Local
    Settings\Apps\2.0\Data\ND4AO93W.0VD\RZ08BA32.KBH\aird..tion_d16aeb438fc48f5e_0001.0001_
    37a6bfd7209f173\Data\DESIGN_MANUFACTURING.mdb;Persist Security Info = True"

    Dim i As Integer

    myConn.Open (connectionString)

    Dim myRecordset As New ADODB.Recordset
    Dim mySQL As String

    myRecordset.ActiveConnection = myConn

    For i = 1 To 10
        'The following sql statement needs to be updated as it always reads roller design type id 1 and
        paper type id 1 currently. It is written this way for illustration purpose. When data are calibrated, it
        needs to be updated, so that it can read settings for the appropriate cushion.
        mySQL = "SELECT STEPPER_MOTOR_POSITION FROM [ROLLER_SETTING]" & _
        "WHERE ROLLER_DESIGN_TYPE_ID = '1' AND PAPER_TYPE_ID = '1'" & _
        " AND INSTALLED_POSITION =" & CStr(i)

        myRecordset.Open mySQL, , adOpenStatic, adLockOptimistic
        myRecordset.MoveFirst

        gTagDb("ROLLER" & CStr(i) & "_PRE").Value =
        myRecordset.Fields("STEPPER_MOTOR_POSITION").Value
        myRecordset.Close

    Next i

    myConn.Close

    Set myRecordset = Nothing
    Set myConn = Nothing

End Sub
```

Appendix 5

VBA code for (a) Cushion ID lookup dialog and (b) operator screen

(a) VBA code for Cushion ID lookup (USER FORM)

```
Private Sub CommandButton1_Click()  
    If TextBox1.Text = "" Then  
        MsgBox ("Please enter a valid design ID!!")  
        Exit Sub  
    End If  
    Dim ValidDID As Boolean  
    gTagDb("DESIGN_ID").Value = CInt(TextBox1.Text)  
    ValidDID = infeed.ThisProject.DesignID  
    If ValidDID = True Then  
        TextBox2.Text = gTagDb("C1_ID").Value  
        TextBox3.Text = gTagDb("C2_ID").Value  
        TextBox4.Text = gTagDb("C3_ID").Value  
    End If  
    If ValidDID = False Then  
        TextBox2.Text = ""  
        TextBox3.Text = ""  
        TextBox4.Text = ""  
    End If  
End Sub  
  
Private Sub CommandButton1_MouseDown(ByVal Button As Integer, ByVal Shift As Integer, ByVal  
X As Single, ByVal Y As Single)  
    gTagDb("RESET").Value = 1  
End Sub  
  
Private Sub CommandButton1_MouseUp(ByVal Button As Integer, ByVal Shift As Integer, ByVal X  
As Single, ByVal Y As Single)  
    gTagDb("RESET").Value = 0  
End Sub  
  
Private Sub CommandButton2_Click()  
    If OptionButton1.Value = True Then  
        gTagDb("CUSHION_ID").Value = gTagDb("C1_ID").Value  
    ElseIf OptionButton2.Value = True Then  
        gTagDb("CUSHION_ID").Value = gTagDb("C2_ID").Value  
    ElseIf OptionButton3.Value = True Then  
        gTagDb("CUSHION_ID").Value = gTagDb("C3_ID").Value  
    Else  
        MsgBox ("Please select a cushion!!")  
        Exit Sub  
    End If  
  
    Me.Hide  
  
End Sub  
  
Private Sub CommandButton3_Click()  
    Me.Hide
```

End Sub

Private Sub UserForm_Click()

End Sub

(b) VBA code for Operator screen

Sub Init()

 gTagDb("CUSHION_ID").Value = 0

 gTagDb("C_QUANTITY_COUNTER").Value = 0

 gTagDb("NO_OF_LAYERS_COUNTER").Value = 0

 gTagDb("DESIGN_ID").Value = 0

 gTagDb("PAPER_TYPE_ID").Value = ""

 gTagDb("C_LENGTH").Value = 0

 gTagDb("C_WIDTH").Value = 0

 gTagDb("C_THICKNESS").Value = 0

 gTagDb("CUSHION_IDENTIFIER").Value = 0

 gTagDb("POSITION_ID").Value = 0

 gTagDb("PARAM_DONE").Value = 0

 gTagDb("SENSOR_MSW").Value = 0

 gTagDb("SENSOR_LSW").Value = 0

 UserForm1.Show

End Sub

Function DesignID() As Boolean

 Dim myConn As New ADODB.Connection

 Dim connectionString As String

 connectionString = "Provider = Microsoft.Jet.OLEDB.4.0;Data Source = C:\Documents and

Settings**USERNAME**\Local

Settings\Apps\2.0\Data\ND4AO93W.0VD\RZ08BA32.KBH\aird..tion_d16aeb438fc48f5e_0001.0001_
37a6bfcd7209f173\Data\DESIGN_MANUFACTURING.mdb;Persist Security Info = True"

 myConn.Open (connectionString)

 Dim myRecordset As New ADODB.Recordset

 Dim mySQL As String

 Dim i As Integer

 myRecordset.ActiveConnection = myConn

 mySQL = "SELECT CUSHION_ID FROM [CUSHION]" & _
 "WHERE DESIGN_ID = " & gTagDb("DESIGN_ID").Value

 myRecordset.Open mySQL, , adOpenStatic, adLockOptimistic

 If myRecordset.RecordCount <> 0 Then

 myRecordset.MoveFirst

 For i = 0 To (myRecordset.RecordCount - 1)

 gTagDb("C" & CStr(i + 1) & "_ID").Value =

CInt(myRecordset.Fields("CUSHION_ID").Value)

 myRecordset.MoveNext

 Next i

 DesignID = True

 Else

```

        MsgBox ("Design ID does not exist!!")
        DesignID = False
    End If
    myConn.Close
End Function

Sub PARAM()
    Dim myConn As New ADODB.Connection
    Dim connectionString As String
    connectionString = "Provider = Microsoft.Jet.OLEDB.4.0;Data Source = C:\Documents and
Settings\USERNAMELocal
Settings\Apps\2.0\Data\ND4AO93W.0VD\RZ08BA32.KBH\aird..tion_d16aeb438fc48f5e_0001.0001_
37a6bfd7209f173\Data\DESIGN_MANUFACTURING.mdb;Persist Security Info = True"

    myConn.Open (connectionString)

    Dim myRecordset As New ADODB.Recordset
    Dim mySQL As String

    myRecordset.ActiveConnection = myConn

    mySQL = "SELECT
DESIGN_ID,C_LENGTH,C_WIDTH,C_THICKNESS,C_QUANTITY,PAPER_TYPE_ID,NO_OF_LAY
ERS,
ABSOLUTE_INDEXER_MOVE,RELATIVE_INDEXER_MOVE,POSITION_ID FROM [CUSHION]" &
- "WHERE CUSHION_ID = " & gTagDb("CUSHION_ID").Value

    myRecordset.Open mySQL, , adOpenStatic, adLockOptimistic
    If myRecordset.RecordCount <> 0 Then
        gTagDb("C_QUANTITY_COUNTER").Value =
CInt(myRecordset.Fields("C_QUANTITY").Value)
        gTagDb("C_QUANTITY_LESS_1").Value = CInt(myRecordset.Fields("C_QUANTITY").Value -
1)
        gTagDb("NO_OF_LAYERS_COUNTER").Value =
CInt(myRecordset.Fields("NO_OF_LAYERS").Value)
        gTagDb("NO_OF_LAYERS_LESS_1").Value =
CInt(myRecordset.Fields("NO_OF_LAYERS").Value - 1)
        'gTagDb("ABSOLUTE_INDEXER_MOVE1").Value =
CInt(myRecordset.Fields("ABSOLUTE_INDEXER_MOVE").Value \ 1000)
        'gTagDb("ABSOLUTE_INDEXER_MOVE2").Value =
CInt(myRecordset.Fields("ABSOLUTE_INDEXER_MOVE").Value Mod 1000)
        gTagDb("RELATIVE_INDEXER_MOVE1").Value =
CInt(myRecordset.Fields("RELATIVE_INDEXER_MOVE").Value \ 1000)
        gTagDb("RELATIVE_INDEXER_MOVE2").Value =
CInt(myRecordset.Fields("RELATIVE_INDEXER_MOVE").Value Mod 1000)

        gTagDb("DESIGN_ID").Value = CInt(myRecordset.Fields("DESIGN_ID").Value)
        gTagDb("PAPER_TYPE_ID").Value = CStr(myRecordset.Fields("PAPER_TYPE_ID").Value)
        gTagDb("C_LENGTH").Value = CDbI(myRecordset.Fields("C_LENGTH").Value)
        gTagDb("C_WIDTH").Value = CDbI(myRecordset.Fields("C_WIDTH").Value)
        gTagDb("C_THICKNESS").Value = CDbI(myRecordset.Fields("C_THICKNESS").Value)

```



```

gTagDb("POSITION_ID").Value = CInt(myRecordset.Fields("POSITION_ID").Value)

Dim temp As Double
temp = CDbl(myRecordset.Fields("C_LENGTH").Value)
gTagDb("SENSOR_MSW").Value = CInt(((30 - temp) * 1200) \ 1000)
gTagDb("SENSOR_LSW").Value = CInt(((30 - temp) * 1200) Mod 1000)

gTagDb("PARAM_DONE").Value = 1

.....

"Temporary chages for the demo on 06/10/2010
.....

If gTagDb("CUSHION_ID").Value = 19 Then
    gTagDb("CUSHION_IDENTIFIER").Value = 1
ElseIf gTagDb("CUSHION_ID").Value = 20 Then
    gTagDb("CUSHION_IDENTIFIER").Value = 2
ElseIf gTagDb("CUSHION_ID").Value = 21 Then
    gTagDb("CUSHION_IDENTIFIER").Value = 1
End If
.....

If (gTagDb("C_LENGTH").Value > 30 Or gTagDb("C_LENGTH").Value < 10) Then
    gTagDb("PARAM_DONE").Value = 0
    MsgBox ("Critical ERROR!!!\n\nCushion length should be between 10 and 30 inches!")
Else
    MsgBox ("***   Download complete!!   ***")
End If
Else
    MsgBox ("Cushion ID does not exist!!")
    gTagDb("PARAM_DONE").Value = 0
End If

myConn.Close

End Sub

Sub LoadUserForm1()
    UserForm1.Show
End Sub

```

Appendix 6

Machine Design

This Appendix is prepared by B. B. Basily

The machine design includes the design of individual units which are then assembled to make the final assembly of the machine. These units are listed below and their design details are given in Appendix 6.

- 1) The machine frame
- 2) The laminate hot melt glue unit
- 3) The laminating conveyor
- 4) The Web takeoff conveyor
- 5) The Web deflector
- 6) The web feed in rollers
- 7) The slab cutting unit
- 8) The slab holding unit
- 9) The slab measure to length/ positioning unit
- 10) The shuttle unit
- 11) The slab pick and place unit
- 12) The slab hot melt glue unit
- 13) The slab stacking unit
- 14) The pad labeling unit
- 15) The pad ejection Unit
- 16) The build in fork lift for loading the laminate feed roll stock
- 17) Construction an installation of built-in forklift for loading the core rolls
- 18) Design and construction of the sensor deploying unit for slab cut/pickup
- 19) The pneumatic operating circuit
- 20) The signal/power interface circuit
- 21) The PLC control box
- 22) The Parker 6K8 control box

A5.1 Design and Manufacture of the Machine Frame

The design and manufacture of the machine frame was based on the use of aluminum extrusion profiles the frame, constructed from heavy duty section profiles, provided rigidity and simplified assembly. After major design considerations the machine frame was capable of accommodating all operating units, with ease of modifications/ repositioning which resulted in an extremely compact machine. Design details of the frame with operating units attached is shown in Figure A5.1 and the assembled frame is shown in Figure A5.2

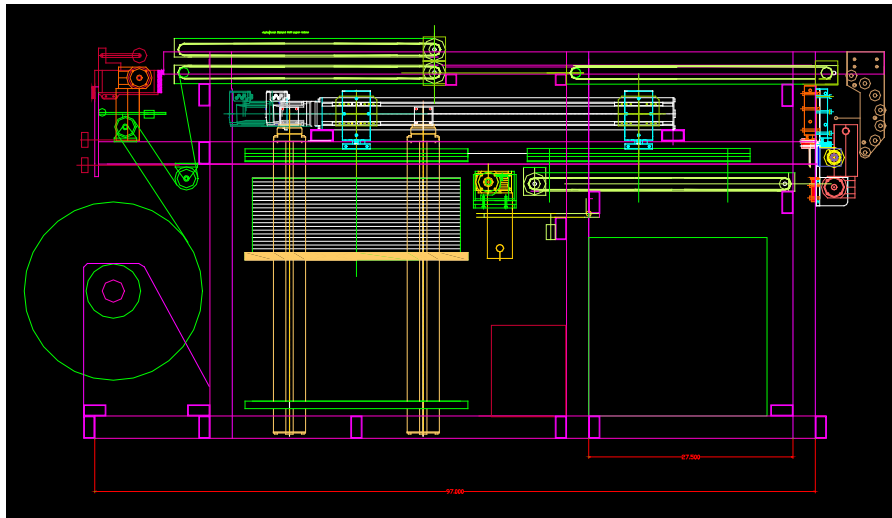


Figure A5.1. The machine frame with all operating units attached

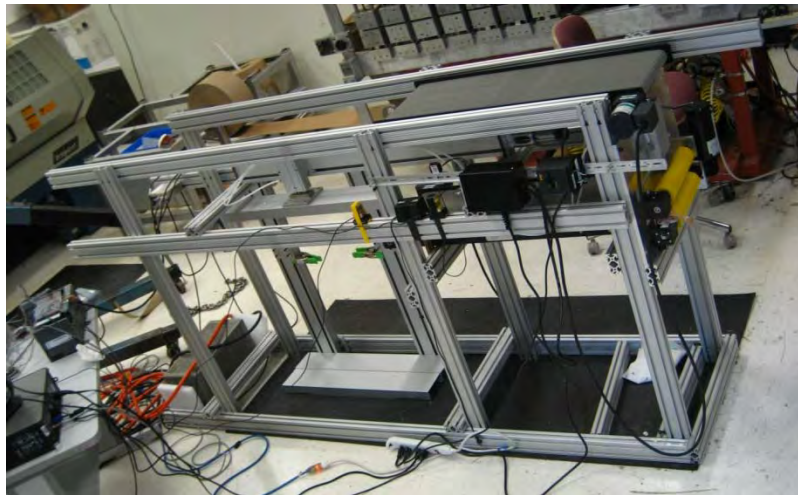


Figure A5.2. Photograph of the frame assembled from heavy duty Aluminum extruded profiles

A5.2 The design and manufacture of the core hot melt glue unit

The core glue unit (glue unit1) has been designed and manufactured based on a rotary applicator drum and a doctor blade. The roll applicator speed is being synchronized with the web speed for optimum glue application efficiency. The unit has a built in 1500 watt heating element, thermostatically controlled with overheating protection sensor. The unit is also provided with

electronic safety circuit that insures enabling power supply to the roll driving motor only when glue is in molten state, this eliminates motor burn out in case of failure in heating circuit.

The glue unit is also encapsulated in a box made of phenol laminate sheets which acts as a heat insulator and as an extra safety precaution against personal burns/injury by containing the heat generated from such large heating source. The unit is constructed from 0.5 inch aluminum plates with the 1.5 KW cast in heating element that forms an integrated part of the unit base, the design ensures uniform and efficient heat transfer for melting the glue at the required rate by avoiding the direct exposure of the hot melt glue to the heating element. Design drawing of the self contained hot melt glue unit is shown in Figure A5.3..

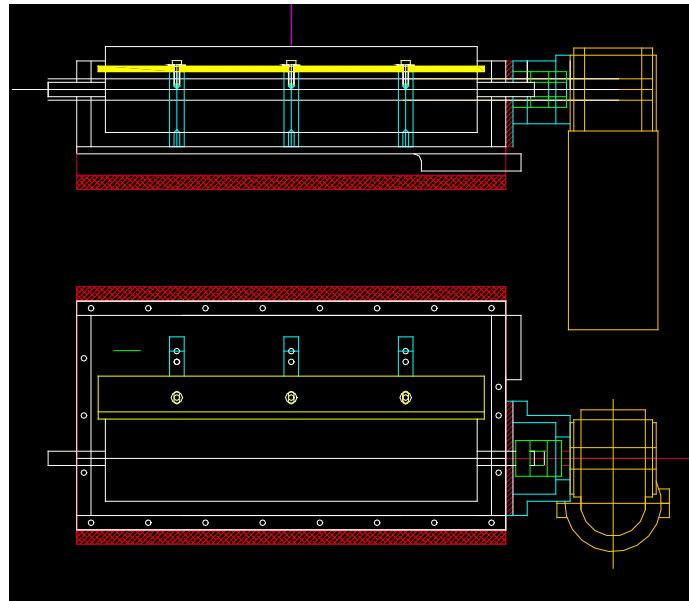


Figure A5.3. Design drawing of the Core Glue Unit (Glue Unit 1)

Additionally, the Doctor blade is supported on three peers that are fixed to the base to insure direct heat transfer to brass Doctor's blade. The blade which is fitted to the peers with set screws for adjusting the gap between the doctor blade and the knurled roll for controlling the amount of glue transferred to the paper core edges. The knurled roll is directly driven by a variable speed DC geared motor, with a chosen gear ratio that satisfies both the torque and speed requirements. Detailed design of the Doctor's blade/ peers assembly is shown in Figure A5.4.

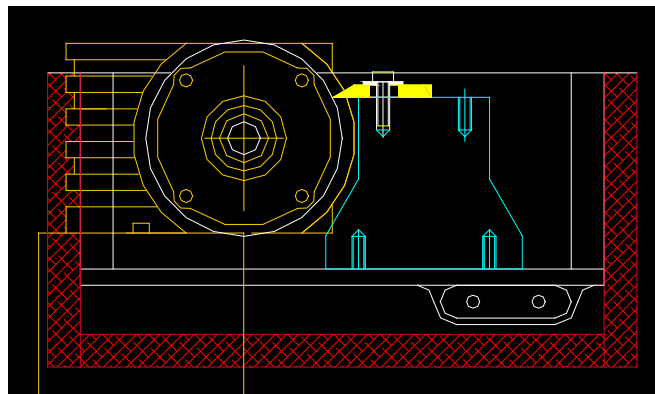


Figure A5.4. Detailed design of the Doctor's blade/ peers assembly

The knurled glue applicator roll is composed of a main body roll constructed from aluminum for efficient heat transfer, with press fitted steel shaft on roll both ends, for maximum rigidity. The shafts run in plain bearings with hot melt acting as the lubricant which ensures maintenance free operation.

The unit is also fitted with a swinging free rotating top roll that applies the required pressure for maintaining the contact between the core bottom edges and the glue roll, to ensure uniform coating of the core bottom ridges with the hot melt glue. Photograph of the core hot melt glue applicator is shown in Figure A5.5.

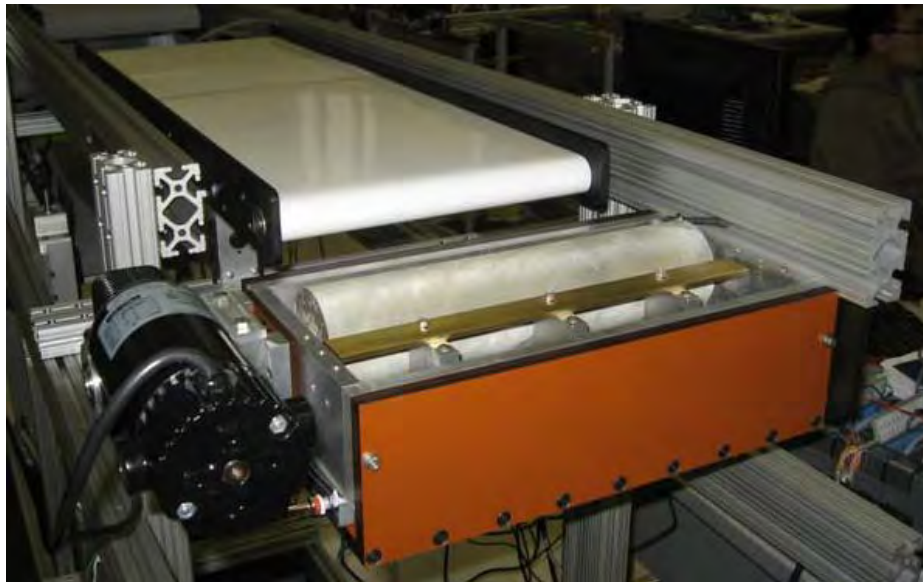


Figure A5.5. Photograph of the Core hot melt glue applicator

A5.3 The design and construction of the double conveyor laminating unit

This unit is positioned directly after the core hot melt glue unit, its function is to perform the laminating process by uniformly pressing the facing sheet material to the core that has hot melt glue already applied to its bottom contours. The design of this laminating unit has to fulfill the following three design requirements;

- a) Provide a controllable laminating speed that is synchronized with the speed of folded core emerging from the continuous sheet folding machine.
- b) Provide means of applying uniform pressure across the entire conveyor laminating area with means of varying this pressure from a minimum of zero to a maximum of 3.0 psi for a web width varying from 4 to 12 inch, and laminating speed up to 25 ft/min.
- c) Provide means of quick separating/engaging of the top and bottom conveyor at will. This is needed for the initial web feed in, and quick adjusting/ alignment of laminated core/facing during continuous non-stop operation. It also should provide a non adjustable separating gap that varies from a minimum of zero to a maximum of three inches.

All of the above design requirements were fulfilled by developing a pneumatically operated bridge suspension arrangement with spring loaded points. Assembly drawing of the double conveyor laminating unit is shown in Figure A5.6

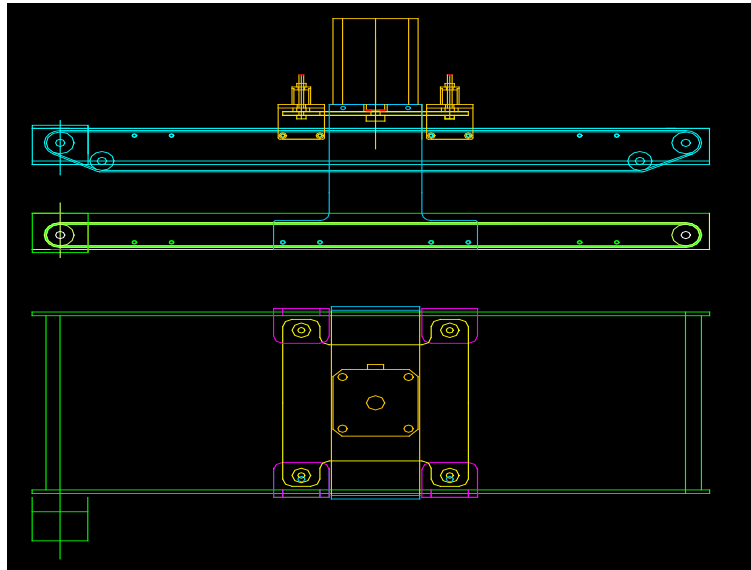


Figure A5.6. Assembly drawing of the pneumatically operated suspended bridge arrangement

The pneumatic circuit operating the unit top conveyor consists of a four inch diameter double acting compact cylinder, two three-way solenoid valves, two high precision pressure regulators, and two flow control valves, the upward stroke pressure is pre-adjusted to just lift up the upper conveyor to top end position.

The lower stroke pressure is adjusted to overcome the upward pressure plus the added psi requirements. Hence, for a 90 psi air supply and 40 lb top conveyor weight, a maximum laminating pressure of 0.3 psi is achieved which exceeds the practical requirements.

On the other hand, the design totally eliminates the dead weight effect of the top conveyor, thus allowing the application of a laminating pressures varying from zero to a maximum of 3.0 psi, This is very essential to avoid crushing of cores made of light paper weight.

To perform the laminating operation two identical servo motors fitted with reduction gear-heads were used, Speed synchronization relative to each other and with respect to the speed of the incoming folded core web are closed loop controlled by the Parker 6K8 controller

Both top and bottom conveyors are identical off-the-shelf units, however, an essential modification has been made on the top conveyor to achieve the zero gap requirements, by adding two extra rollers to the conveyor bottom surface, this enabled the conveyor belt to protrude downward and maintain contact with top surface of the lower conveyor. Photograph of the constructed unit is shown in Figure A5.7.

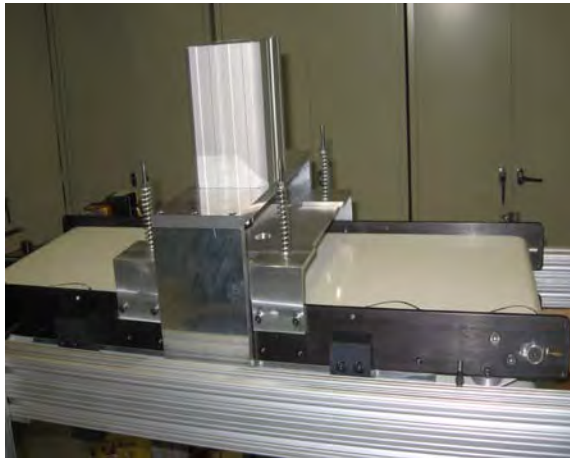


Figure A5.7. Photograph of the constructed Top Laminator unit

A5.4 The design and construction of the web takeoff conveyor

The web takeoff conveyor is positioned directly after the laminating conveyor and it serves the purpose of receiving the one sided laminated hot melt glued core from the laminating conveyor and transferring the web to the feed in roll unit, without stagnation/build up problems

The conveyor used, is off-the-shelf standard unit, Figure A5.8, fitted at the top rear end of the machine frame through 4 L shaped brackets that allows fixation of the unit with minimal modification. The conveyor is operated by 3 phase geared motor, which adjusts the belt speed by frequency converter.

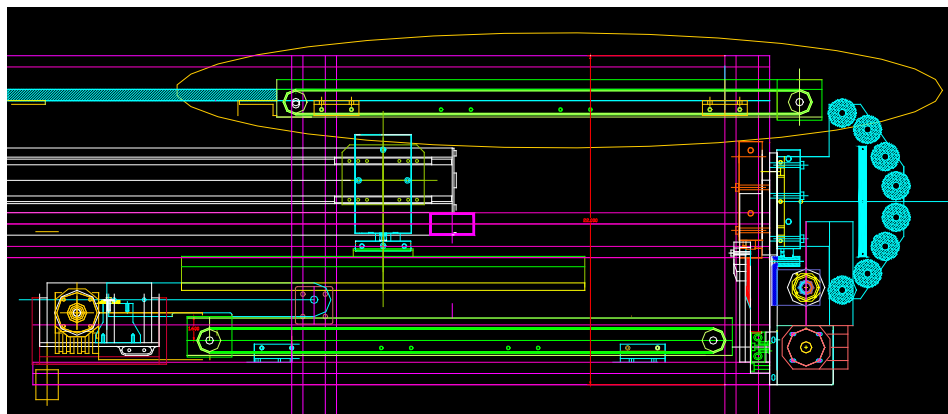


Figure A5.8. Web takeoff conveyor

The gap between the laminating conveyor and the web take off conveyor is covered by a flat platen to eliminate web sagging / trapping in between the two conveyors (see Figure A5.9)

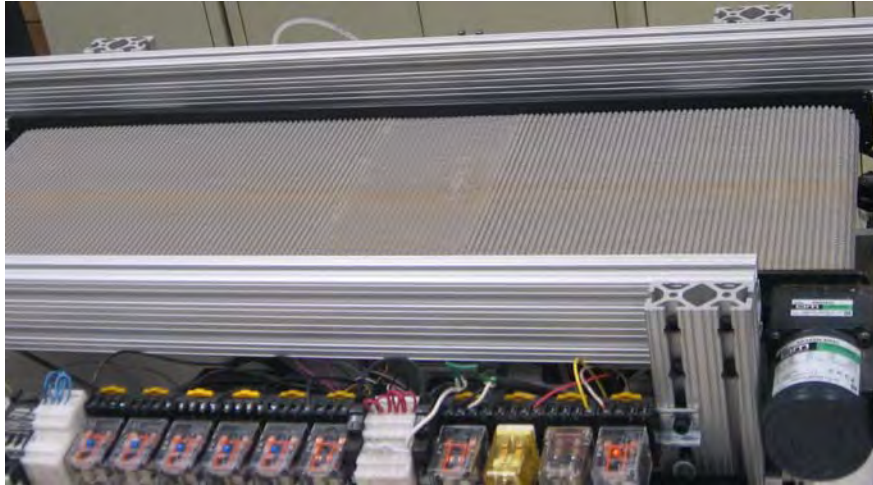


Figure A5.9. Web takeoff conveyor

A5.5 The web deflector unit

The web deflector, Figure A5.10, is used to deflect the incoming web by 180 degrees in order to enter the feed in rollers. It consists of set of free rotating rollers placed on a semicircular arc of 12 inch radius. The unit also has adjustable side platens, for web positioning and guiding through the feed in roller unit.

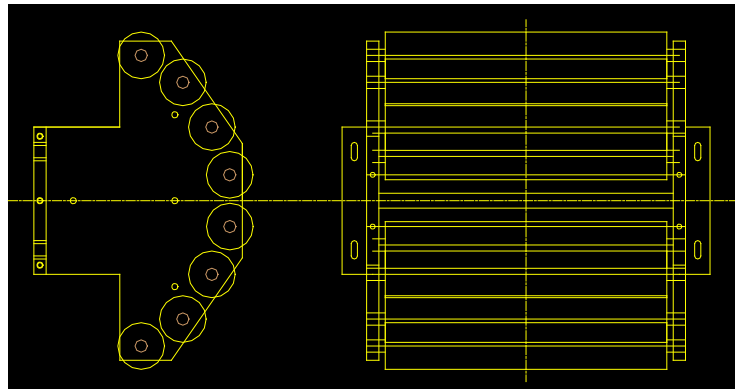


Figure A5.10. The web deflector guide platens

The free rotating rolls of the web deflector are off-the-shelf standard PVC coated conveyor roll, and the adjustable web guide platens slides on frame cross beam and locked in position by thumb screws. The web deflecting unit is shown in Figure A5.11.



Figure A5.11. The web deflector unit

A5.6 The web feed in rollers

The function of the nibbling roll unit is to feed the correct length of the incoming single sided laminated core web to be cut by the shearing unit, then glued to previous slab to form the final cushioning pad. For proper functioning of the feed in roll unit, both the top and bottom feed rolls should be power driven at same angular speed and opposite direction, they also should maintain a predetermined gripping force to eliminate slippage while preventing crushing of the folded core. Additionally the gap between the two rolls should be automatically adjustable to accommodate different web heights. All the above constraints were met by use of pneumatically operated variable gap roll arrangement as shown in Figure A5.12.

The unit is driven by a single 90 VDC geared motor, directly coupled to the lower feed roll, while the power is transmitted to the top roll through the gear train arrangement, A selected web feed speed up to 26 ft/min is set by variable speed controller driving the 40 rpm geared motor from main 115 ACV power supply

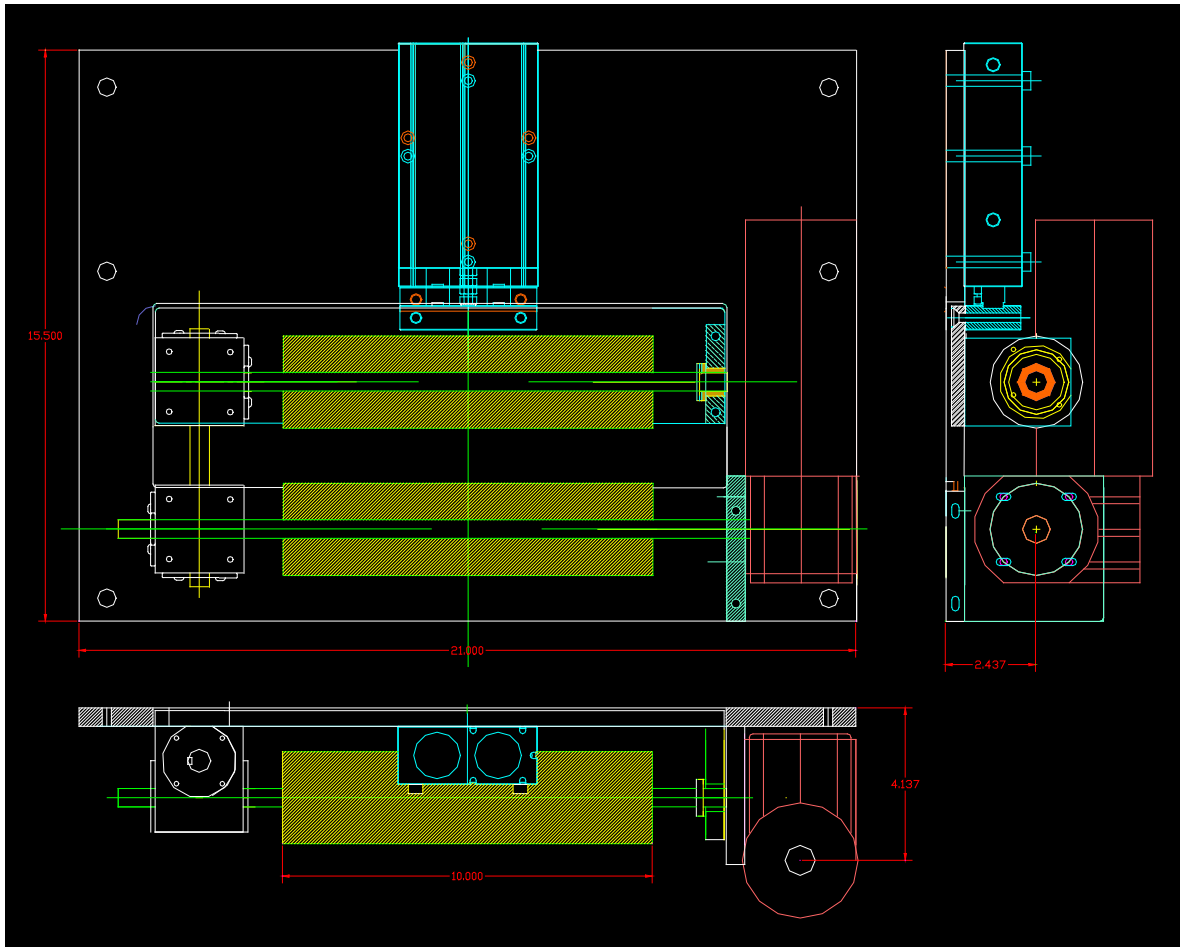


Figure A5.12. Design drawing of the nibbling roll feed unit

Speed synchronization of upper roller and lower roller through use of two right angle gearboxes and keyed shafting arrangement as shown in Figure A5.13.

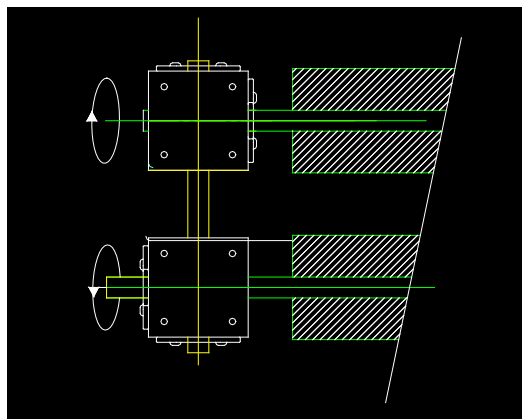


Figure A5.12. Feed rollers synchronization by two right angle gearboxes

The Feed roll unit design eliminated use of an extra stepper motor/drive/ control arrangement, separate mounting platform and simplified control by requiring only single initiating signal and enabled automatic adjusting for any web thickness up to 2 inch, it also Improved safety by blocking

the accesses to the shearing blade during cutting operation. Slippage, between the web and the rollers was eliminated by use of composite feed rolls coated with high friction polyurethane top layer, and application of controllable gripping force. Photograph of the feed in roll unit is shown in Figure A5.13



Figure A5.13. Photograph of the nibbling roll feed unit

A5.7 The Slab Cutting Unit

The slab cutting operation is performed by the shearing action between a fixed and a moving shearing blades, the moving blade is operated by a pneumatic actuator of predetermined impact speed, and blade also has an inclined shearing angle for progressive cutting action Figure A5.14.

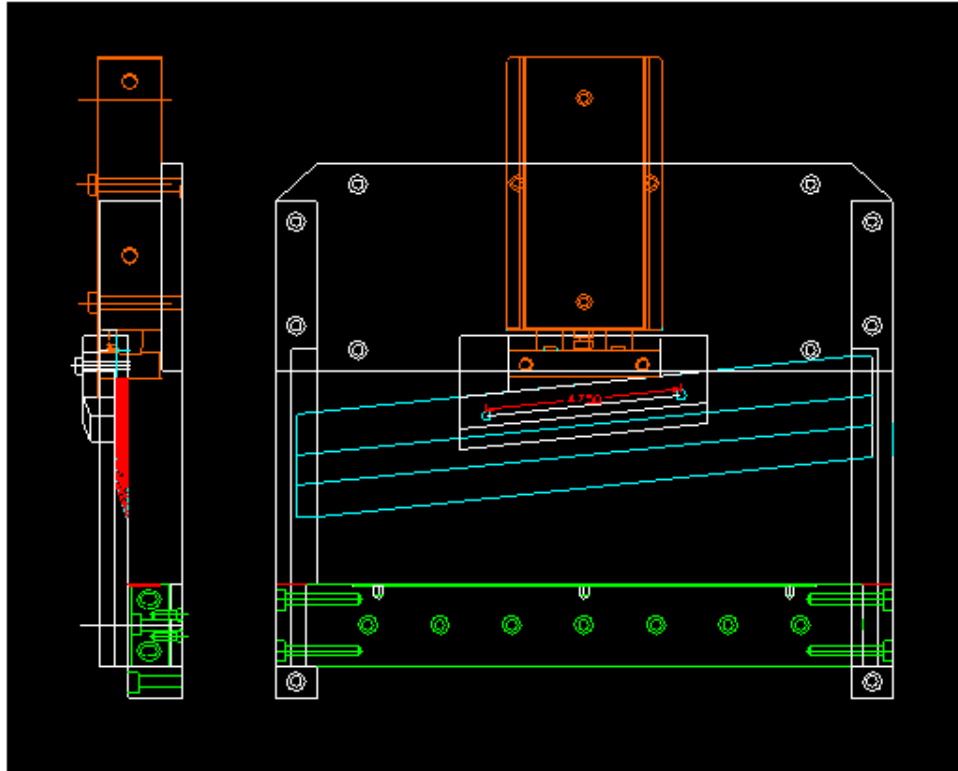


Figure A5.14. Cutting of the incoming web by shearing unit

The slab cutting unit is located directly after the feed rolls and operated pneumatically through a signal from the slab length measuring sensor. The operating pneumatic linear actuators will maintain the paper cutting blade in the upper position until receives the sensor signal then performs the following operation:

- a) The blade moves down cutting the slab of predetermined length from the web
- b) The blade moves up and waits for the progress of the nest slab signal.

The slab cutting unit has the moving blade inclined at 6 degrees angle for smooth cutting operation and also means of adjusting the blade cutting clearance enabling the unit to operate properly and provides clean cuts and smooth action, Figure A5.15..

An electronic circuit was also constructed, that enable the cutting operation to be initiated by a signal from the slab length measuring sensor. Upon receiving the 24V DC signal results in the following function occurs:

- a) The Feed in rolls stops immediately while maintain the hold of the incoming web
- b) The slab centering conveyor stops waiting for the web cutting operation
- c) The blade cuts a slab of predetermined length from the incoming web
- d) The cutting blade moves up and waits for the next slab signal.

- e) The slab maneuvering conveyor start moving to position the cut slab at the centre of the pick and place unit ready for transfer by the shuttle then stops



Figure A5.15. the slab cutting unit

To ensure personnel safety during maintenance operations, the operating circuit was fitted with a manual override shut off valve, Figure A5.16.

Figure2.16: Photograph of the web cutting unit,



Figure 2.17: The safety valve for operating the web cutting unit.

Figure A5.16. The manual override shut off valve,

A5.8. The slab holding unit

To ensure the uniformity and the stacking precision of the cut slabs, during the buildup of the pad, the incoming web should be held in place during cutting operation to eliminate any shifting /tilting, this has been achieved by the construction of web hold down unit Figure A5.17.

The unit consists of a pneumatic cylinder when actuated it forces a guided transverse beam to move down and clamps the web during the cutting operation, after cutting, it retracts upward to allow the conveyor to move forward and place the cut to size slab in the pickup position

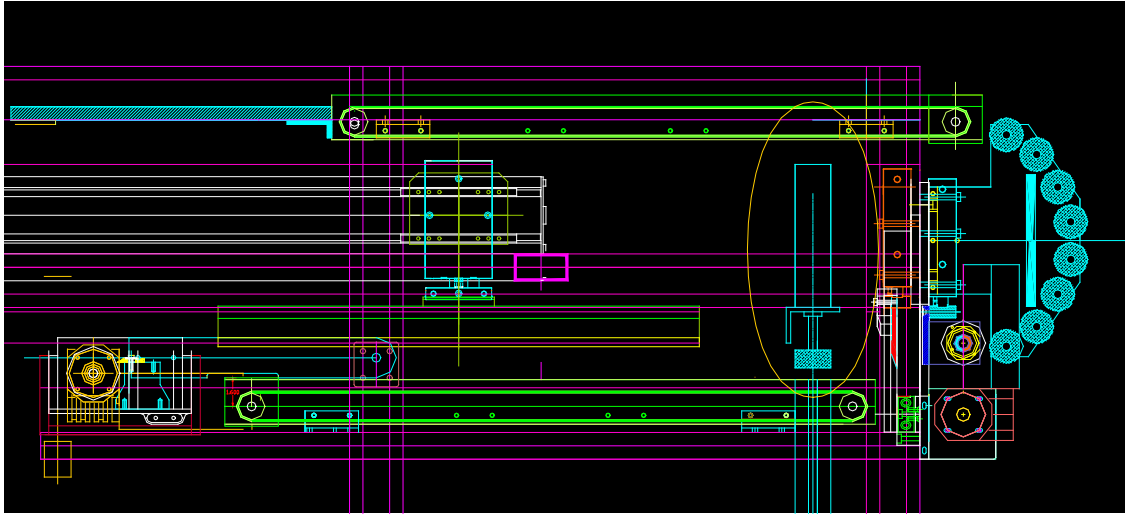


Figure A5.17. The slab clamping unit

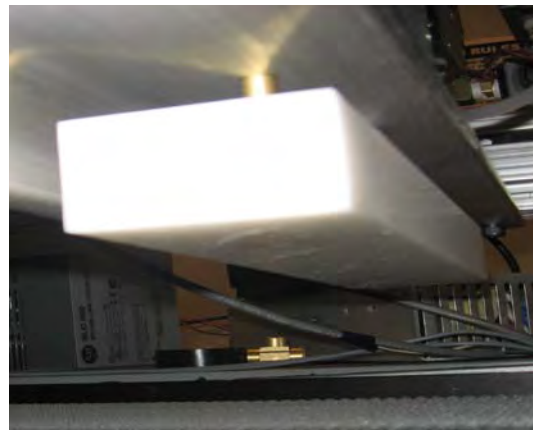


Figure A5.18. The slab clamping unit

A5.9 The slab measuring / positioning unit

The operation of slab cut to length from the incoming web, then properly positioned for pick up is achieved by an arrangement composed of two optical sensors and a transporting conveyor. This arrangement greatly simplified the controlling process of shuttle displacement of follow up operation of pick place of the slab, in that, it eliminates the need to adjust the shuttle stroke according to slab length, by prepositioning the slab to be picked up from its centre position regardless of its length. Figure A5.19

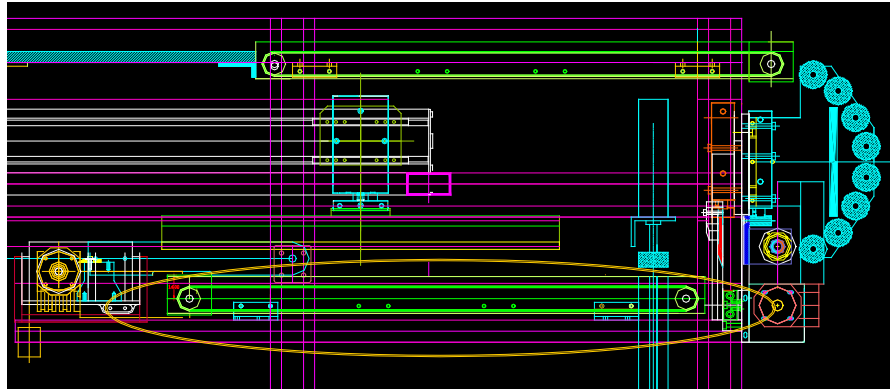


Figure A5.19. Position of transporting conveyor relative to the shuttle

When first optical sensor (slab measure to length sensor) senses the edge of incoming web, driven by the feed in rolls, the clamping pad descends and holds the web in position this action is immediately followed by the cutting operation to produce a slab of predetermined length. As the clamp holder moves up the conveyor moves the slab forward until its edge is detected by the second optical sensor (slab positioning sensor), this causes the conveyor to stop ready for slab pickup. The positioning of the second sensor is calculated based on the location of the first sensor and the length of the cut slab, which results in positioning the center of the cut slab in a fixed coordinate position ready for the pickup irrespective of slab length. This fixed position coincides with far end stroke of the shuttle (see Figure A5.20)



Figure A5.20. Transporting conveyor and the two optical sensors

A5.10 The shuttle

The shuttle unit arrangement performs the slab transporting/positioning operation. The unit is composed of a power screw linear actuator, fitted with a double cylinder pneumatic actuator vertically attached to the linear actuator moving carriage. The pneumatic actuator provides the ascending/descending movement of the pick and place platform operation, Figure A5.21.

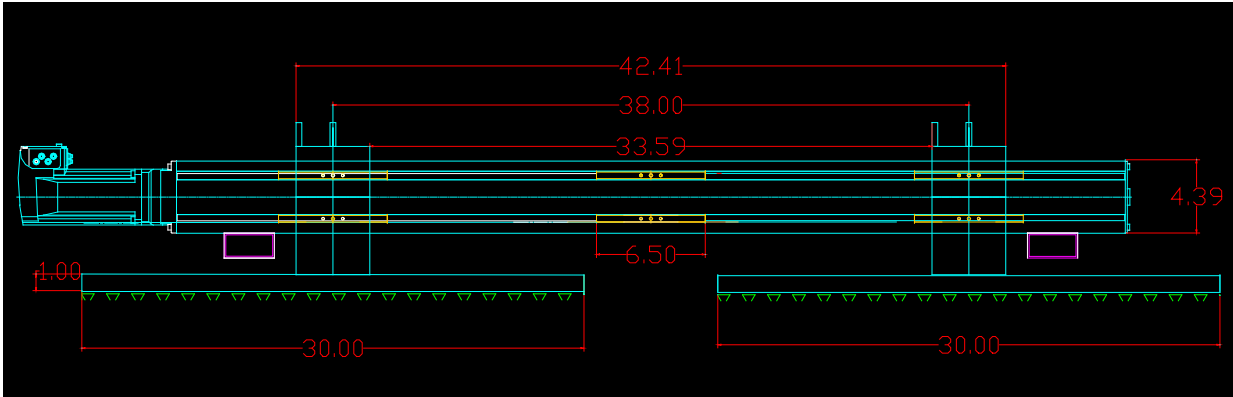


Figure A5.21. The shuttle unit arrangement

The use of power screw linear actuator in the design of the design of the shuttle arrangement provided precise movement, high reliability and ease of control, additionally, the use of the pneumatic actuator for pick up an place greatly simplified the control operation by providing automatic stroke adjustment required for the pick and place process. The shuttle driven by a PLC controlled servomotor, Figure A5.22.



Figure A5.21. Shuttle unit arrangement

A5.11 The slab pick and place unit

The slab pick and place unit consists of the vertically operated pneumatic actuator that carries the pressing platform that moves down to pick up the slab, then lifts the slab up, moves forward over the second hot melt glue applicator to coat the core bottom zigzagged ridges glue, then moves down to press/glue the slab on top of the previous one, thus gradually building the cushioning pad of a predetermined height based on the total number of slabs glued together. Figure A5.22.

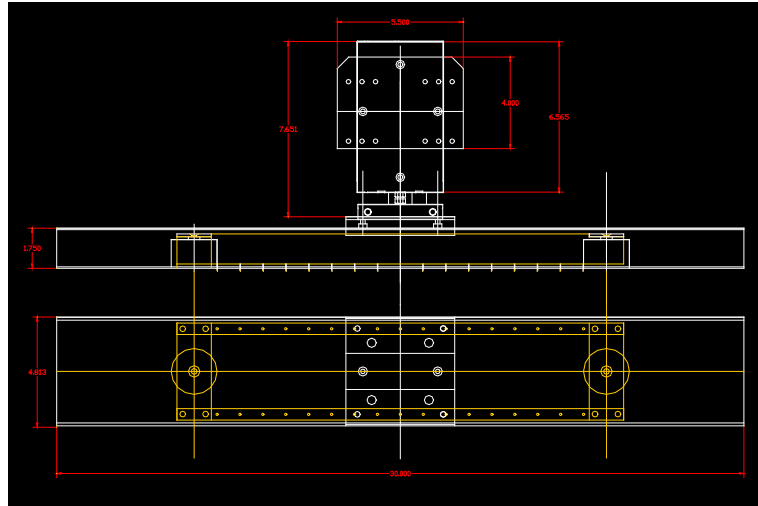


Figure A5.22. The slab pick and place unit

The novel slab pinch/retract nail system, developed by the author, replaces the traditional suction cup technique, with the advantage of eliminating both the slab slippage, and the use of cumbersome vacuum hoses/solenoids attachments, The slab pinch/retract nail system consists of two rows of needles pushed down/retracted by two compact pneumatic cylinders housed in the platform, Figure A5.23.



Figure A5.23. Slab pinch/retract nail system

A5.12 The slab hot melt glue unit

The slab gluing unit (the second glue unit) performs a selective gluing operation by applying a predetermined thickness of a hot melt glue to the tips of bottom side zigzagged ridges of the folded core structure using a hot melt roll applicator. The unit is similar to the first hot melt unit (the core glue unit).

However the method of transferring the glue to the slab differs, in that, the whole glue unit is lifted up to make contact with the bottom side of the slab, carried by the pick and place platform and passing over the glue unit. This is achieved by pivoting the glue unit and lifting it up by an adjustable stroke pneumatic cylinder, Figure A5.24.

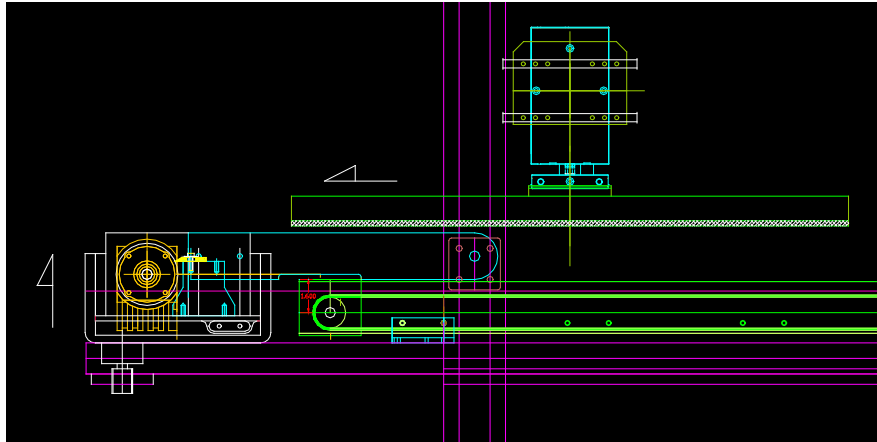


Figure A5.24. The slab hot melt glue unit

This technique enables slab selective glue application, which is essential to avoid gluing the constructed pad to the delivery platform by eliminating glue application to the first slab in contact with the delivery platform. Photograph of the unit is shown in Figure A5.25.

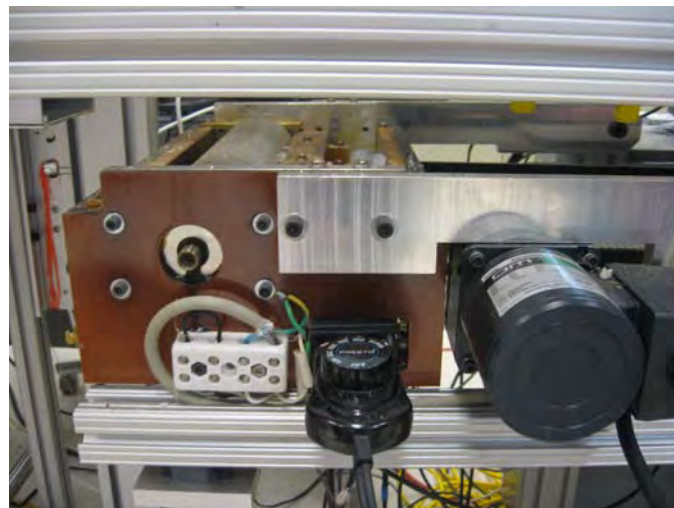


Figure A5.25. The slab glue unit

A5.13 The slab stacking unit

The slab positioning/pressing/gluing operation is also performed by the shuttle unit arrangement, in which the slab carried by the pick and place platform with glue already applied to the bottom ridges of its folded core surface and exactly aligned is then pressed down for it to be glued previous slab of the constructed pad.

As the slab being glued to the previous one the delivery platform descends an increment equal to the slab thickness thus creating a room for next slab application. This is achieved by the stacker unit which carries the delivery platform and consists of two linear actuators, with synchronized motion driven by a PLC controlled single servomotor operating the two power screws at the same speed, Figure A5.26.

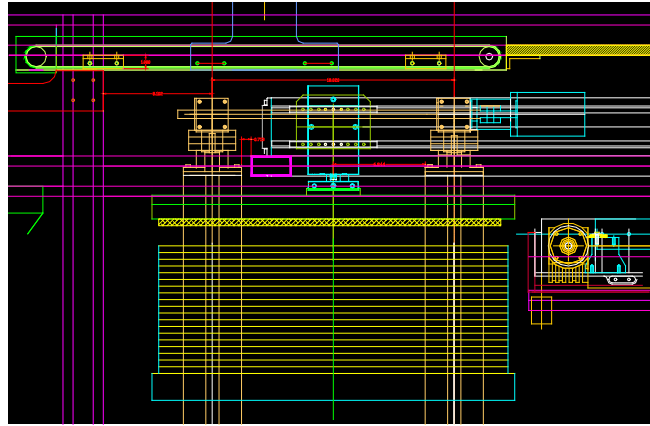


Figure A5.26. The slab stacking unit

As the pad build up is completed and ejected, the two actuators bring the delivery platform to its initial top position ready for the construction of the next pad, Photograph of the stacker unit is shown in Figure A5.27.



Figure A5.27. Slab stacking unit

A5.14 The pad labeling unit

The construction free airdrop subpack consists of three identical pairs of energy absorbing pads the dimension of each pair is determined by the software based on item dimensions, weight, fragility level drop height and air speed, accordingly they will vary in size, shape and dimensions. To facilitate the differentiation between these three pads for correct assembly of the subpack they have to be given distinctive marking, therefore a simple and an expensive labeler was developed for that purpose. Figure A5.28.

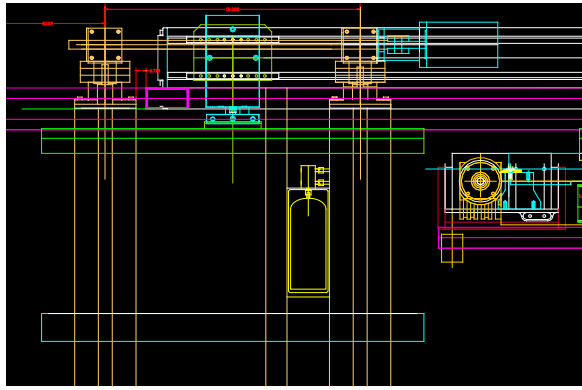


Figure A5.28. The pad labeling unit

The labeling unit consists of a miniature pneumatic cylinder when actuated it presses on knob of an off shelf paint spray can causing the nozzle to squirt a pre determined amount of paint forming a defined spot on the pad, Figure A5.29. Accordingly, the pair of the first type pad have one round paint spot, the second pair have two round paint spots, and the third pair have three round paint spots



Figure A5.29. The pad labeling unit

A5.15 The Pad Ejection Unit

The ejection operation is performed at the end of compellation of the formed pad and is conducted by the pneumatically operated ejecting cylinder, fitted at the frame back columns and facing the delivery platform, Figure A5.30. Upon pad completion the delivery platform descends to floor position, and the ejector platen, ejects the completed pad off the machine compartment, the delivery platform then moves to the upward position ready for the construction of the next pad.

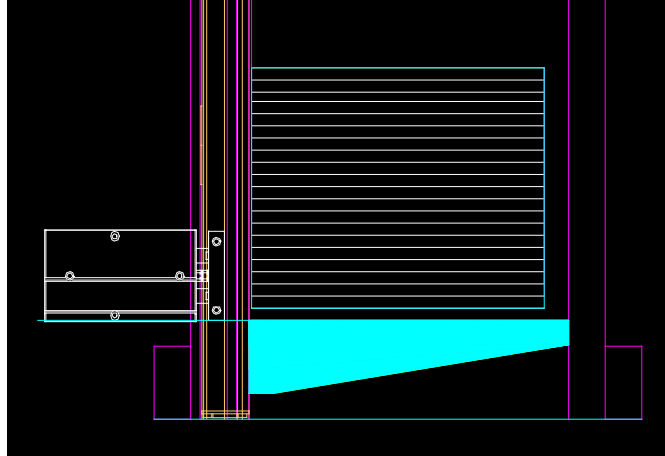


Figure A5.30. Pad ejection unit

The ejection unit consists simply of an ejection platen attached to a pneumatic cylinder of a non rotating cylinder rod. Upon activation the platen ejects the completed pad and immediately retracts to avoid crashing with the ascending delivery platform. Photograph of the unit is shown in Figure A5.31.



Figure A5.31. The pad ejection unit

A5.16 The build in fork lift for loading/Unloading the laminate feed roll stock

The build-in forklift for loading the laminate rolls was constructed and fitted to the machine, , Figure A5.32. It is successfully loading roll weighing up to 250 lb and with external diameter up to 36 inch, which was extremely difficult to load manually due to the compact space allocated for the laminate feed compartment, The built in forklift unit design enable it to operate in a very smooth manner and with ease of control by using an electrically operated an SKF force actuator manipulating the machine vertical pillars as a loading frame. Photograph of the fork lift is shown in Figure A5.33.

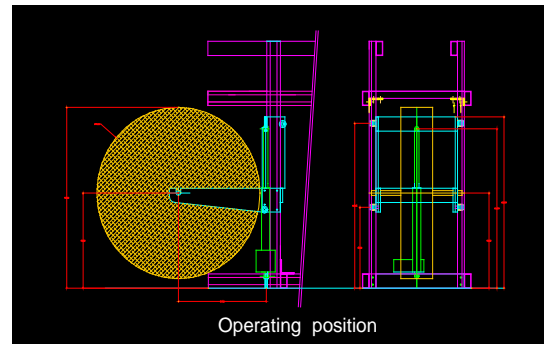
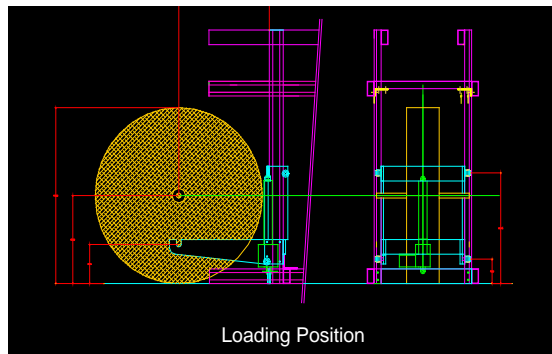


Figure A5.32. The built-in fork lift for loading/unloading Laminate rolls



Figure A5.33. The built-in fork in loading position

A5.17 Construction and installation of built-in forklift for loading the core rolls

A built-in forklift for loading the core rolls was designed, constructed and installed in the continuous folding machine stationed behind the pad making machine, and enabled the loading of the core heavy rolls with ease, simplicity and great saving in floor area.

The unit construction is similar to that of the built-in forklift of the laminating rolls, previously constructed and fitted in the pad making machine, however the detailed design differs in order to accommodate heavier core rolls weighing up to 400 lb, roll width up to 18 inches, and roll diameters

up to 42 inches. The design also overcome severe restrictions due to limited space allocated for the forklift underneath the pre-gathering rolls arrangement of the continuous folding machine.

The constructed forklift unit greatly simplified the loading of these heavy weight core rolls with ease and eliminated the need for the existing roll feeding station and the need for separate crane for lifting the rolls as shown in Figure A5.34

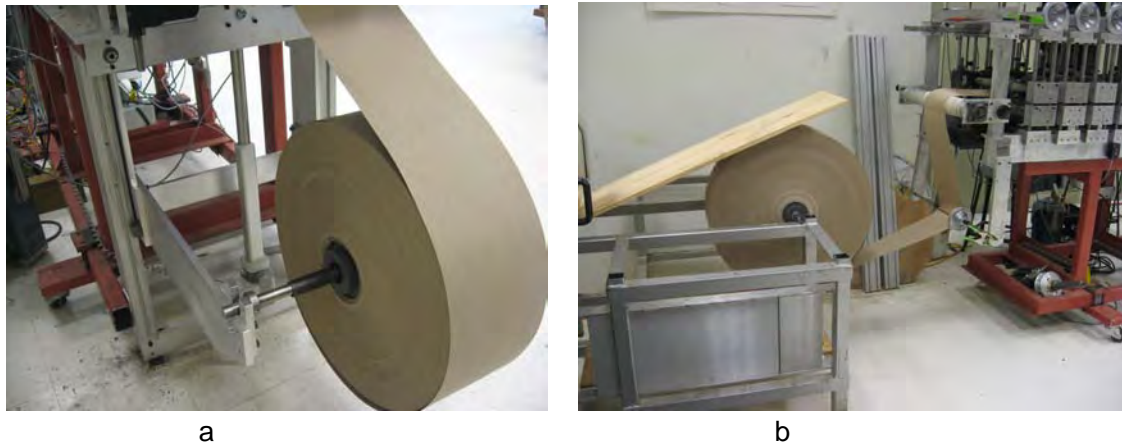


Figure A5.34. The constructed built-in fork lift

A5.18 Design and construction of the sensor deploying Unit for Slab Cut/pickup

The main function of this unit is to position two sensors in a pre-specified locations defined by the software, based on GUI data input and corresponding calculations that determine the required length of each pair of the three lengths of pads that form a sub-pack of given dimensions. Typical arrangement is the use of two separate linear actuators driven by stepper motors, where the first actuator carriage is fitted with a sensor for detecting the edge of the incoming web and placed at will at a distance from the paper shear equal to that of pad required length using a stepper motor.

Additionally the second actuator carriage is fitted with a second sensor for detecting the cut slab edge and placed at will at a distance equal to the half the length of the slab from that of the centre of the pickup platform, driven by the second stepper motor. An innovative design has been implemented where only one stepper driving motor position the two edge detecting sensors in the proper positions irrespective of the required slab length. This has been achieved by use of a left hand power screw driving a right hand power screw at half the speed through pair of gears with gear ratio of 1:2, resulting in driving the two carriages with sensors along a common slider.

The compact design provided a simple solution for slab cutting to measure and positioning operation, and eliminated the need for complicated driving system and the associated software, as shown in Figure A5.35.

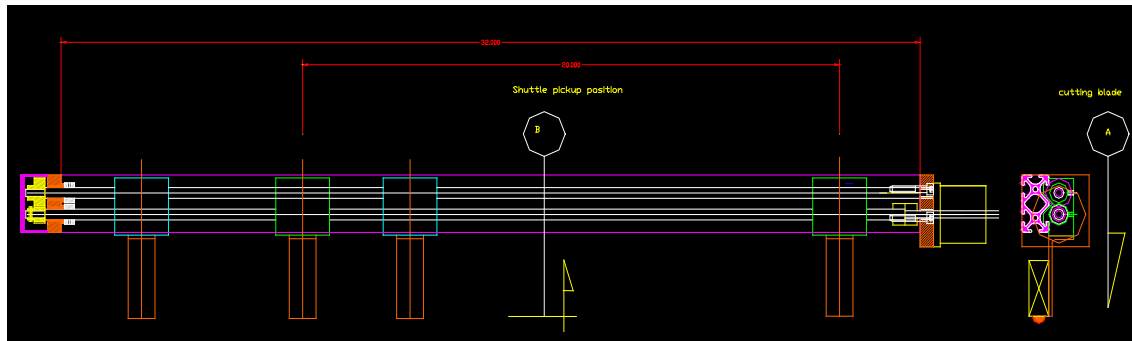


Figure A5.35. The sensors deploying unit for slab cut/pickup operation

Further simplification of the construction of the unit has been achieved through use of existing 20/80 extruded profiles as dual linear actuator guide for the moving sensor carriages. Detailed design drawing of the sensor deployment unit is shown in Figure A5.36, and photograph of the unit is shown in Figure A5.37.

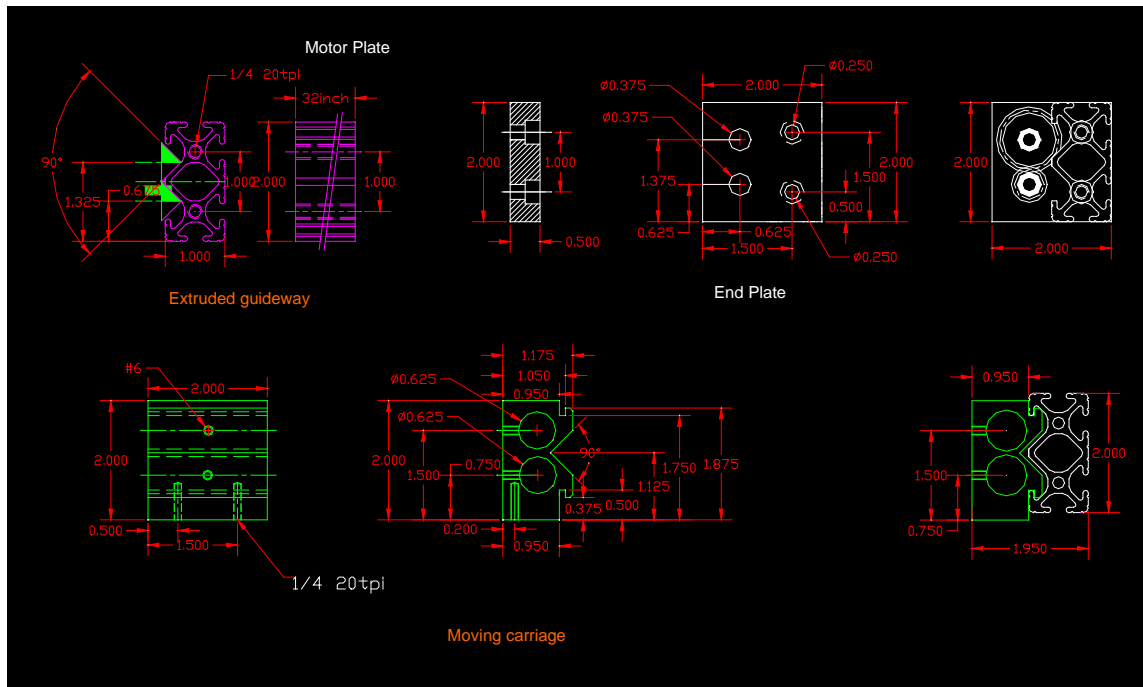


Figure A5.36. Detailed design drawing of the component of the sensor deployment unit

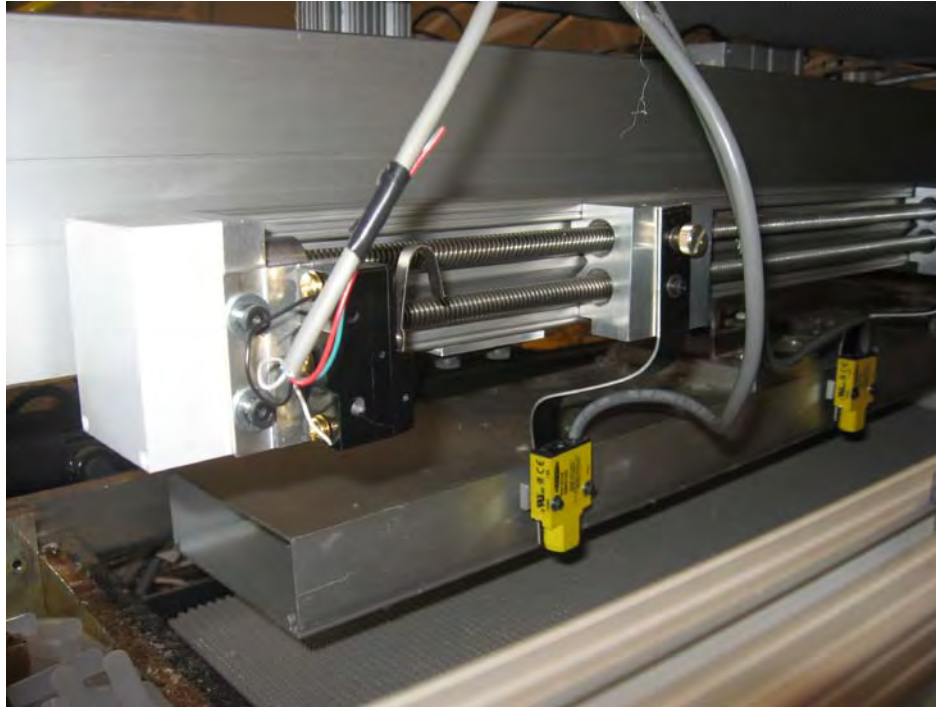


Figure A5.37. Photograph of the sensor deployment unit

A5.19 The pneumatic system

A pneumatic system has been designed and constructed, Figure A5.38, to operate the all the pneumatic cylinders of the machine modular units upon receiving 24VDC signal from the PLC control unit. The unit consists of solenoids, pressure regulators and flow rate control valves, which ensure each of the pneumatic actuator is operating with the required motion, speed, acceleration and applied force, the circuit operates the six pneumatic actuators to provide the following actions:

- The up and down motion of the top laminating conveyor
- The up and down motion of the feed nibbling rolls
- The up and down motion of the pick and place moving platen of the shuttle
- The up and down motion of the extending/retracting nails of pick & place moving platen
- The up and down motion of the labeling paint squirt action
- The forward and return motion of the ejector platen

The constructed pneumatic system enabled precise application of laminating pressure, varying from a minimum value of $\text{psi}=0$ by compensating for the weight of the top laminator, to a maximum laminating pressure of 3.0 psi over the entire laminating area, the appropriate gripping pressure for the nibbling rolls, the required pressure for slab gluing, enough force for nail penetrating/retraction, proper action for paint squirting and proper force and speed for ejecting of the finished pad.



Figure A5.38. Basic concept of the laminator unit

A5.20 The signal/power interface circuit

To operate all the above pneumatic actuators, the solenoid valves are activated by set of relays that deliver the proper high/low tension power source needed to operate these devices upon receiving the signal from the PLC controller. The circuit was also designed on the fail safe principle, in that the actuators resume safe positions in case of power failure, or sudden interruption of the operating cycle.

The circuit also operates the periphery units including the speed controllers of the core glue roll unit, the feed in nibbling rolls, the web take off conveyor, the slab positioning conveyor, and the slab glue roll unit.

The circuit is fitted with manual override for controlling, the up and down operation of the laminating conveyor, the slab cutting operation, the web feed in operation and the pick and place operation. Photograph of the signal/power interface circuit is shown in Figure A5.39.

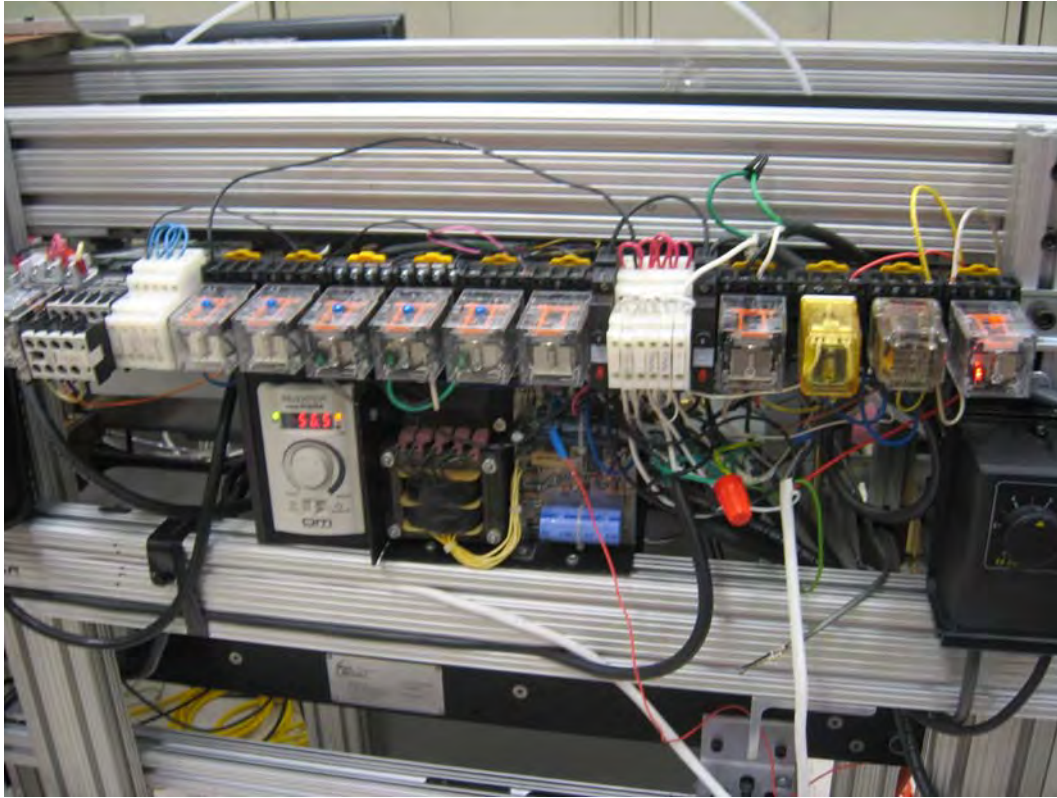


Figure A5.39. The signal/power interface circuit

A5.21 The PLC control box

The hardware of the PLC control unit for the machine has been partially constructed and fitted to the back of the machine frame, it consists of the following components:

- a) The PLC unit composed of : TTL unit, two servo modules, input and output modules
- b) The 5 VDC power Pack
- c) The servo drive for the shuttle
- d) The servo drive for the stacker
- e) The filter unit for the 220 VAC power supply for the two servo drives

The unit is housed in 24x20x8 inch steel enclosure attached to the back of the machine frame next to the 6K8 control unit cabinet. the unit receives input signals and forward output signals to drive the relay control unit which is housed at the front of the machine, The relay control unit drives the slab cutter, the feed roll, the hot melt glue unit, the ejector and labeling unit. The circuit diagram of the PLC control unit is shown in the Figure A5.40. Photograph of PLC control unit under construction is shown in Figure A5.41.

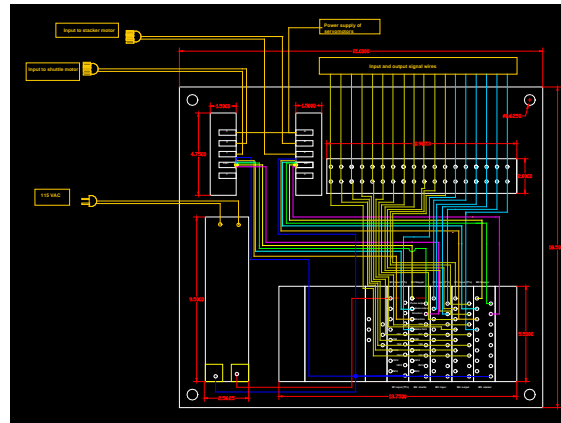


Figure A5.40. The circuit diagram of the PLC control unit

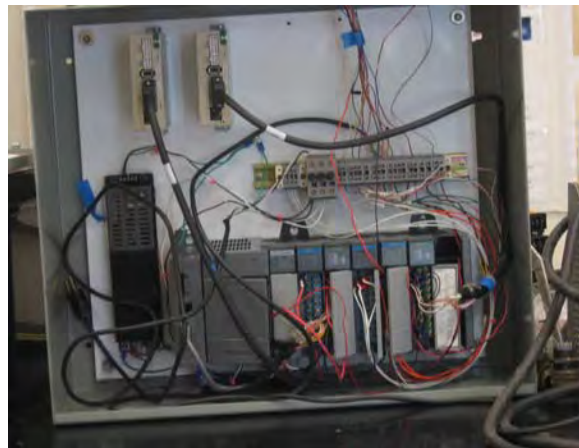


Figure A5.41. The constructed PLC control circuit under construction

A5.22 The Parker 6K8 control box

The hardware of the Parker 6K8 control unit consists of the following main components:

- a) The Parker 6K8 unit
- b) The 24 VDC power supply
- c) The 90 VDC drive for the main folding motor
- d) The 90VDC drive for the main pre-folding motor
- e) The servo drive for the laminator top conveyor motor
- f) The servo drive for the laminator bottom conveyor motor

The unit is housed in 30x24x12 inch steel enclosure attached to the back of the machine frame next to the PLC control unit cabinet. the unit receives input signals, from both the encoders and tachometers and forward output signals to drive the folding roll motor(the master motor) and the pre-folding motor(a slave motor) and both top and bottom laminating conveyor (slave motors) at predetermined electronic speed reduction ratios that can be over ride manually using the screen interface unit. The circuit diagram of the 6K8 control unit is shown in the Figure A5.42. Photograph of 6K8 control unit under construction is shown in Figure A5.43.

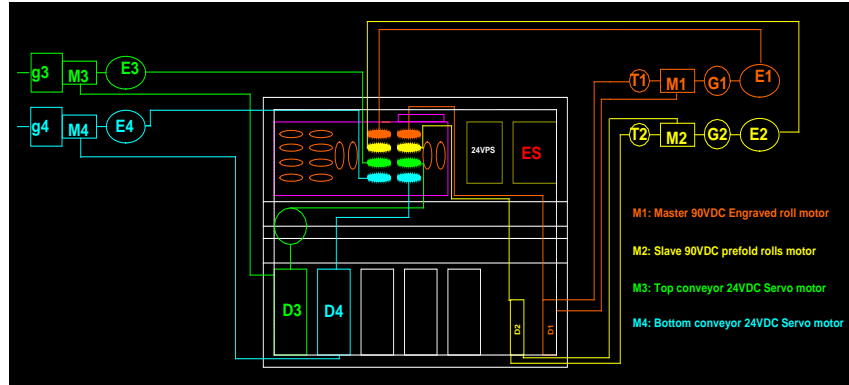


Figure A5.42.The circuit diagram of the Parker 6K8 control unit

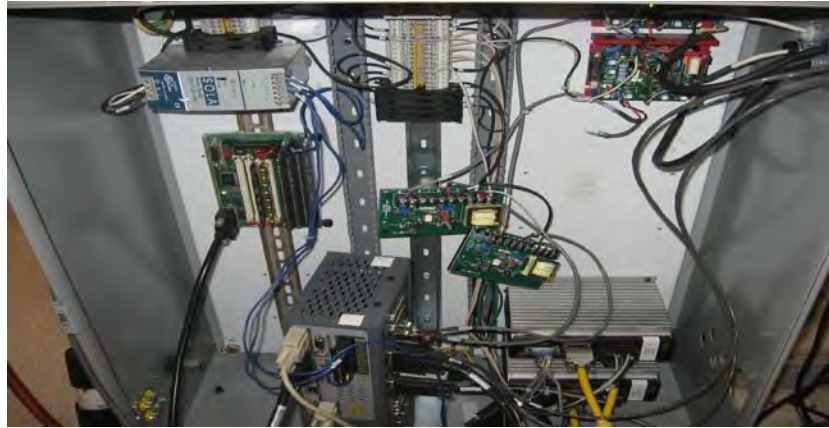


Figure A5.43. Photograph of the Parker 6K8 control unit under construction

Conclusion

The development of the pad making machine from a basic design concept to fully operational unit has been achieved. All design tasks have been completed for the proposed machine basic concept, shown in Figure A5.44 to a fully automated machine shown in Figure A5.45. (Please see video title “folding machine operation”)

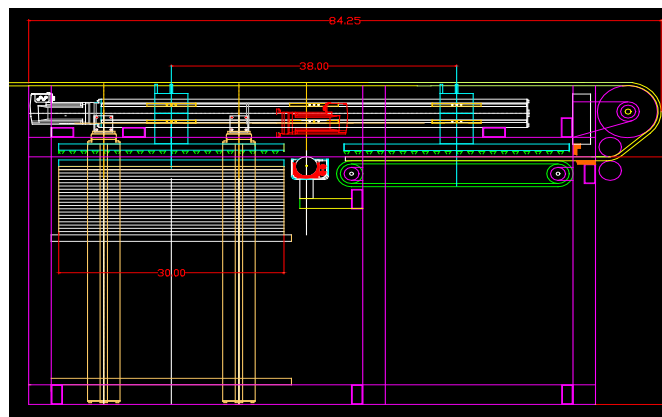


Figure A5.44. CAD drawing of the proposed Machine basic design concept

The machine main work tasks included the design, development and construction of the following 21 sub assemblies/units:

- 1) The machine frame
- 2) The laminate hot melt glue unit
- 3) The laminating conveyor
- 4) The web takeoff conveyor
- 5) The web deflector
- 6) The web feed in rollers
- 7) The slab cutting unit
- 8) The slab holding unit
- 9) The slab measure to length/ positioning unit
- 10) The shuttle unit
- 11) The slab pick and place unit
- 12) The slab hot melt glue unit
- 13) The slab stacking unit
- 14) The pad labeling unit
- 15) The pad ejection Unit
- 16) The build in fork lift for loading the laminate feed roll stock
- 17) The pneumatic operating circuit
- 18) The signal/power interface circuits
- 19) The PLC control unit
- 20) The Parker 6K8 control unit
- 21) The close loop periphery attachments

The fully constructed machine with above modules attached to it is shown in Figure A5.45. Where it receives the folded sheet core from the continuous sheet folding machine placed directly behind

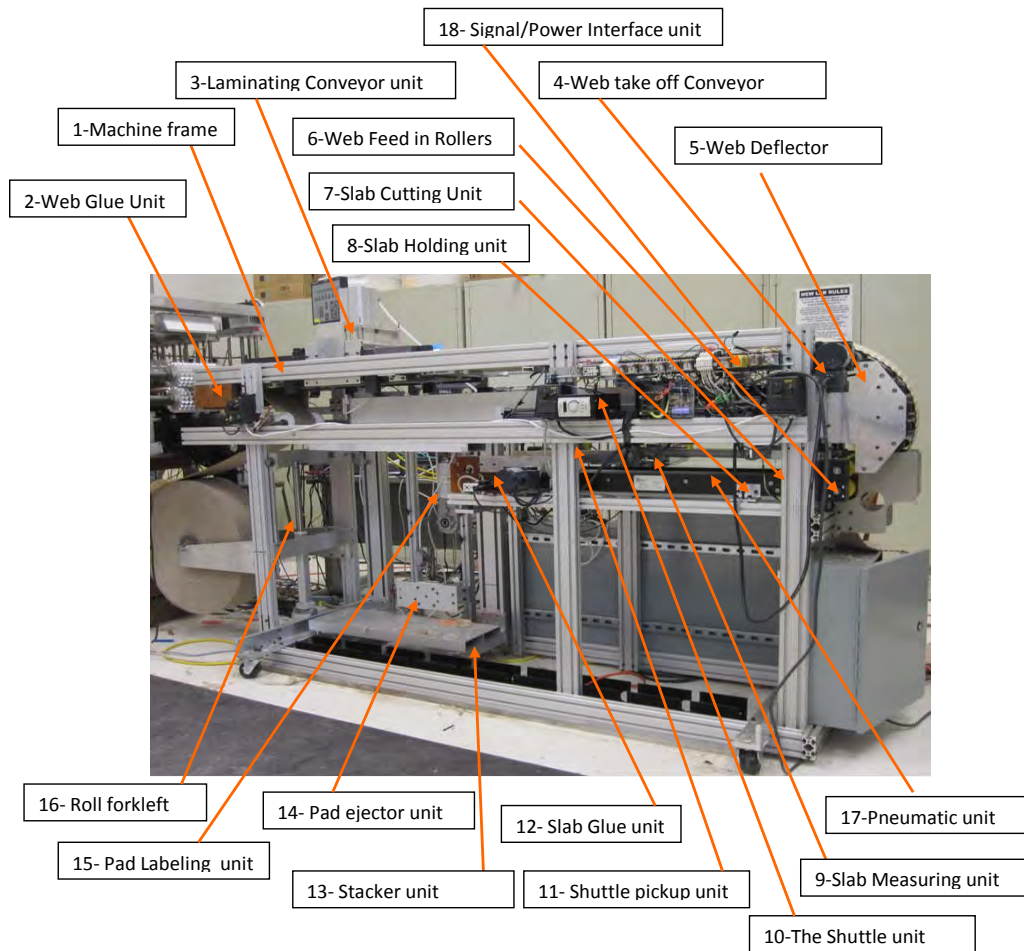


Figure A5.45. Photograph of the fully automated pad making machine

Appendix 6
Setting Folding Machine Bridges

INTRODUCTION

This working paper documents the control program logic and code for setting bridge heights on the folding machine. There are nine bridges the height of which is set in accordance with the paper type that is being used to form the cushion layers. Each bridge height is independently set using stepper motors. The control sequence sets each motor position sequentially such that each roller has a proper gap with its opposing roller. This roller positioning is a one time setup that takes place at the beginning of a production run. Once set, the roller positions do not change during the production run. The roller position will change only when the paper type is changed or a new set of rollers are introduced.

A roller setting consists of moving the roller upward to find a home position limit switch and then moving the roller down a predefined distance to close the gap to the desired size. The actuator is a stepper motor. Closing the gap amounts to moving the stepper motor a predefined number of steps.

The control program has three parts. In the first part a test is run on the home position limit switches. Limit switches are wired as normally closed contacts because the predominant mode for a limit switch failure is as an open circuit. The program first tests that each limit switch reading is true, or closed. If a switch is false, or open, it has either failed or the bridge is at the limiting position. In that case, the stepper for that position is backed away from the limit switch by one turn of the motor. If the switch continues to indicate it is open, the operator is notified and must investigate the wiring. No further action is allowed. When the wiring problem is corrected, the operator can rerun the first part of the program. A successful run of the first part of the program will set a bit in controller memory that allows the bridge gaps to be set.

The second part of the control program is allowed to run when all limit switches have past initial testing. Here the bridges are first homed and, following that, they are moved to the nominal gap position. Indicator lamps on the operator panel will be lighted to show the operator that all positions are set.

The third part of the program is for jogging the rollers. Although the nominal roller setting is considered correct for a specific paper type, differences in manufacture as between lots of the same paper type may require slight adjustments of the roller. The jog buttons are available to the operator to make minor adjustments to the settings.

PROGRAM LOGIC

In order to ease transfer of control programs to commercial producers and to users, the program model is structured as a set of state diagrams. The state diagrams will make the program logic clear to anyone familiar with control programming and will make trouble shooting and further program development easier for the final user.

The next section describes the state diagrams for each function. The subsequent section is the actual program code. This is followed by a description of the operator graphical user interface.

STATE MACHINE DIAGRAMS

Figure 1 is the state diagram of the overall program structure. Macro State S1 is the limit switch testing sub program. When it successfully completes the test, it sets a bit and returns to the initial step. The operator can then use a momentary contact push button to begin the homing cycle. If the limit switch test bit is true, the homing cycle will run and the rollers will be set. Macro State S2 is the roller setting sub program. Finally, the operator can jog the rollers down or up, as indicated in Macro States S3 and S4.

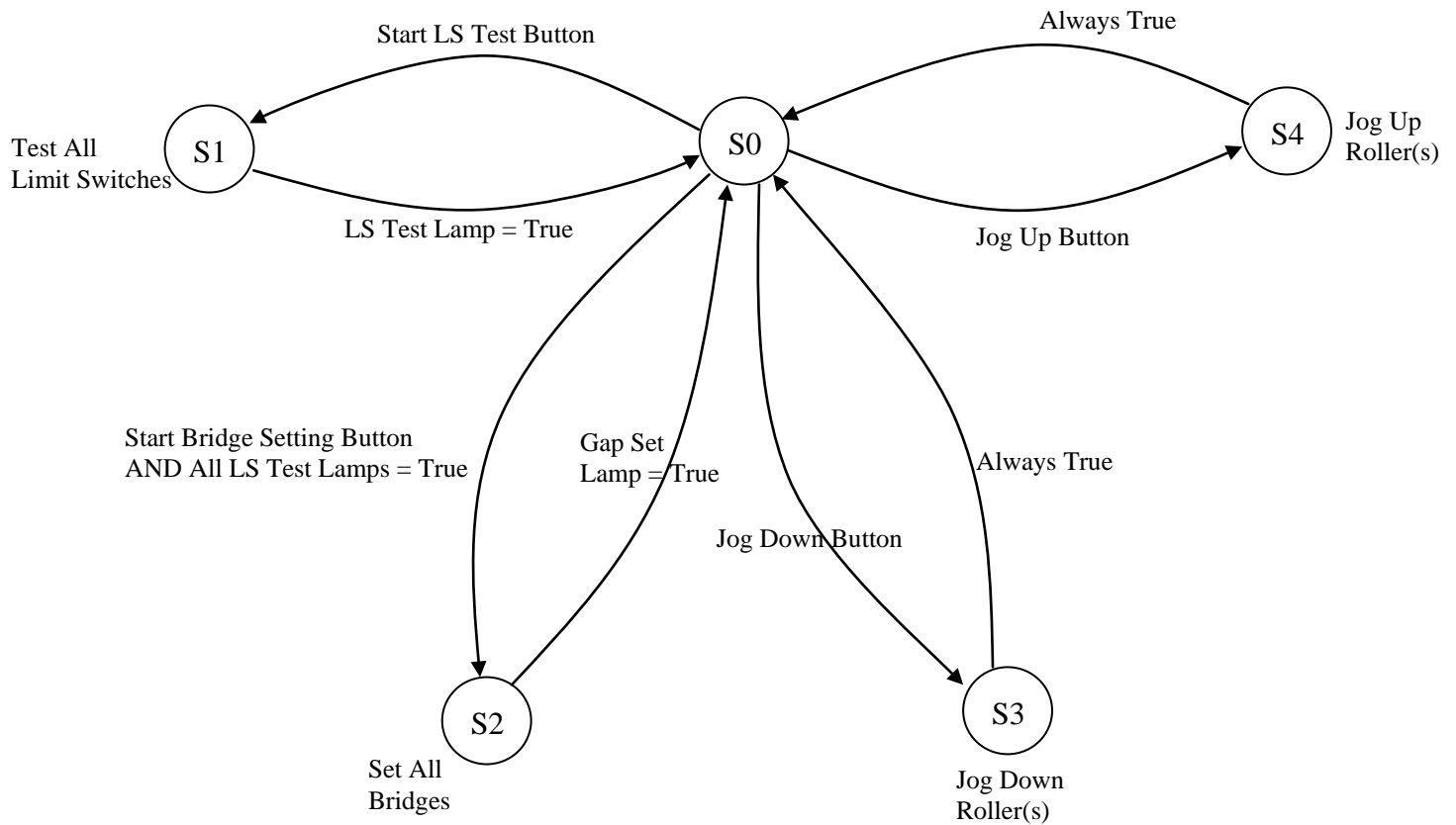


Figure 1 Overall Structure of Program

STATE MACHINE: Limit Switch Test Program

Figure 2 provides the details of S1. It is shown only for one motor (roller position 1). All of the other roller positions are a simple repetition of this program done sequentially (shown in the dotted box below). The “Driver Enable Bit” that is executed in steps S1.2 and S1.3 simply closes a contact for the appropriate bridge circuit driver to be energized. Each motor has its own dedicated driver.

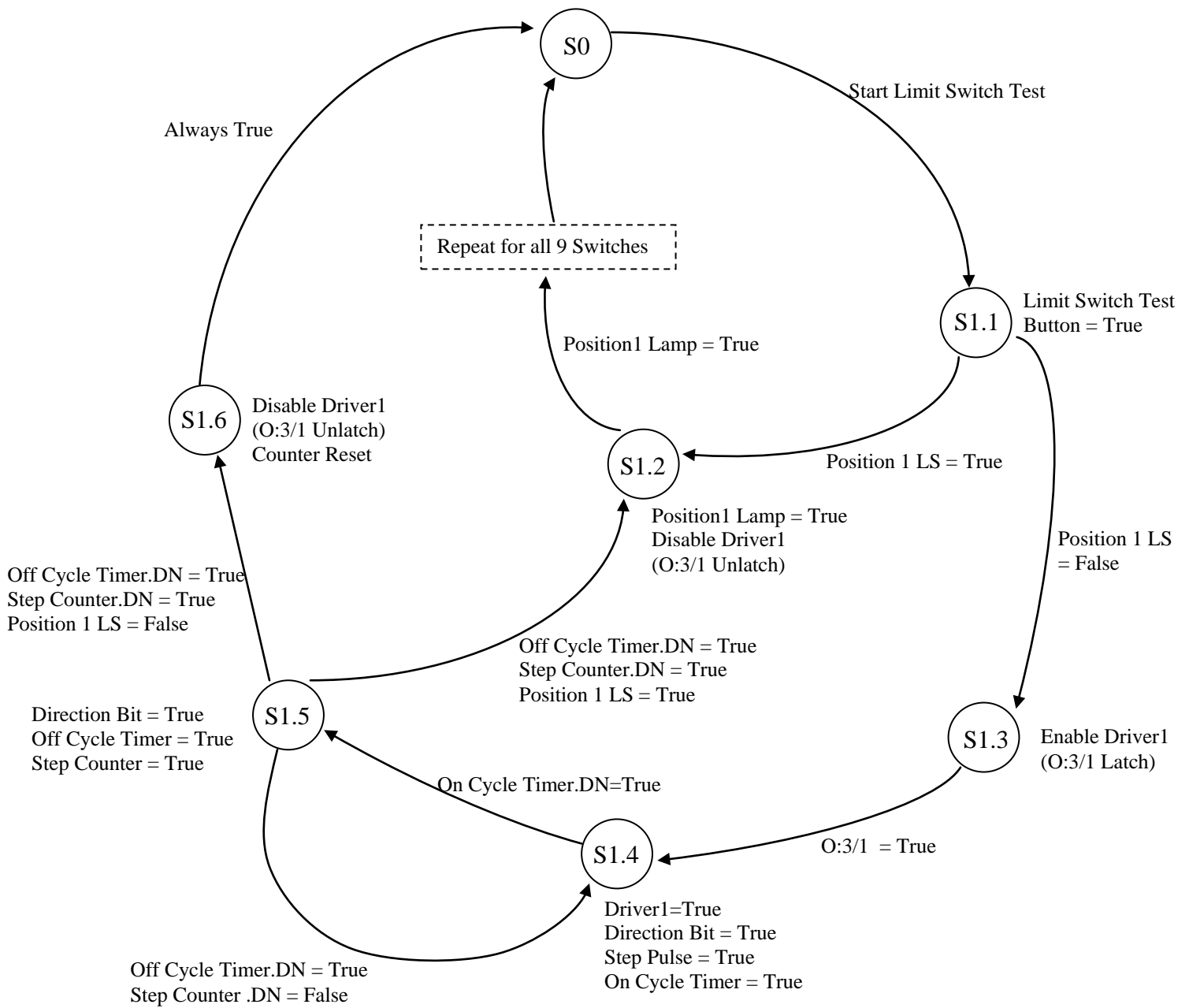


Figure 2 Expansion of Macro State S1

STATE MACHINE: Roller Positioning Program

Figure 3 shows the details of Macro State S2. During the first three steps the program is raising the roller until it engages the upper limit switch. When this occurs the limit switch opens and the program reads the input as false. This is followed by moving the motor position to the appropriate predetermined gap size based on the paper type and roller set being used. Again, this is shown for only one bridge position; the remaining eight positions are simply a repetition of the state machine diagram.

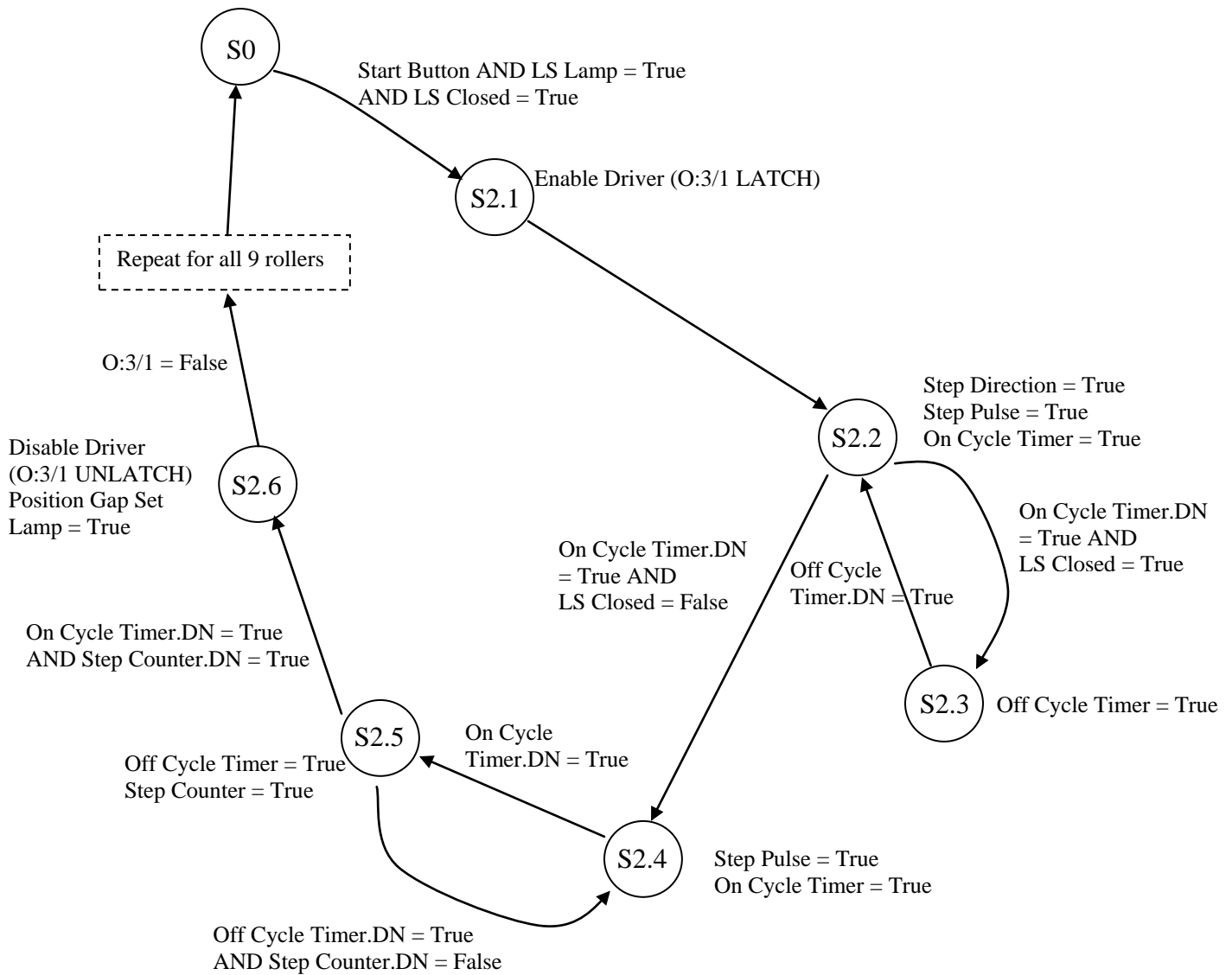


Figure 3 Expansion of Macro Step S2

STATE MACHINE: Roller Jogging Programs

When an operator finds out that the predetermined gap size didn't set the rollers at an appropriate position, s/he can jog down or up rollers one step a time. This is accomplished by pressing the jog down or up button. Following two figures, Figure 4 and 5, show the state machine diagrams for these two functions. As before, they are shown for only roller 1; the rest of the rollers will have the same program except the driver and lamp numbers, etc.

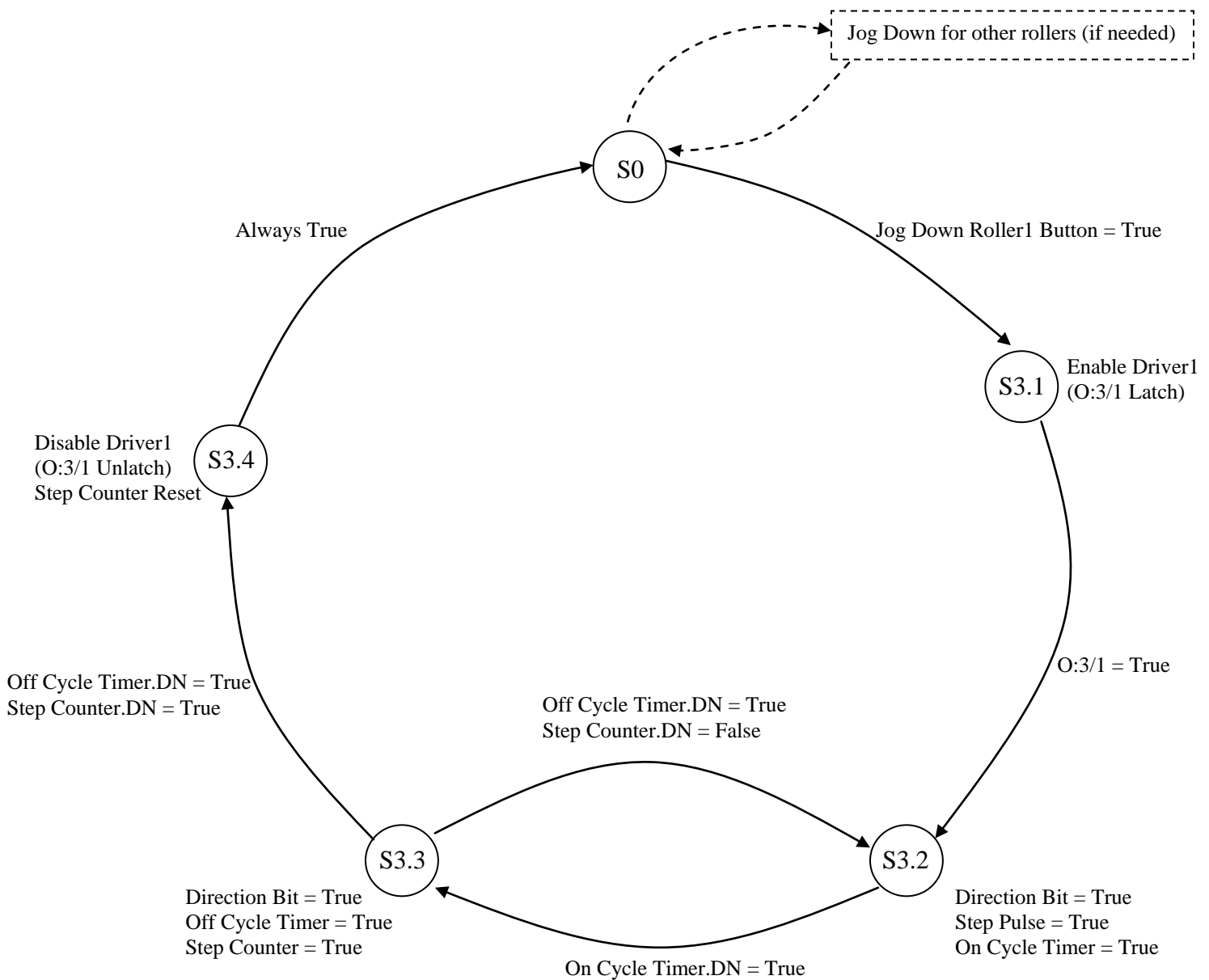


Figure 4 Jog Down Program

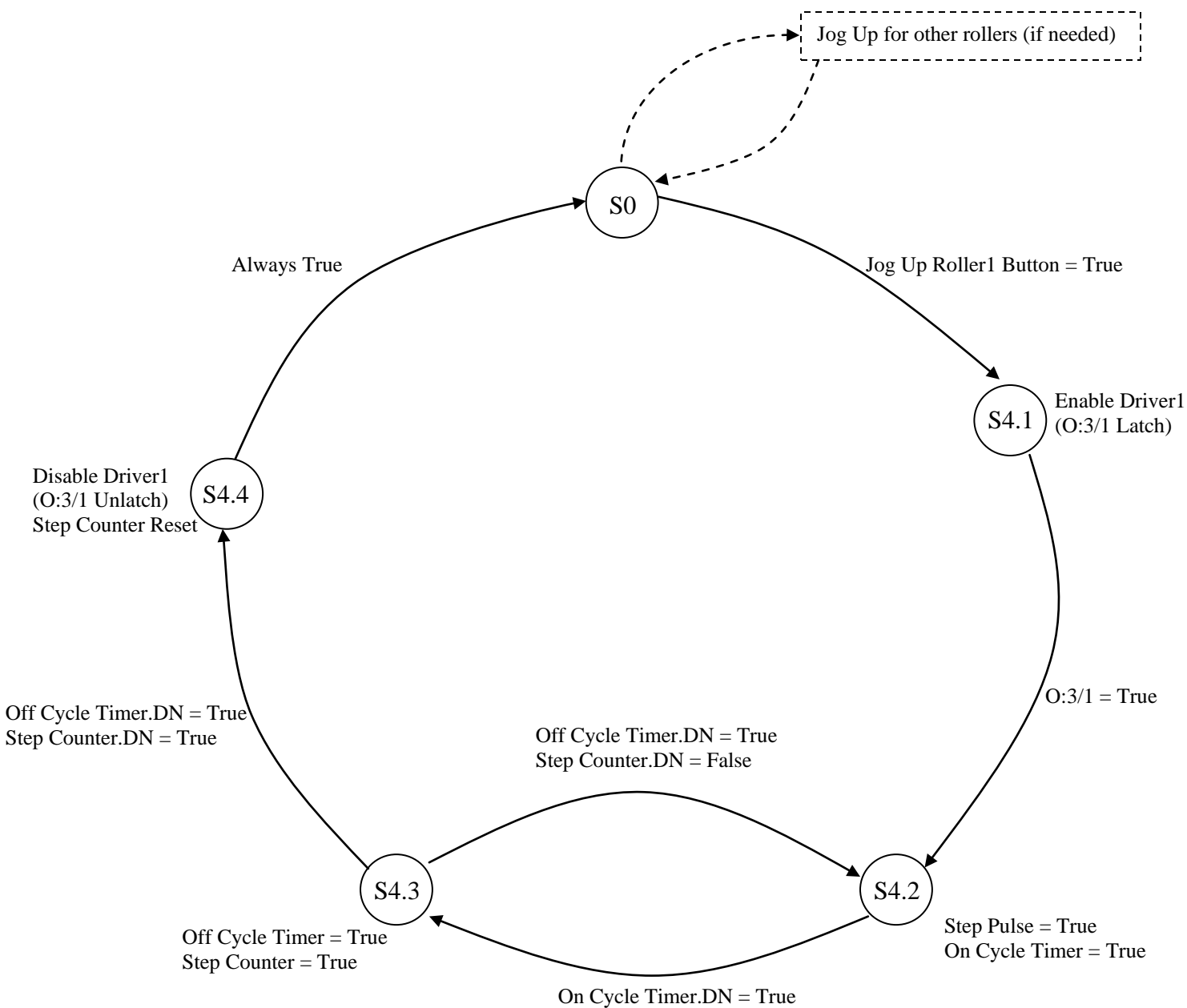


Figure 5 Jog Up Program

GRAPHICAL USER INTERFACE

Figure 6 shows the graphical user interface of the roller setting program. In this figure, only two rollers have been activated for the demonstration purpose. As explained in earlier sections, the first thing for an operator to do is to test all the limit switches. This is done by pressing “TEST” button at the bottom left portion of the screen.

Initially, all the indicator lamps are red. Once the limit switch test is initiated, the program checks if there is any limit switch that is open. If all the limit switches are closed, the limit switch test indicator lamps will turn to green. In Figure 6, we can see that two limit switch test indicator lamps have turned to green. If there is any open limit switch, the program will try to lower the corresponding roller a little bit and checks the limit switch again. If the switch is closed, the indicator lamp becomes green and the program proceeds to the next limit switch test.

If the switch is still open, the indicator lamp remains red and the operator cannot continue. The operator should then check the integrity of the limit switch manually and run the limit switch test again before move on.

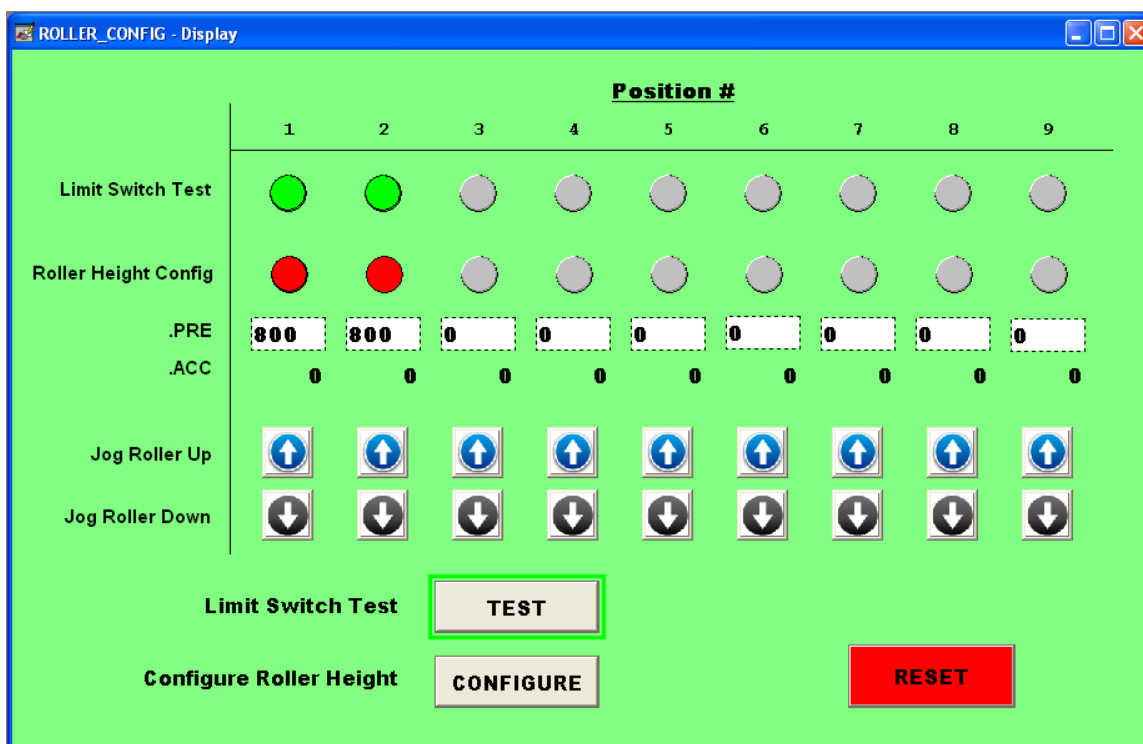


Figure 6 Operator Interface

Once limit switch test is done successfully, we are ready to position the rollers according to the predetermined gap settings. Press the “CONFIGURE” button to configure the roller positions. Starting from roller1, it will move upward until it hits the limit switch and then automatically moves down to the predetermined position. The predetermined value for each roller is shown in the text boxes which are labeled as “.PRE”. During setting the rollers, the accumulated step numbers will be shown in the space (which is labeled as “.ACC”) below the text boxes. If setting has been successfully done, the gap position indicator lamp (the Roller Height Config lamps in the figure) will turn to green.

Due to some uncertainties in paper thickness, the predetermine position may not allow the folding machine work properly. Should this happen, the operator needs to adjust the roller gap manually by jogging the rollers up and down. This is done by pressing the jog buttons. There are two jog buttons, up and down, for each roller. This will turn the motor for the roller by one step. The operator should not press the jog button several times without checking whether the roller is in position or not.

At any time, the operator can stop operation and go to initial state by pressing the “RESET” button at the bottom right on the screen.

LADDER LOGIC PROGRAM

Table 1 assigns specific memory addresses to steps, transitions, and other variables for the nine bridge positions. This table links the SFC to the actual control program, which is shown in the next section.

Table 1 PLC Image Table Assignments

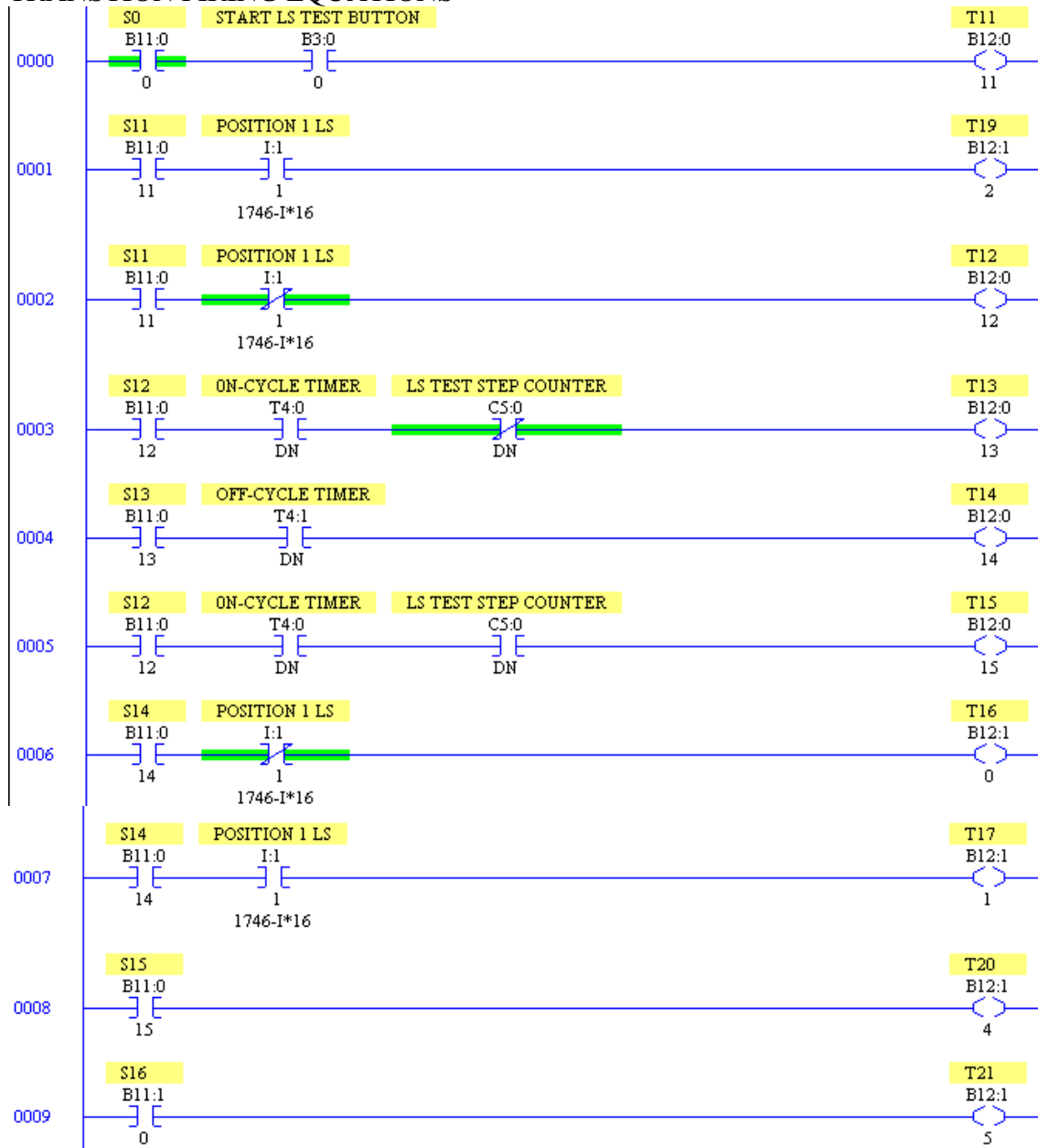
	Stepper Motor / Bridge Position								
	1	2	3	4	5	6	7	8	9
Driver Enable Bit	O:2/0	O:2/3	O:2/6	O:2/9	O:2/12	O:3/0	O:3/3	O:3/6	O:3/9
Step Direction Bit	O:2/1	O:2/4	O:2/7	O:2/10	O:2/13	O:3/1	O:3/4	O:3/7	O:3/10
Step Pulse Bit	O:2/2	O:2/5	O:2/8	O:2/11	O:2/14	O:3/2	O:3/5	O:3/8	O:3/11
Upper Limit Switch	I:1/1	I:1/2	I:1/3	I:1/4	I:1/5	I:1/6	I:1/7	I:1/8	I:1/9
Position Step Counter	C5:1	C5:2	C5:3	C5:4	C5:5	C5:6	C5:7	C5:8	C5:9
Position LS Set LAMP	B30/1	B30/2	B30/3	B30/4	B30/5	B30/6	B30/7	B30/8	B30/9
Position Gap Set LAMP	B31/1	B31/2	B31/3	B31/4	B31/5	B31/6	B31/7	B31/8	B31/9
	Limit Switch Test Steps and Transitions								
Step File Start	B11/11	B11/21	B11/31	B11/41	B11/51	B11/61	B11/71	B11/81	B11/91
Step File End	B11/16	B11/26	B11/36	B11/46	B11/56	B11/66	B11/76	B11/86	B11/96
Transition File Start	B12/11	B12/20	B12/30	B12/40	B12/50	B12/60	B12/70	B12/80	B12/90
Transition File End	B12/17	B12/26	B12/36	B12/46	B12/56	B12/66	B12/76	B12/86	B12/96
	Homing Cycle Steps and Transitions								
Step File Start	B21/11	B21/21	B21/31	B21/41	B21/51	B21/61	B21/71	B21/81	B21/91
Step File End	B21/16	B21/26	B21/36	B21/46	B21/56	B21/66	B21/76	B21/86	B21/96
Transition File Start	B22/11	B22/20	B22/30	B22/40	B22/50	B22/60	B22/70	B22/80	B22/90
Transition File End	B22/17	B22/26	B22/36	B22/46	B22/56	B22/66	B22/76	B22/86	B22/96

PROGRAMMING CODE

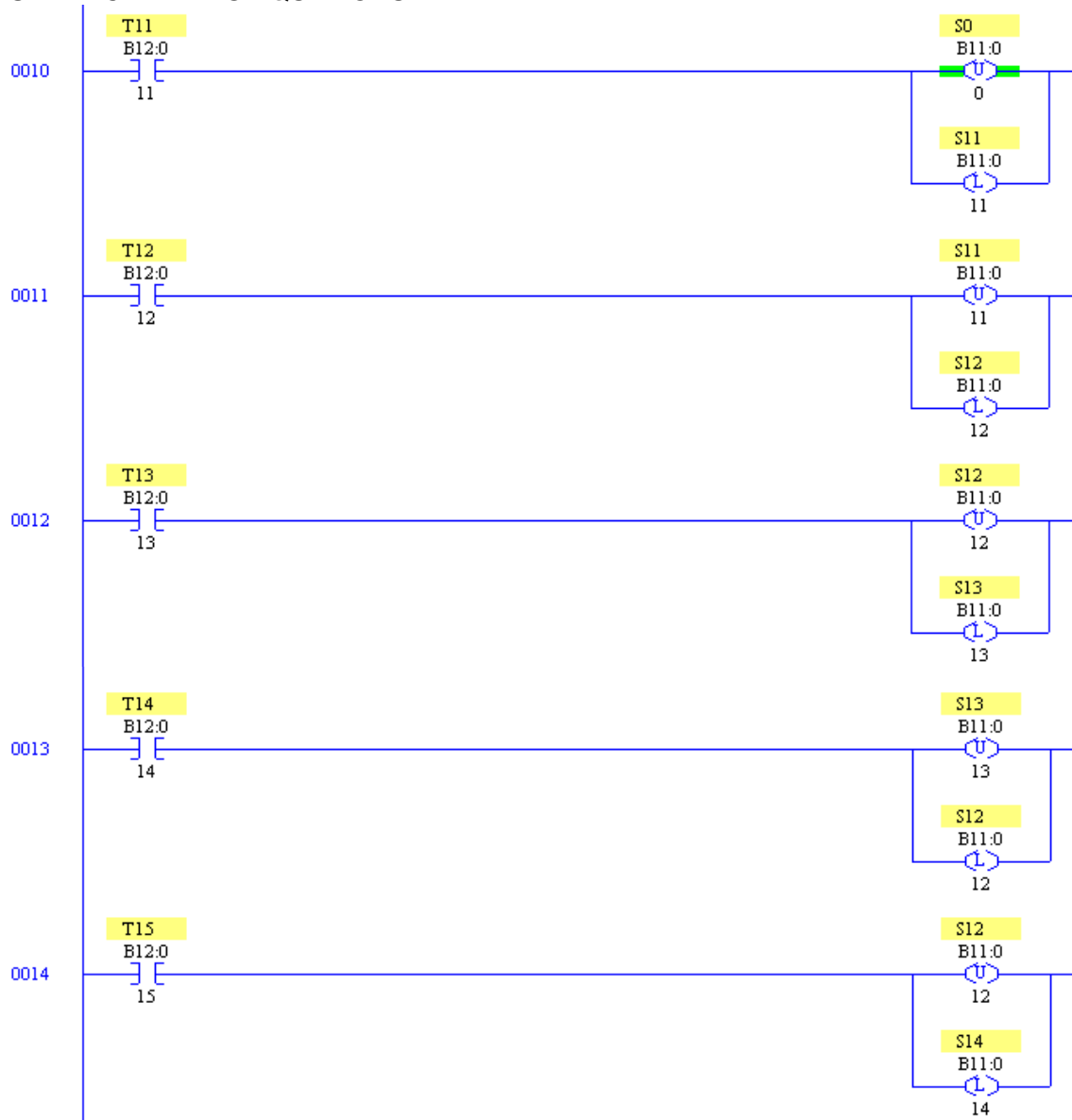
The control program consists of three parts for each repetition of M1 and M2. These parts are labeled as 1) transition firing equations, 2) step activating equations, and 3) output action equations. In addition, there is a section for initialization of M1 and M2, which includes a reset function. The code is shown in Figure 4 for two

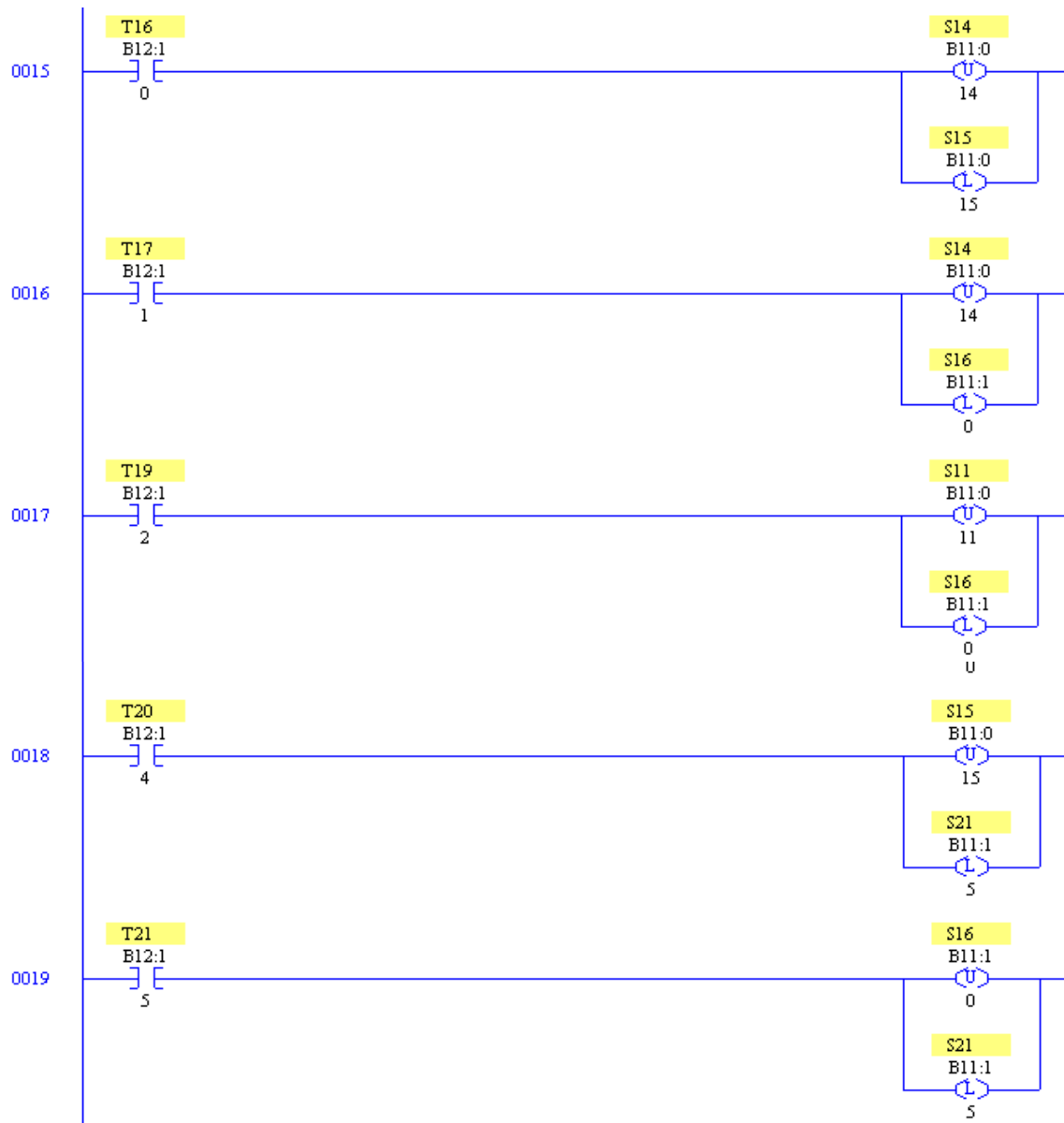
bridges. It is left to the reader to examine the actual code in the PLC to see that it is just repetition of Figure 4 to obtain a program for setting nine bridges.

TRANSITION FIRING EQUATIONS

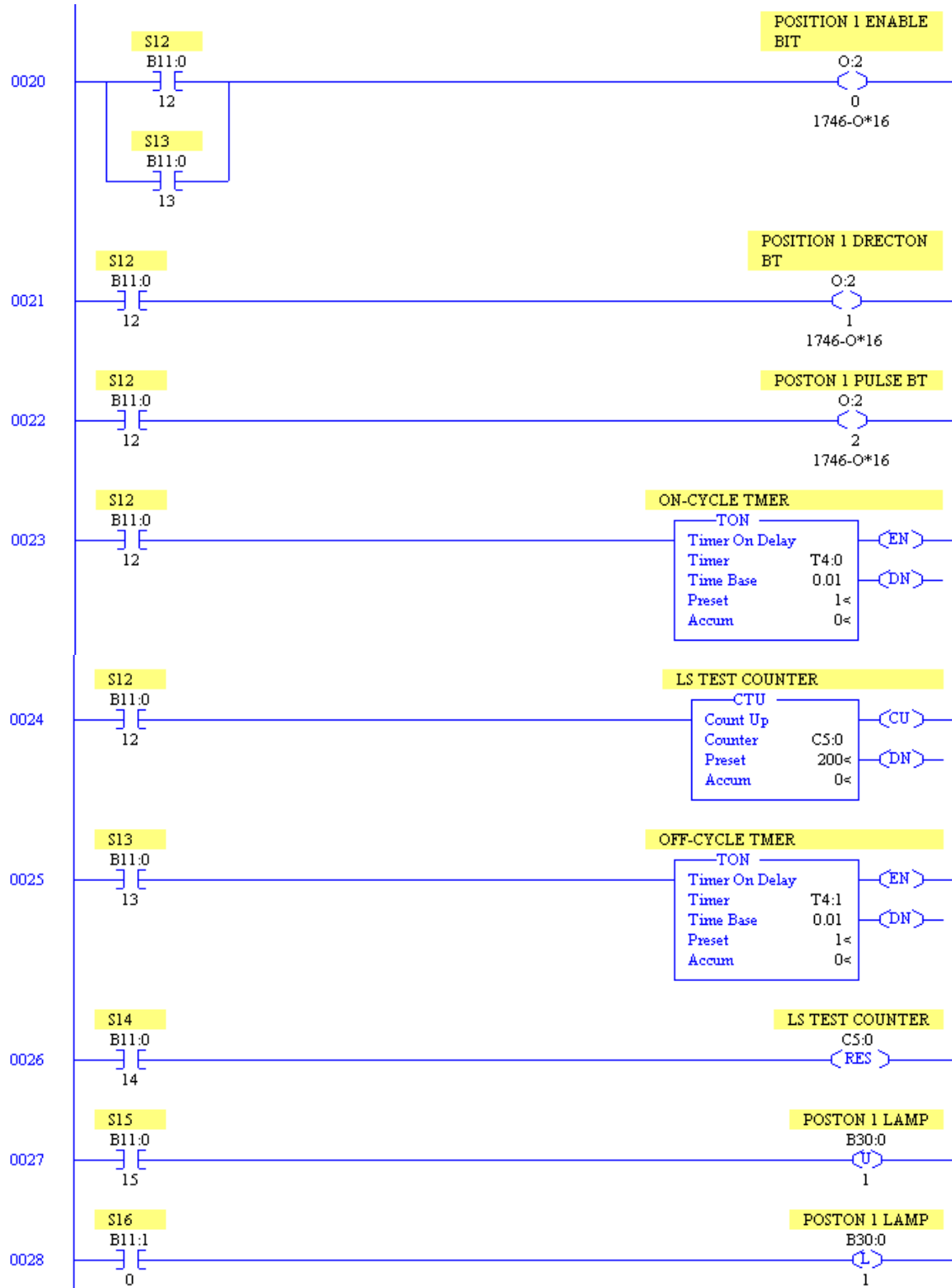


STEP ACTIVATING EQUATIONS





OUTPUT ACTION EQUATIONS



SUMMARY

This working paper has documented the control program for setting folding machine bridges during machine set up prior to going into the run mode. The program is shown in SFC format for logical expression and has been programmed according to the rules of a state machine in order to enhance readability and ease of transfer to machine producers and technicians who support machine maintenance.

It should be noted that the machine design and program is based on using limit switches and an open loop positioning system for the bridges. Therefore, one enhancement that could be considered in the future is to add encoders to the motors and augment the program for closed loop control.

Appendix 8

Sensor Positioning for Pad Cutting Operation

1.0 INTRODUCTION

An important component of the cushion fabrication subsystem is the sensor positioning mechanism that measures the length of pads that are to be cut, consistent with the design of the cushion that is assembled by gluing pads together. A two-sensor mechanism is implemented as shown in the drawing of Figure 1. Before material is fed into the gluing subsystem (from the right of Figure 1), sensor 1 has to be positioned to detect the material when it has reached the cushion design length. At that point the material is cut at the infeed rollers by a knife under program control. The material is then transported along a conveyor until it reaches sensor 2, which is used to signal the control program that the material has reached the pickup point. From there it is picked up by a linear transport pick up arm and taken to the gluing and stacking operation to become part of the cushion.

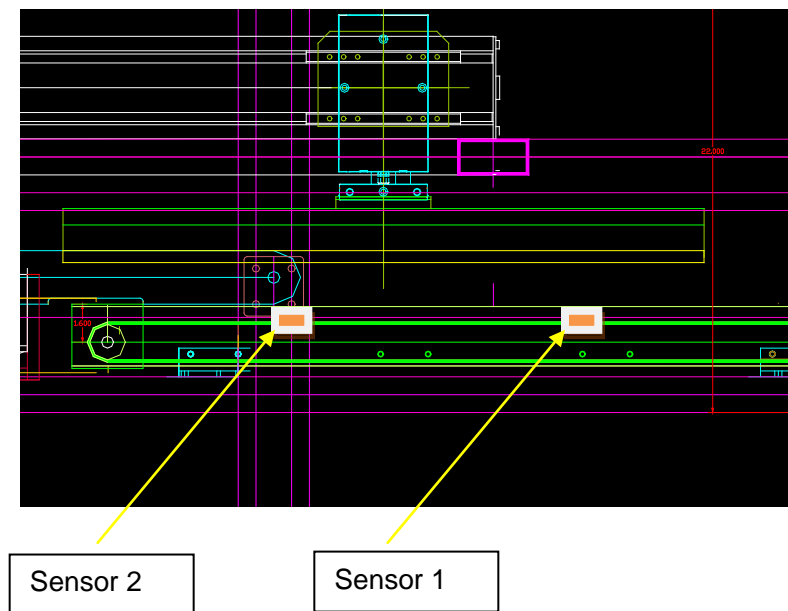


Figure 1 Sensors for length of cut and stopping point for pick up

This technical report documents the control program for the proper positioning of the sensors. The control program receives information on the length of the pad from the design program since the appropriate length of the cushion is defined at design time. The sensors are positioned by a set of lead screws that move them laterally along the conveyor. The lead screw for sensor 1 is driven by a stepper motor and the lead screw for sensor 2 is driven off the sensor 1 lead screw through a gear box having a 1:2 gear ratio. When sensor 1 is correctly positioned for the length of cut, sensor 2 will be automatically correctly positioned for the pick up of a pad of the designed length.

The lead screw pitch for sensor 1 is six revolutions per inch and the stepper motor resolution is 200 steps per revolution. Hence, 1200 steps are commanded from the control program for every inch of travel.

The stepper motor is driven from a PLC by the Allen Bradley 1746-HSTP1 stepper control module. In Section 2.0 we will describe the files that are used to command this module to control the stepper motor. Section 3 explains the program logic used to run the stepper control module. Section 4 contains the PLC ladder logic code for the sensor positioning program.

2.0 Integer Files for Operation of the 1746-HSTP1 Stepper Module

Integer file N31 of the PLC is dedicated to the control of the stepper motor for the sensor position setting. We are using the Allen Bradley Stepper Controller Module to drive the RMS Technologies R710-R0 stepper drive. Since the controller module is the same module we use for controlling the slider and stacker, most of the parameters are the same and they have been described in detail in the technical report: “Program for Controlling the Cushion Fabrication and Gluing Subsystem.” The reader is referred to that report for more details. However, the stepper control module we use for sensor setting uses some different parameters which will be described here. Integer file N31 is configured as shown in Table 1.

Table 1 Integer File N31

	0	1	2	3	4	5	6	7	8	9
N31:0	-31725	19	1	0	0	0	0	0	0	0
N31:10	0	0	0	0	0	0	0	0	0	0
N31:20	1	0	0	0	2	0	1	1	0	0
N31:60	16	0	0	0	0	0	0	0	0	0
N31:80	64	0	0	0	2	0	0	0	0	0

2.1 EXPLANATION OF INTEGER FILE N31

N31:0 = Configuration mode, used to configure the module for specific functionality.

N31:10 = Command mode initiation, used to put the module in the command mode, when it awaits the next move command.

N31:20 = Command mode absolute move, used to turn the stepper motor clockwise to an absolute position. The actual position values will be written to N31:22 and N31:23 (the most significant word and the least significant word, respectively), when the parameters for a production are downloaded from the database by the user using the user interface. The position information cannot be written in advance because it will be changed according to the cushion length.

N31:60 = Command mode emergency stop, used to cancel operation.

N31:80 = Command mode homing in counter clockwise, used to turn the stepper motor counter clockwise until it triggers the home limit switch.

Further details on the use of the 1746-HSTP1 Stepper Module can be found in the user manual, “Stepper Controller Module User Manual (1746-HSTP1),” Allen Bradley Corporation.

3.0 Control Program Logic

The control program logic, shown in Figure 2, is described as a state/event diagram based on the Grafset principle of PLC program documentation.

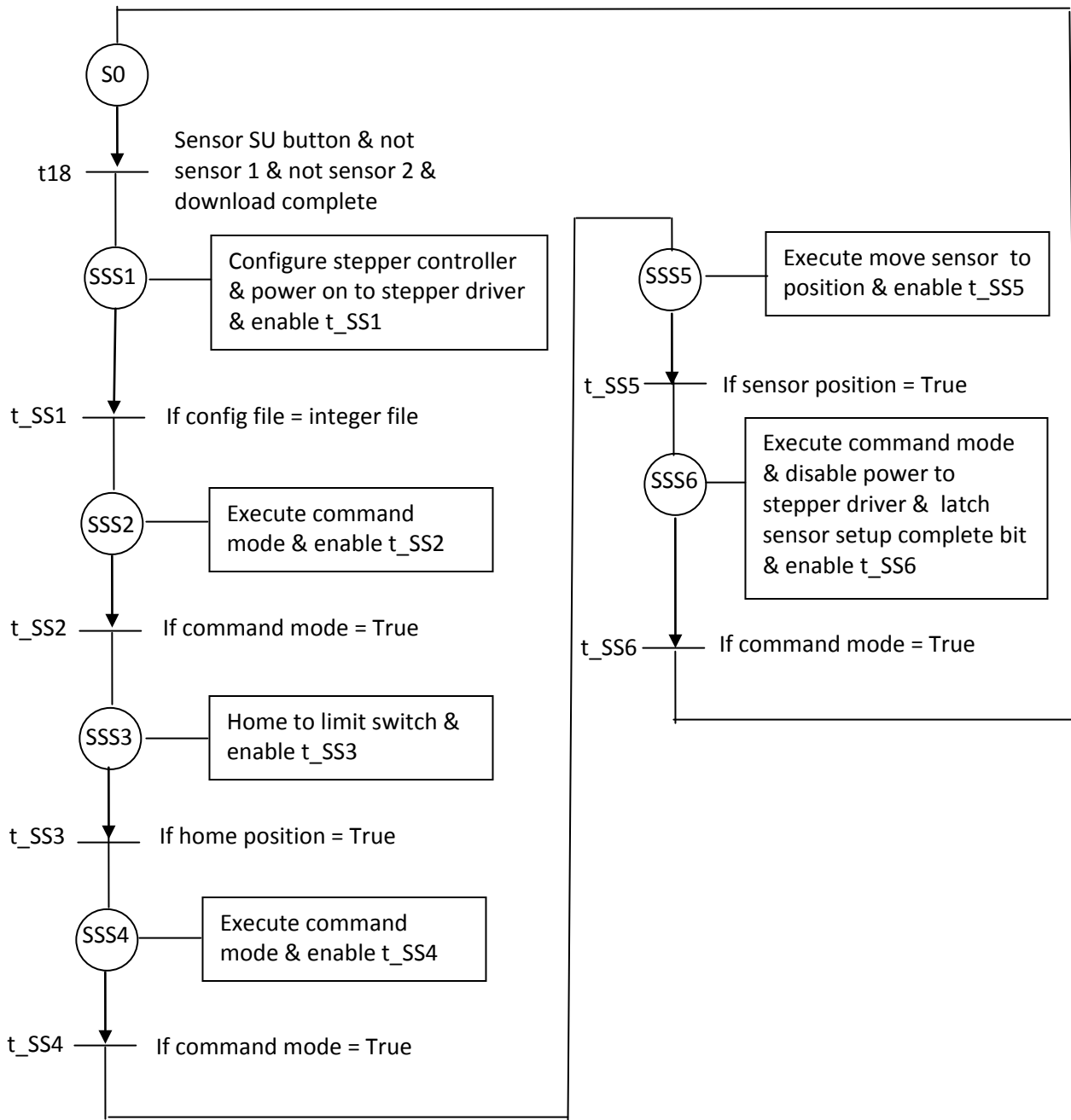
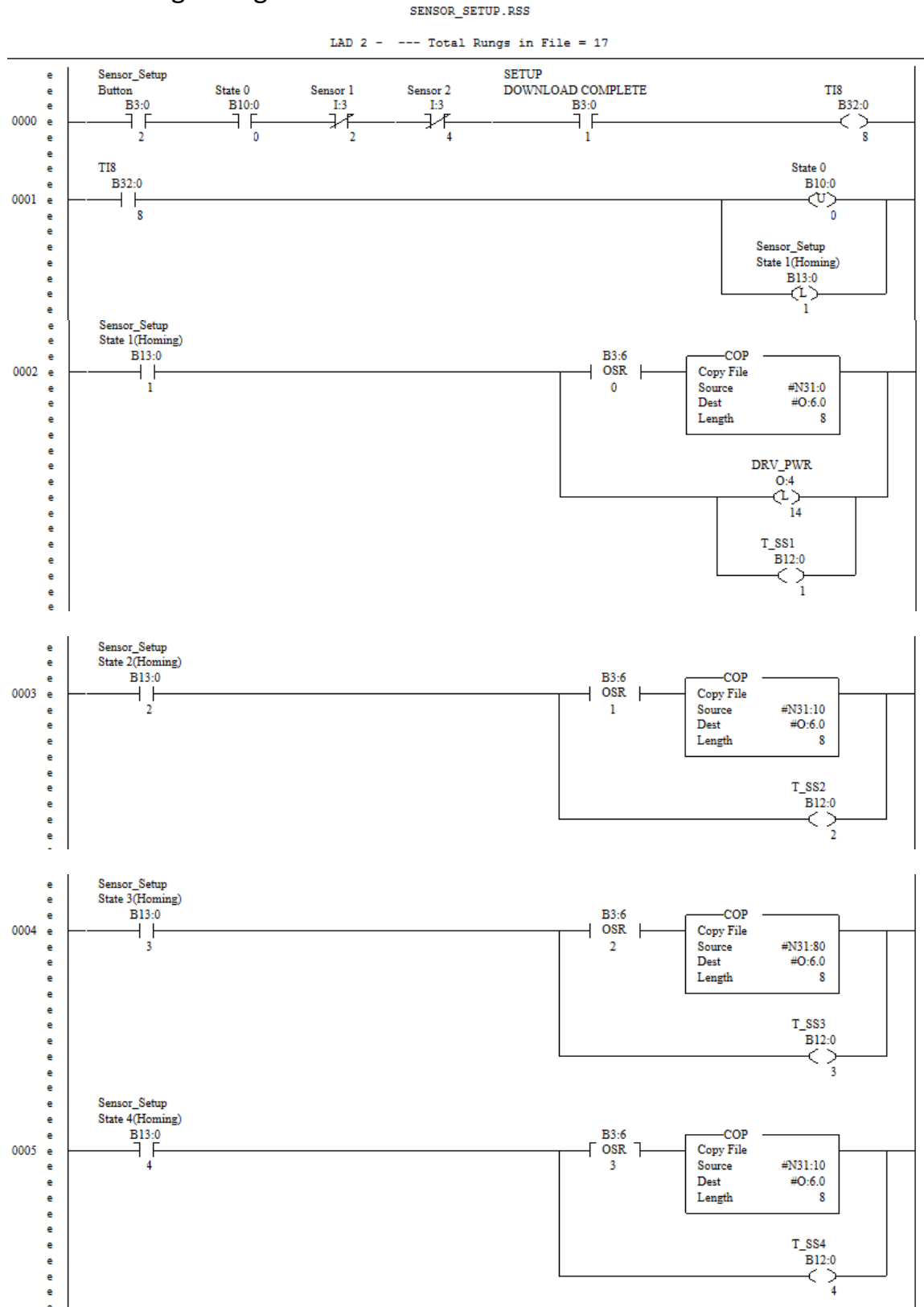
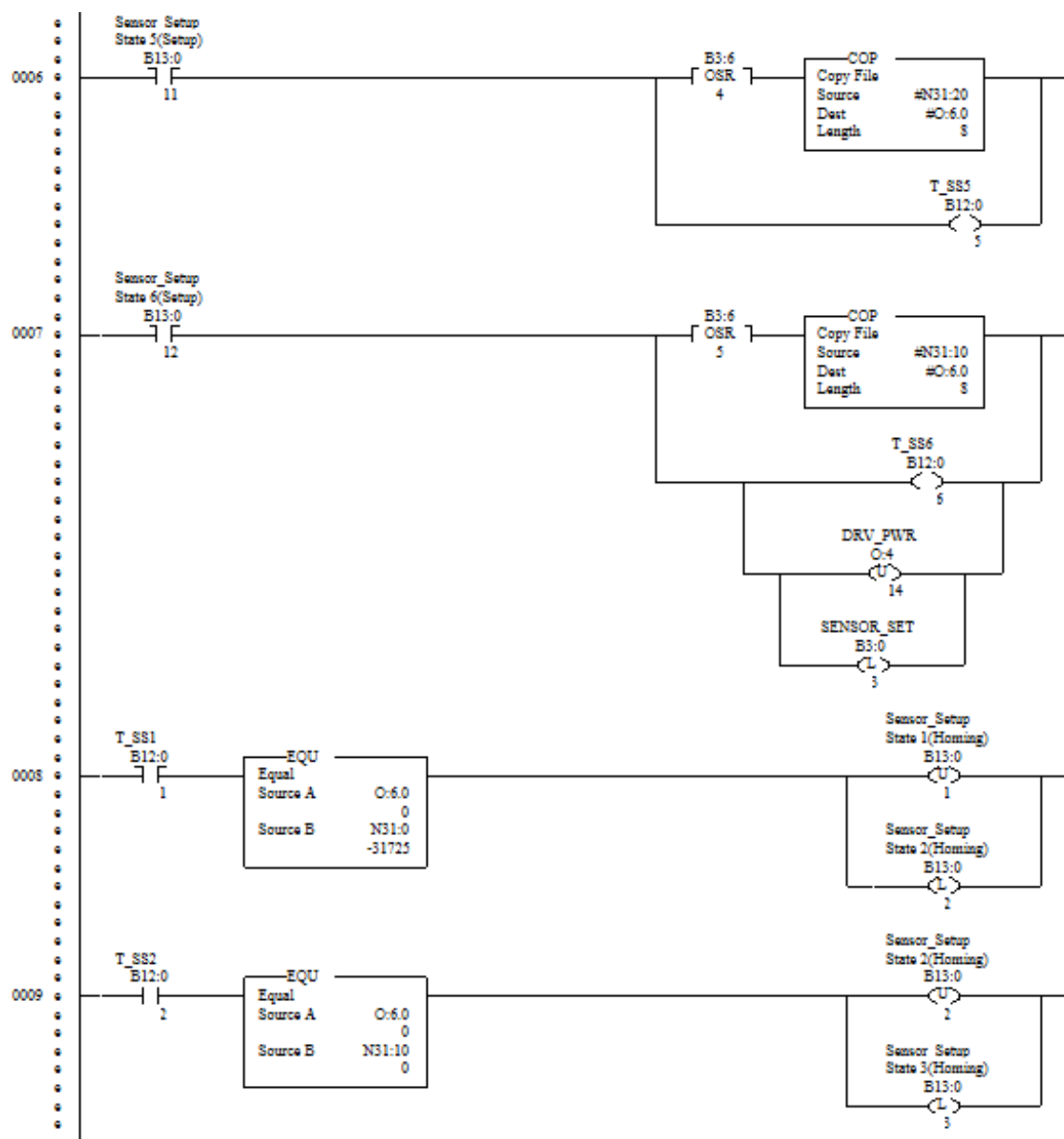
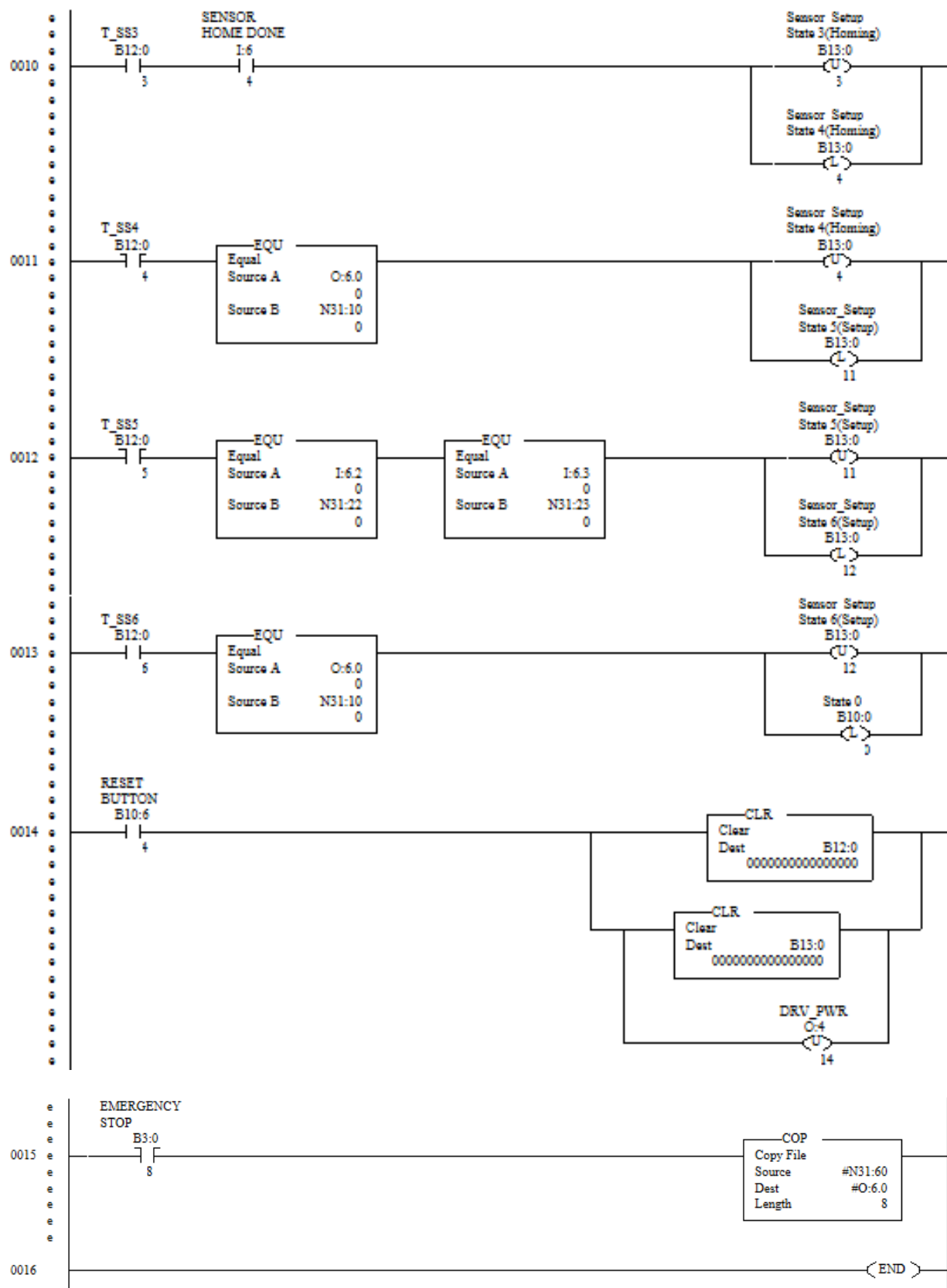


Figure 2 Program Logic

4.0 Ladder Logic Program







Appendix 9
Supervisor/Controller (6K Controller)

1.0 INTRODUCTION

This technical report documents the 6K control program. A 6K controller is used to control the speeds of the first ten rollers on the folding machine and of the upper conveyor belts on the sub-pack system, so that they can be appropriately adjusted according to the speed of master folding roller, which is also controlled by the 6K controller. The control program described in this report is written for the 6K controller, so that we can achieve desired responses from the motors which run the rollers.

The master folding roller DC motor is connected to axis 8 on the controller. The rest of the rollers on the folding machine are run by the other DC motor (axis 7 on the controller), and the sub-pack system upper conveyor belts are run by two servo motors (axes 5 and 6.) The program regulates the speed of the master motor and also adjusts the speed of other motors according to a programmed ratio of the speed of the master motor. The program also displays relevant information on a user interface, the RP-240 panel, and a user can manually override the control using this panel.

This report explains the concept of following and how it is applied in the control of folding machine and sub-pack system. It also explains how to use the RP-240 panel to override the control manually. The program is listed with description on each line. Most of the important commands that are used in the program are given with description in the Appendix.

2.0 CONCEPT OF FOLLOWING

Following is controlled motion between a master device and follower axes. Standard motion is expressed through velocity. However, following motion is expressed through a follower-to-master ratio. That is, once the velocity of the master device is set, the velocity of a follower axis is determined by the ratio.

In our application, the DC motor that runs the master folding roller (axis 8) is the master device. The other DC motor (axis 7) and two servo motors that run the conveyor belts (axes 5 and 6) are followers. The follower-to-master ration is specified by two inputs: a numerator and a denominator. These following ratios are affected by the scale factor, if the scale is enabled (SCALE1.) The numerator is scaled by SCLD scale factor and the denominator is scaled by SCLMAS scale factor.

The master/follower program can be set to run for a specific target distance or to run continuously. There is no target distance to move in our application, so it should be run continuously until the cushion production is done or the user stops running the machine. Therefore, we set the mode of our program to be continuous (MC1) and disable the maximum allowed position error (SMPER).

3.0 PROGRAM

The control program can be run by typing 'RUTGERS' on a terminal screen in Motion Planner ®. If this is the first time after the program was downloaded to the 6K, then the user should run the setup program before running the 'RUTGERS' program by typing 'SETUP' or 'MAIN.'

The machine should start running at the preset velocity and ratios. Should a user want to change the velocity of the master motor or the ratios between the master axis and follower axes, one can use the RP240 panel. It displays the current master motor velocity. To increase the velocity, press '2' (up-arrow), to decrease the velocity, press '8' (down-arrow), to increase the velocity faster, press '6' (right-arrow), to decrease the velocity, press '4' (left-arrow), to pause/resume, press '5,' and to kill all the motion, press 'C/E' button. (It is not recommended to use 'STOP' button on RP240.) Once you pressed 'C/E' button, you have to run the 'RUTGERS' program again to restart. Table 1 summarizes this.

Table 1 Explanation of use of keys on RP240

Action	Key
Increase the velocity	2 (up-arrow)
Increase the velocity faster	5 (right-arrow)
Decrease the velocity	8 (down-arrow)
Decrease the velocity faster	4 (left-arrow)
Pause/Resume	5
Stop (Kills all motion)	C/E

By pressing 'F1' key, you can change the RP240 display to the axis 7 following ratio adjustment screen. Keys that are used in adjustment are the same as they were in master velocity adjustment. Instead of adjusting velocity, this time the ratio is adjusted and the current ratio is displayed on RP240. By pressing 'F2' key, you can enter axes 5-6 following ratio adjustment screen. Again, keys are the same. The following ratios for axes 5-6 are changed at the same time. To go back to the master velocity adjustment screen, press 'Recall' button.

The control program is listed below. In the following program, anything behind a semicolon (;) in a line is a comment and can be ignored. The program shown below is actually comprised of four different programs. The first part is setup program where one can define properties of the system and parameters that will be used. The second part is main program, which would normally be the main execution part. In our application, it just runs the setup program. The third part is a crash handling code, which is currently empty. The last part is the main execution code for our application. The setup code of the following code was generated using a wizard and there are comments that were written by the wizard. To differentiate the comments that we wrote to explain the code from the comments by the wizard, we use *italic font* for our comments. If the reader can see the color, words in blue are the keywords/commands that are used in 6K. Please remember that we are using axes 5 through 8 only. So, ignore any settings for axes 1-4 in the following.

```

; WIZID = 00020020
;Product Setup Code
; Wizard developed for 8 axes with a 6K8 using RS232 COM1

; WIZID = 00020100
;Scaling Setup ;This should be done even before the setup. Not allowed in a program.
;Distance Units - counts,counts,counts,counts,counts,counts,counts,counts
SCLD 1,1,1,1,8000,8000,5000,5000 ; Distance scale factor. This affects FOLRN
;Velocity Units - rev/s,rev/s,rev/s,rev/s,rev/s,rev/s,rev/s,rev/s
SCLV 4000,4000,4000,4000,8000,8000,5000,5000 ;Velocity scale factor
;Acceleration Units - rev/s/s,rev/s/s,rev/s/s,rev/s/s,rev/s/s,rev/s/s,rev/s/s,rev/s/s
SCLA 4000,4000,4000,4000,8000,8000,5000,5000 ;Acceleration scale factor
SCALE0 ;Disable scaling. Although we set the factors above, we don't use them.

;COMEXC1 ;Ensure immediate execution of commands.

; WIZID = 00020040
;-----
;Setup Program
DEL SETUP ;Delete a possible pre-existing program with the same name.
DEF SETUP ;Define program 'Setup'
FOLMAS 0,0,0,0,0,0,0,0 ;Ignore this. It will be overridden.
FOLEN00000000 ;Ignore this. It will be overriede.

; WIZID = 00020060
;Enable Mode Code
DRIVE00000000 ;Shut down drives for all axes.
; WIZID = 00020080
;Drive Setup
;Axis 1, Servo Control, No Drive

```

```

;Axis 2, Servo Control, No Drive
;Axis 3, Servo Control, No Drive
;Axis 4, Servo Control, No Drive
;Axis 5, Servo Control, Aries Drive
;Axis 6, Servo Control, Aries Drive
;Axis 7, Servo Control, No Drive
;Axis 8, Servo Control, No Drive
AXSDEF 11111111 ;Sets all axis to be a servo control(1) or a stepper(0).
DRFLVL 11111111 ;Drive fault input level 0-active low, 1-active high.
DRFEN 00000000 ;Check for driver fault input active 0-disable 1-enable
KDRIVE 00001111 ;Disable drive when a user kills the motion.

; WIZID = 00020100
;Scaling Setup
;Because scaling commands are not allowed in a program,
;the scaling commands will be placed at the beginning
;of the program file. This insures that motion programs
;in subsequent programs will be scaled correctly.

; WIZID = 00020120
;Feedback Setup
SFB 1,1,1,1,1,1,1,1 ;Set feedback source 0-open loop 1-encoder 2-analog
ERES 4000,4000,4000,4000,8000,8000,5000,5000 ;Encoder resolution
SMPEP 4000,4000,4000,4000,0,0,0,0 ;Maximum allowed position error 0-disable
EFAIL 00000000 ;Encoder failure detection
ENCPOL 00000000 ;Encoder polarity
ENCSND 00000011 ;Encoder type 0-quadrature 1-step and direction
; WIZID = 00020140
;Hardware Limit Setup
LH 3,3,3,3,0,0,0,0 ;Hardware End-of-Travel Limit enable 0-disable
LHAD 100,100,100,100,100,100,100,100 ;Hardware limit deceleration
LHADA 100,100,100,100,100,100,100,100 ;Hardware limit average deceleration

;Software Limit Setup
LS 0,0,0,0,0,0,0,0 ;Disable software End-of-Travel limit
LSAD 100,100,100,100,100,100,100,100
LSADA 100,100,100,100,100,100,100,100
LSNEG 0,0,0,0,0,0,0,0
LSPOS 0,0,0,0,0,0,0,0

;Home Limit Setup
;We are not using homing. The following setting was generated by the wizard.
HOMA 10,10,10,10,10,10,10,10
HOMAA 10,10,10,10,10,10,10,10
HOMV 1,1,1,1,1,1,1,1
HOMAD 10,10,10,10,10,10,10,10
HOMADA 10,10,10,10,10,10,10,10
HOMBAC 00000000
HOMZ 00000000
HOMDF 00000000
HOMVF 0.1,0.1,0.1,0.1,0.1,0.1,0.1,0.1
HOMEDG 00000000

LIMLVL 000000000000000000000000 ;Limit and Homing active level
; WIZID = 00020160

;Servo Tuner Setup
;Servo Tuner Setup
SGP 0.5,0.5,0.5,0.5,3.0,3.0,15.0,0.5 ;Proportional gain
SGI 0,0,0,0,0,0,0,0 ;Integral gain
SGILIM 0,0,0,0,0,0,0,0 ;Integral Windup Limit
SGV 0,0,0,0,0,0,0,0 ;Velocity gain
SGVF 0,0,0,0,0,0,0,0 ;Velocity feedforward gain
SGAF 0,0,0,0,0,0,0,0 ;Acceleration feedforward gain

```



```

;
;
5FOLMAS-81      ;Set axis 5 to follow axis 8, opposite direction, source=encoder
6FOLMAS81       ;Set axis 6 to follow axis 8, positive direction, source=encoder
7FOLMAS81       ;Set axis 7 to follow axis 8, positive direction, source=encoder
FOLEN 00001110  ;Enable following for axes 5-7
; 5FOLRN1
; 6FOLRN1
; 5FOLRD1
; 6FOLRD1
MC00001111      ;Set mode continuous for axes 5-8

A 10,10,10,10,10,10,250,1    ;Set accelerations

;

;Error Setup
;To modify the error bits,
;Please double-click on your Error Program

; Error program setup
ERRORP CRASH ; Error program setup      ;Specifies error program
ERROR XXXXXXXXXXXXXXXXXXXXXXXXXXXXXXXX ; Bits tested

END          ;End of definition of program 'setup'

; WIZID = 00020180
;-----
;Main Program
DEL MAIN
DEF MAIN

; WIZID = 00020200
GOSUB SETUP

END

STARTP MAIN ;Specifies startup program (program that's started when power-up/reset

; WIZID = 00020220
;-----
;Error Program
DEL CRASH
DEF CRASH

END

DEL RUTGERS
DEF RUTGERS

COMEXC1

```

```

VAR1=0.250      ; Master velocity variable
V,,,,,,,,(VAR1) ; Setting velocity for axis 8 (master)
;8V0.25

VAR2=41      ;Numerator for axis 5
VAR3=41      ;Numerator for axis 6
VAR4=1       ;Denominator for axis 5
VAR5=1       ;Denominator for axis 6
VAR6=118     ;Numerator for axis 7
VAR7=100     ;Denominator for axis 7

VAR101=-1    ;Temporary variable used in the program
VAR102=0     ;TEMP2
VAR103=0     ;TEMP3
VAR104=0     ;PAUSE/RESUME FLAG

DSTP0        ;Enable/Disable RP240 Stop key

5FOLRN(VAR2)  ;Set following ratio numerator for axis 5 using var2
6FOLRN(VAR3)  ;Set following ratio numerator for axis 6 using var3
5FOLRD(VAR4)  ;Set following ratio denominator for axis 5 using var4
6FOLRD(VAR5)  ;Set following ratio denominator for axis 6 using var5
7FOLRN(VAR6)  ;Set following ratio numerator for axis 7 using var6
7FOLRD(VAR7)  ;Set following ratio denominator for axis 7 using var7

VAR11=-1      ; RP240 key input variable

DRIVE00001111 ;Enable drives 5-8
GO00001111    ;Initiate motion for axes 5-8

DREADI1      ; Enable immediate data read mode. Does not wait for the user input.
VAR100=0     ; Defalut menu value variable

L      ;Starting loop (infinite times)
VAR100 = DREADF      ;Assigns function key (Fkey) input from RP240 to var100
VAR11=DKEY           ;Assigns other key input from RP240 to var11

DCLEAR0             ;Clears RP240 display.

IF (VAR11=12)       ;Key input is 'C/E'
    K11111111      ;Kill the motion
    BREAK          ;jump out of the loop
NIF

IF (VAR100=0 OR VAR100>2) ;No Fkey input or unknown Fkey input

    DWRITE"ADJUST SPEED W/ARROWS FOLLOW RATIO F1/F2" ;Write to RP240
    DPCUR2,0      ;Set cursor position on RP240 at the specified location
    DWRITE"CURRENT SPEED= "
    DVAR1,1,3,0   ;Write the variable value in the specified format
    DPCUR2,26
    DWRITE"5=PAUSE/RESUME"

    IF (VAR11=8)   ;Key '8' down-arrow
        DLED10000000 ;Turn on the 1st LED indicator
        VAR1=VAR1-0.025 ;Decrease master velocity variable
        IF (VAR1<0)
            VAR1=0 ;Minimum velocity
        NIF
        V,,,,,,,,(VAR1) ;Assign velocity for axis 8 (master axis)
    NIF
    IF (VAR11=2)   ;Key '2' up-arrow
        DLED01000000 ;Turn on the 2nd LED indicator
        VAR1=VAR1+0.025 ;Increase master velocity variable

```

```

    IF (VAR1>0.42)
        VAR1=0.42      ;Maximum V is 0.42 before we exceeds 10 volts output.
    NIF
    V,,,,,,,,(VAR1)    ;Assign V
NIF
IF (VAR11=4)          ;Key '4' left-arrow
    DLED00100000      ;Turn on the 3rd LED indicator
    VAR1=VAR1-0.05     ;Decrease master velocity variable faster
    IF (VAR1<0)
        VAR1=0         ;Minimum velocity
    NIF
    V,,,,,,,,(VAR1)    ;Assign V
NIF
IF (VAR11=6)          ;Key '6' right-arrow
    DLED00010000      ;Turn on the 4th LED indicator
    VAR1=VAR1+0.05     ;Increase master velocity variable faster
    IF (VAR1>0.42)
        VAR1=0.42      ;Maximum V
    NIF
    V,,,,,,,,(VAR1)    ;Assign V
NIF
IF (VAR11=5 AND VAR104=0) ;'5'Key and pause flag is false(var104=0)
    DLED00000010      ;Turn on 7th LED Indicator
    VAR101=VAR1        ;Temporary variable var101 Store current velocity
    VAR1=0             ;Set velocity to be zero
    VAR104=1          ;Set pause flag to be true
    V,,,,,,,,(VAR1)    ;Assign V
ELSE
    IF (VAR11=5 AND VAR104=1) ;'5'Key and pause flag is true(var104=1)
        DLED00000001    ;Turn on 8th LED Indicator
        VAR1=VAR101      ;Restore velocity
        VAR104=0         ;Set pause flag to be false
        V,,,,,,,,(VAR1)  ;Assign V
    NIF
NIF

DPCUR2,16             ;Place cursor on RP240 at specified location
DVAR1,1,3,0           ;Write the variable value in the given format
NIF

IF (VAR100=1)          ;'F1' key input. Axis 7 ratio adjustment

DWRITE"ADJUST FOLLOWING RATIO OF AXIS7 W/ARROWS"
DPCUR2,0
DWRITE"CURRENT RATIO= "
DVAR6
DPCUR2,26
DWRITE"5=PAUSE/RESUME"

IF (VAR11=8 AND VAR6>0)
    DLED10000000
    VAR6=VAR6-1
NIF
IF (VAR11=2)
    DLED01000000
    VAR6=VAR6+1
NIF
IF (VAR11=4)
    DLED00100000
    VAR6=VAR6-5
    IF (VAR6<0)
        VAR6=0
    NIF
NIF

```

```

IF (VAR11=6)
    DLED00010000
    VAR6=VAR6+5
NIF
IF (VAR11=5 AND VAR104=0)
    DLED00000010
    VAR102=VAR6
    VAR6=0
    VAR104=1
ELSE
    IF (VAR11=5 AND VAR104=1)
        DLED00000001
        VAR6=VAR102
        VAR104=0
    NIF
NIF

DPCUR2,16
DVAR6
NIF

IF (VAR100=2)          ;'F2' key input.  Axes 5-6 ratio adjustment

DWRITE"ADJUST FOLLOWING RATIO OF CONVEYOR BELTS"
DPCUR2,0
DWRITE"CURRENT RATIO= "
DVAR2
DPCUR2,26
DWRITE"5=PAUSE/RESUME"

IF (VAR11=8 AND VAR2>0 AND VAR3>0)
    DLED10000000
    VAR2=VAR2-1
    VAR3=VAR3-1
NIF
IF (VAR11=2)
    DLED01000000
    VAR2=VAR2+1
    VAR3=VAR3+1
NIF
IF (VAR11=4)
    DLED00100000
    VAR2=VAR2-10
    VAR3=VAR3-10
    IF (VAR2<0 OR VAR3<0)
        VAR2=0
        VAR3=0
    NIF
NIF
IF (VAR11=6)
    DLED00010000
    VAR2=VAR2+10
    VAR3=VAR3+10
NIF
IF (VAR11=5 AND VAR104=0)
    DLED00000010
    VAR103=VAR2
    VAR2=0
    VAR3=0
    VAR104=1
ELSE
    IF (VAR11=5 AND VAR104=1)
        DLED00000001
        VAR2=VAR103

```

```

        VAR3=VAR103
        VAR104=0
    NIF
NIF

    DPCUR2,16
    DVAR2
NIF

    5FOLRN(VAR2)
    6FOLRN(VAR3)
    7FOLRN(VAR6)
    GO00001111
    DLED00000000
    T0.5          ;Time delay 0.5 sec
LN
END

```

4.0 SUMMARY

This technical report has documented the 6K control program. The report explains the concept of following. Also, it includes the explanation for how the controller and RP240 panel for manual overriding works. The control program is listed with line by line description. Functions used in the program are attached in Appendix with description.

APPENDIX (List of functions)

Here we list all the functions in the order were used in the program and also show brief explanation that is from the 6K manual. Some unused functions were omitted. See 6K user manual for full explanation.

SCLD (Distance Scale Factor)

Type	Scaling
Syntax	<!><@><a>SCLD<i>,<i>,<i>,<i>,<i>,<i>,<i>,<i>
Units	i = counts/unit
Range	1 - 999,999
Default	1
	(Servos auto-detect based on SFB: 1 if encoder, 205 if ANI)
Response	SCLD: *SCLD1,1,1,1,1,1,1,1
1SCLD:	*1SCLD1
See Also	SCALE, SCLA, SCLMAS, SCLV, TSTAT

SCLV (Velocity Scale Factor)

Type	Scaling
Syntax	<!><@><a>SCLV<i>,<i>,<i>,<i>,<i>,<i>,<i>,<i>
Units	i = counts/unit
Range	1 - 999,999
Default	4000
	(Servos auto-detect based on SFB: 4000 if encoder, 205 if ANI)
Response	SCLV: *SCLV4000,4000,4000,4000 ...
1SCLV:	*1SCLV4000

See Also ANIRNG, FMAXV, HOMV, HOMVF, JOGVH, JOGVL, JOYVH, JOYVL, SCALE, SCLA, SCLD, SFB, TSTAT, V

SCLA (Acceleration Scale Factor)

Type Scaling
 Syntax <!><@><a>SCLA<i>,<i>,<i>,<i>,<i>,<i>,<i>,<i>
 Units i = counts/unit
 Range 1 - 999,999
 Default 4000
 (Servos auto-detect based on SFB: 4000 if encoder, 205 if ANI)
 Response SCLA: *SCLA4000,4000,4000,4000,4000,4000,4000,4000
 1SCLA: *1SCLA4000
 See Also ANIRNG, FMAXA, SCALE, SCLD, SCLMAS, SCLV, SFB, TSTAT

SCALE (Scaling Enable)

Type Scaling
 Syntax <!>SCALEUnits n/a
 Range b = 0 (disable) or 1 (enable)
 Default 0
 Response SCALE: *SCALE0
 See Also DRES, ERES, SCLA, SCLD, SCLMAS, SCLV, SFB, TSTAT

DEL (Delete a Program/Subroutine/Path)

Type Program or Subroutine Definition
 Syntax <!>DEL<t>
 Units t = alpha text string (name of a program)
 Range text string of 6 characters or less
 Default n/a
 Response n/a
 See Also \$, DEF, END, ERASE, GOSUB, GOTO, RUN

DEF (Begin Definition of a Program/Subroutine/Path)

Type Program or Subroutine Definition
 Syntax <!>DEF<t>
 Units t = alpha text string (name of a program)
 Range text string of 6 characters or less
 Default n/a
 Response n/a
 See Also \$, DEL, END, ERASE, GOBUF, GOSUB, GOTO, MEMORY, PCOMP, PLCP, PRUN, RUN, [SS], TDIR, TMEM, TPROG, TSS, TSTAT

FOLMAS (Assignment of Master to Follower)

Type Following
 Syntax <!><@><a>FOLMAS<꺆 i>,<꺆 i>,<꺆 i>,<꺆 i>,<꺆 i>,<꺆 i>,<꺆 i>,<꺆 i>
 Units 1st i = master #;
 2nd i = master count source;
 =sets direction of master counts relative to direction of actual master count source
 Range 1st i = 1-8 (axis #, or VARI #);
 2nd i = 1 (encoder),
 2 (analog input),
 4 (commanded position),
 5 (internal count source),

6 (internal sine wave source), or
8 (VARI variable).

NOTE: "1", by itself, selects the master encoder.

"0", by itself, disables the axis from being a follower

Default +0 (disable from being a follower axis)

Response FOLMAS *FOLMAS+0,+0,+0,+0, +0,+0,+0,+0
1FOLMAS *1FOLMAS+0

See Also ANIMAS, FGADV, FOLEN, FOLK, FOLMD, FOLRD, FOLRN, FOLRNF, [FS],
FVMACC, FVMFRQ, SINAMP, SINANG, SINGO, VARI, VARSHO, TFS

FOLEN (Following Mode Enable)

Type Following

Syntax <!><@><a>FOLEN

Units n/a

Range b = 0 (disable), 1 (enable) or X (don't change)

Default 0

Response FOLEN: *FOLEN0000_0000
1FOLEN: *1FOLEN0

See Also FGADV, FOLK, FOLMAS, FOLRD, FOLRN, FOLRNF, [FS], FSHFC, FSHFD,
GOWHEN, JOG, JOY, TFS

DRIVE (Drive Enable)

Type Drive Configuration

Syntax <!><@><a>DRIVE

Units n/a

Range b = 0 (shutdown), 1 (enable), or X (don't change)

Default0 (shutdown)

Response DRIVE *DRIVE1111_1111
1DRIVE *1DRIVE1

See Also [AS], [ASX], AXSDEF, DRFEN, DRFLVL, DRES, KDRIVE, TAS, TASX, TER

AXSDEF (Axis Definition)

Type Controller Configuration

Syntax <!><@>AXSDEF

Units n/a

Range b = 0 (stepper), 1 (servo), or X (don't change)

Default 1 (servo)

Response AXSDEF: *11111111

See Also DRIVE

DRFLVL (Drive Fault Input Level)

Type Drive Configuration

Syntax <!><@><a>DRFLVL

Units n/a

Range b = 0 (active low), 1 (active high), or X (don't change)

Default 1

Response DRFLVL *DRFLVL1111_1111
1DRFLVL *1DRFLVL1

See Also [AS], [ASX], DRIVE, DRES, DRFEN, [ER], TAS, TASX, TER

DRFEN (Check for Drive Fault Input Active)

Type Drive Configuration

Syntax <!><@><a>DRFEN

Units b = enable bit

Range b = 1 (check the state of the drive fault input),
0 (don't check the state of the drive fault input), or
x (don't change)

Default 0 (disabled)

Response DRFEN: *DRFEN0000_0000
1DRFEN: *1DRFEN0

See Also DRFLVL, DRIVE, [AS], [ASX], [ER], ERROR, TAS, TASX, TER
[KDRIVE \(Disable Drive on Kill\)](#)

Type Controller Configuration

Syntax <!><@><a>KDRIVE

Units b = enable bit

Range 0 (disable), 1 (enable), or X (don't change)

Default 0

Response KDRIVE: *KDRIVE0000_0000
1KDRIVE: *KDRIVE0

See Also DRIVE, INFNC, K, <ctrl>K, LIMFNC
[SFB \(Select Servo Feedback Source\)](#)

Type Controller Configuration or Servo

Syntax <@><a>SFB<i>,<i>,<i>,<i>,<i>,<i>,<i>,<i>

Units i = feedback source identifier

Range i = 0 (open loop, disable gains), 1 (encoder), or 2 (ANI input)

Default 1

Response SFB *SFB1,1,1,1,1,1,1,1
1SFB *1SFB1

See Also [ANI], ANIFB, ANIRNG, AXSDEF, ERES, [FB], OUTPn, [PANI], [PCE], [PE], PSET, SCALE, SCLD, SGAF, SGI, SGILIM, SGP, SGV, SGVF, SMPER, SOFFS, TANI, TFB, TPANI, TPE
[ERES \(Encoder Resolution\)](#)

Type Encoder Configuration

Syntax <!><@><a>ERES<i>,<i>,<i>,<i>,<i>,<i>,<i>,<i>

Units i = counts/rev

Range 1 - 65535 (stepper axes); 200 to 1024000(servo axes)
Updated to 1,073,741,823 in Rev 6.4

Default 4000

Response ERES: *ERES4000,4000,4000,4000,4000,4000,4000,4000
1ERES: *1ERES4000

See Also DRES, EFAIL, ENCCNT, ESTALL, TSTAT
[SMPER \(Maximum Allowable Position Error\)](#)

Type Servo

Syntax <!><@><a>SMPER<r>,<r>,<r>,<r>,<r>,<r>,<r>,<r>

Units r = feedback device steps (scalable with SCLD)

Range 0-200,000,000 (0 = do not monitor position error condition)

Default 4000

Response SMPER: *SMPER4000,4000,4000,4000 ...
1SMPER: *1SMPER4000

See Also [AS], CMDDIR, ENCPOL, [ER], ERES, ERROR, ERRORP, KSMPER, SCALE, SCLD, SFB, SGILIM, TANI, TAS, TER, TFB, TPC, TPE, TPER

(applicable to servo axes only)

[EFAIL \(Encoder Failure Detection\)](#)

Type Encoder Configuration

Syntax <!><@>EFAIL

Units n/a

Range b = 0 (disable), 1 (enable), or X (don't change)

Default 0

Response EFAIL: *EFAIL0000_0000
1EFAIL: *1EFAIL0

See Also [ASX], [ER], ERROR, ERRORP, TASX, TER

[ENCPOL \(Encoder Polarity\)](#)

Type Encoder; Controller Configuration

Syntax <!><@><a>ENCPOL

Units b = polarity bit

Range 0 (normal polarity), 1 (reverse polarity) or X (don't change)

Default 0

Response ENCPOL *ENCPOL00000000
1ENCPOL *1ENCPOL0

See Also CMDDIR, EFAIL, [FB], FOLMAS, MEPOL, [PCE], [PE], [PER], PSET, SFB, TFB, TPE, TPCE, TPER

[ENCSDND \(Step and Direction from Encoder\)](#)

Type Encoder; Counter

Syntax <!><@><a>ENCSDND

Units n/a

Range b = 0 (quadrature signal),
1 (step & direction)
or X (don't care)

Default 0

Response ENCSND: *ENCSND0000_0000
1ENCSND: *1ENCSND0

See Also MESND, [PE], SFB, TPE

[SGP \(Proportional Feedback Gain\)](#)

Type Servo

Syntax <!><@><a>SGP<r>,<r>,<r>,<r>,<r>,<r>,<r>,<r>

Units r = millivolts/step

Range 0.00000000-2,800,000.00000000

Default 0.5

Response SGP: *SGP0.5,0.5,0.5,0.5 ...
1SGP: *1SGP0.5

See Also SFB, SGAF, SGENB, SGI, SGSET, SGV, SGVF, TGAIN, TSGSET

[MC \(Preset/Continuous Positioning Mode Enable\)](#)

Type Motion

Syntax <!><@><a>MC

Units n/a
Range b = 0 (incremental mode), 1 (absolute mode), or x (don't change)
Default 0
Response MC: *MC0000_0000
1MC: *1MC0
See Also A, AD, COMEXC, COMEXS, D, FOLMD, [FS], FSHFC, FSHFD, GO, GOBUF, K, MA, PSET, S, TFS, V

A (Acceleration)

Type Motion
Syntax <!><@><a>A<r>,<r>,<r>,<r>,<r>,<r>,<r>,<r>
Units r = units/sec/sec (Scalable by SCLA)
Range 0.00025 - 39,999,998 (depending on the scaling factor)
Default 10.0000
Response A: *A10.0000,10.0000,10.0000,10.0000 ...
1A: *A10.0000
See Also [A], AA, AD, ADA, DRES, ERES, GO, MC, SCALE, SCLA, TSTAT

ERRORP (Error Program Assignment)

Type Error Handling
Syntax <!><%>ERRORP<t>
Units t = text (name of error program)
Range Text name of 6 characters or less
Default n/a
Response ERRORP: *ERRORPerr1
See Also [ER], ERRLVL, ERROR, STARTP, TER

ERROR (Error-Checking Enable)

Type Error Handling
Syntax <!><%>ERROR... (32 bits)
Units n/a
Range b = 0 (disable), 1 (enable), or X (don't change)
Default 0
Response ERROR: *ERROR0000_0000_0000_0000_0000_0000_0000_0000
See Also [ASX], DRFEN, DRFLVL, DSTALL, EFAIL, [ER], ERRORP, ESTALL, GOWHEN, INFNC, K, LH, LIMFNC, LS, S, TASX, TER, TRGFN

END (End Definition of Program/Subroutine/Path)

Type Program or Subroutine Definition
Syntax <!>END
Units n/a
Range n/a
Default n/a
Response n/a
See Also \$, DEF, DEL, ERASE, GOBUF, GOSUB, GOTO, RUN

STARTP (Start-Up Program Assignment)

Type Subroutines
Syntax <!>STARTP<t>
Units t = text (name of program)
Range Text name of 6 characters or less
Default n/a

Response STARTP: *STARTP MAIN
 See Also DEF, RESET, SCALE
COMEXC (Continuous Command Processing Mode)
 Type Command Buffer Control
 Syntax <!!>COMEXC
 Units b = 0, 1 or X
 Range 0 = Disable, 1 = Enable, X = don't change
 Default 0
 Response COMEXC: *COMEXC0
 See Also [!], A, AA, AD, ADA, COMEXL, COMEXS, D, ERRORP, FOLRD, FOLRN, GO, GOWHEN, MA, MC, V
VAR (Numeric Variable Assignment)
 Type Variable
 Syntax <!!>VAR<i><=r>
 Units i = variable number
 r = number or expressionRange i = 1-225
 r = ±99,999,999.99999999
 Default n/a
 Response VAR1: *VAR1=+0.0
 See Also DVAR, VARB, VARCLR, VARI, VARS, VARSHI, VCVT, WRVAR
V (Velocity)
 Type Motion
 Syntax <!!><@><a>V<r>,<r>,<r>,<r>,<r>,<r>,<r>,<r>
 Units r = units/sec
 Range Stepper Axes: 0.00000-2,048,000 (max. depends on SCLV and PULSE)
 Servo Axes: 0.00000-6,500,000 (max. depends on SCLV)
 Default 1.0000
 Response V: *V1.0000,1.0000,1.0000,1.0000 ...
 1V: *1V1.0000
 See Also GO, MC, PULSE, SCALE, SCLV, TSTAT, TVEL, TVELA, [V], [VEL], [VELA], VF
DSTP (Enable/Disable RP240 Stop Key)
 Type Display (RP240) Interface
 Syntax <!!>DSTP
 Units b = enable bit
 Range b = 1 (enable) or 0 (disable)
 Default 1 (enable)
 Response DSTP *DSTP1
 See Also DLED, [DREAD], [DREADF]
FOLRN (Numerator of Follower-to-Master Ratio)
 Type Following
 Syntax <!!><@><a>FOLRN<r>,<r>,<r>,<r>,<r>,<r>,<r>,<r>
 Units r = follower distance in steps
 Range r = 0 - 999,999,999.99999 (scalable by SCLD)
 Default 1
 Response FOLRN *FOLRN1,1,1,1,1,1,1,1
 1FOLRN *FOLRN1
 See Also FGADV, FOLEN, FOLK, FOLMAS, FOLRD, FOLRNF, SCLD

FOLRD (Denominator of Follower-to-Master Ratio)

Type Following
Syntax <!><@><a>FOLRD<r>,<r>,<r>,<r>,<r>,<r>,<r>,<r>
Units r = master distance in counts
Range r = 1 - 999,999,999 (scalable by SCLMAS)
Default 1
Response FOLRD *FOLRD1,1,1,1,1,1,1,1
1FOLRD *FOLRD1
See Also COMEXC, FGADV, FOLEN, FOLK, FOLMAS, FOLRN, FOLRNF, SCLMAS

GO (Initiate Motion)

Type Motion
Syntax <!><@>GO
Units n/a
Range b = 0 (don't go), 1 (go), or X (don't change)
Default 1
Response GO: No response; instead, motion is initiated on all axes
See Also A, AA, AD, ADA, COMEXC, D, DRFLVL, GOBUF, GOWHEN, K, LH, LS, MA, MC, PSET, S, SCLA, SCLD, SCLV, V

DREADI (RP240 Data Read -- Immediate Mode)

Type Display (RP240) Interface
Syntax <!>DREADI
Units n/a
Range 1 (enable) or 0 (disable)
Default 0
Response DREADI: *DREADI0
See Also DPCUR, [DREAD], [DREADF], LOCK, VAR, VARI

L (Loop)

Type Loops; Program Flow Control
Syntax <!>L<i>
Units i = number of times to loop
Range 0-999,999,999
Default 0- infinite loop
Response L: No response; instead, this has the same function as L0
See Also LN, LX, PLN, PLOOP

[DREADF] (Read RP240 Function Key Entry)

Type Display (RP240) Interface
Syntax See below
Units n/a
Range n/a
Default n/a
Response n/a
See Also [DREAD], DREADI, DVAR, DWRITE, [SS], TSS, VAR, VARI

[DKEY] (Value of RP240 Key)

Type Display (RP240) Interface; Assignment or Comparison
Syntax See below
Units n/a
Range n/a

Default	n/a
Response	n/a
See Also	DCLEAR, DPCUR, [DREAD], DREADF, DREADI, DVAR, DWRITE
Value of DKEY	Key currently active

-1	None or multiple keys
0	0
1	1
2	2
3	3
4	4
5	5
6	6
7	7
8	8
9	9
10	.
11	+/-
12	C/E
13	ENTER
14	Menu Recall
15	STOP
16	PAUSE
17	CONTINUE
21	F1
22	F2
23	F3
24	F4
25	F5
26	F6

DCLEAR (Clear Display)

Type	Display (RP240) Interface
Syntax	<!>DCLEARi
Units	n/a
Range	i = 0 (clear all lines), 1 (clear line 1), or 2 (clear line 2)
Default	n/a
Response	n/a
See Also	DLED, DPASS, DPCUR, DSTP, DVAR, DVARB, DVARI, DWRITE

IF (IF Condition/Statement)

Type	Program Flow Control or Conditional Branching
Syntax	<!>IF(expression)
Units	n/a
Range	Up to 80 characters (including parentheses)
Default	n/a
Response	n/a
See Also	ELSE, NIF

K (Kill Motion)

Type Motion
 Syntax <!><@>K
 Units n/a
 Range b = 0 (don't kill), 1 (kill), or X (don't change)
 Default n/a
 Response !K No response, instead motion is killed on all axes
 See Also DRFLVL, ERROR, FOLK, GO, HALT, <CTRL>K, KDRIVE, LHAD, LHADA, S, SCANP, TAS

BREAK (Terminate Program Execution)

Type Program Flow Control
 Syntax <!>BREAK
 Units n/a
 Range n/a
 Default n/a
 Response n/a
 See Also BP, C, GOSUB, HALT, K, S

NIF (End of IF Statement)

Type Program Flow Control or Conditional Branching
 Syntax <!>NIF
 Units n/a
 Range n/a
 Default n/a
 Response No response when used in conjunction with the IF command
 See Also ELSE, IF

DWRITE (Write Text String to RP240 Display)

Type Display (RP240) Interface
 Syntax <!>DWRITE"message"
 Units n/a
 Range Message can be up to 80 characters (may not use characters ", \, * or :)
 Default -
 Response n/a
 See Also DCLEAR, DLED, DPASS, DPCUR, DVAR, DVARB, DVARI, PORT

DPCUR (Position the Cursor)

Type Display (RP240) Interface
 Syntax <!>DPCURi,i
 Units 1st i = line number, 2nd i = columnRange line number = 1 or 2, column = 0-39
 Default n/a
 Response n/a
 See Also DCLEAR, DLED, DPASS, DREADI, DSTP, DVAR, DVARB, DVARI, DWRITE

DVAR (Display Numeric Variable on RP240)

Type Display (RP240) Interface
 Syntax <!>DVARi,<i>,<i>,<i>
 1st i = Variable number [Range 1-225]
 2nd i = Number of whole digits displayed (left of decimal point) [Range 0-9]
 3rd i = Number of fractional digits displayed (right of decimal point) [Range 0-8]
 4th i = Sign bit: 0 = no sign displayed, 1 = display + or -
 Units See above

Range	See above
Default	See above
Response	n/a
See Also	[DREAD], [DREADF], DVARB, DVARI, DWRITE, VAR
DLED (Turn RP240 LEDs On/Off)	
Type	Display (RP240) Interface
Syntax	<!--DLED
Units	n/a
Range	b = 0 (off) or 1 (on)
Default	n/a
Response	DLED:*DLED1101_0001
See Also	DCLEAR, DPASS, DPCUR, DSTP, DVAR, DVARB, DVARI, DWRITE
T (Time Delay)	
Type	Program Flow Control
Syntax	<!--T<r>Units r = seconds
Range	0.001-999.999
Default	n/a
Response	n/a
See Also	GOWHEN, PS, [SS], [TIM], TTIM, TSS, WAIT, VAR, VARI
LN (End of Loop)	
Type	Loops or Program Flow Control
Syntax	<!--LN
Units	n/a
Range	n/a
Default	n/a
Response	No response; used in conjunction with the L command
See Also	L, LX